Influence of Electron-poor Conjugated Polymers on the Selective Dispersion of Carbon Nanotubes

Influence of Electron-poor Conjugated Polymers on the Selective Dispersion of Carbon Nanotubes

By

Jack Cruikshank, B.Sc.

A Thesis

Submitted to the School of Graduate Studies

In Partial Fulfillment of the Requirements

For the Degree of

Master of Science

In Chemistry

Master of Science (2022) McMaster University

Chemistry Hamilton, Ontario, Canada

Title: Influence of Electron-poor Conjugated Polymers on the Selective Dispersion of Carbon Nanotubes

Author: Jack Cruikshank

BSc. (Chemistry)

McMaster University, Hamilton, Canada

Supervisor: Professor Alex Adronov

Number of Pages: xix, 103

Abstract

The unique thermal, electronic, and optical properties of single-walled carbon nanotubes (SWNTs) can be used in a variety of applications. However, all currently available production methods result in a heterogenous mixture of semiconducting and metallic species. SWNTs also self-aggregate, resulting in minimal solubility in solvents, preventing their immediate incorporation into many applications. These challenges have resulted in the development of various purification methods, but the use of conjugated polymers is considered to be the most scalable technique. Currently, conjugated polymers have allowed for the complete isolation of semiconducting SWNTs using electron-rich conjugated polymers such as polythiophenes, polycarbazoles, and polyfluorenes. Conversely, the isolation of pure metallic SWNTs still requires improvement. Recently, a two-polymer system was developed for the enrichment of metallic SWNTs using an electron-rich conjugated polymer to remove semiconducting SWNTs, followed by an electron-poor polymer to disperse the remaining metallic SWNTs. This technique represented a significant step forward in the enrichment of metallic SWNT samples using conjugated polymers, but refinement is still possible.

The aim of this thesis is to improve this scalable technique for the enrichment of metallic SWNTs. Specially, two reactions on poly(fluorene-*co*-pyridine) were investigated in an effort to generate a more electron deficient polymer backbone. The first reaction involved the addition of a dinitrobenzene moiety by means of the Zincke reaction. It was found that the functionalization of the polymer backbone using the Zincke reaction was not feasible, likely due to steric hinderance. Research efforts were then redirected to a reaction involving the addition of a less bulky trifluoroacetyl group by reaction of the polymer with trifluoroacetic anhydride. This investigation led to the straightforward and complete functionalization of the polymer backbone producing

acetylated poly(fluorene-*co*-pyridine). Next, the ideal dispersion conditions were tuned for the acetylated poly(fluorene-*co*-pyridine) to be incorporated into the two-polymer extraction system. This novel polymer showed higher dispersion concentration and improved selectivity toward metallic SWNTs than previously developed. Characterization of the polymer-SWNT dispersions were conducted using UV-vis-NIR spectroscopy, and conductivity techniques to evaluate their electronic purity.

Acknowledgements

Throughout all the highs and lows over the last two years I have had a consistent support system, that I would like to acknowledge. Firstly, a sincere thank you to my supervisor, Professor Alex Adronov, for the opportunity to research in a field in which I am interested. First starting at McMaster in an organic chemistry laboratory was intimidating as my previous research experience was in the field of nanotechnology. Despite this, I was given an amazing opportunity with the Adronov group. Alex made himself available through all the growing pains as I learned the exciting but challenging field of organic multi-step synthesis. He showed me numerous ways to improve my critical thinking, experimental design, and laboratory skills that I will remember throughout my chemistry career and for that I am truly appreciative. I also want to thank my committee member Dr. Ryan Wylie for his ideas and help throughout my thesis.

This research would also not be possible without the contributions of NSERC and the Green Electronics Network (GreEN). Being able to be apart of GreEN has allowed me to learn more about other groups research and contribute to a worthy cause, which has been rewarding.

Next, I thank everybody who was apart of the Adronov group over the two years I attended McMaster. Everyone was always willing to help and share ideas about how to solve problems. I am thankful for all the friends in the lab I have made and lifelong connections. Specifically, a special thanks to Dialia Ritaine for training me on the use of the instruments in the lab and many laboratory techniques. Also, a big thanks to Mokha Ranne for attempting to perform Raman on my samples as there were a lot of them and the effort was appreciated. I also appreciated that Mokha took interest in my research and offered advice on many problems.

On both a personal and professional level I could not have finished the last two years without the support of Dayna Bennett. She was there literally any time I needed help; whether it was because a polymerization exploded, or I had a group meeting the next day. She helped take school off my mind by exploring Hamilton and Toronto, going on many adventures like Jays games and the Toronto Zoo. The last two years has been challenging for both of us both personally and academically and knowing I had your support really helped get through it all. Also, coming home was always a bit easier thanks to my fluffiest family member Freddy. Knowing that I had to pay your vet bills really encouraged me to graduate.

Finally, I am very thankful for my family for their support as I moved to a new city. To my parents, Ian and Tammay, I always knew I could count on you to answer the phone and listen to me talk about my day.

As I move on from McMaster, I know that the knowledge I have gained will stay with me throughout my life and I am grateful for having the opportunity to experience all it had to offer.

List of Abbreviations

1D	One Dimension
2D	Two Dimension
AFM	Atomic Force Microscopy
AGE	Agarose Gel Electrophoresis
ANRORC	Addition of the Nucleophile, Ring Opening, and Ring Closure
A-PF-Py	Acetylated Poly(fluorene-*co*-pyridine)
CDNB	1-Chloro-2,4-dinitrobenzene
C_h	Chiral vector
CNTs	Carbon Nanotubes
CoMoCat	Carbon Monoxide Molybdenum Catalyzed
CPs	Conjugated Polymers
CVD	Chemical Vapour Deposition
Đ	Dispersity
DBP	2,5-dibromopyridine
DCM	Dichloromethane
DGU	Density Gradient Ultracentrifugation
DNCB	2,4-dinitro-chlorobenzene
DOS	Density of States
GPC	Gel Permeation Chromatography
HiPCO	High-pressure Carbon Monoxide Disproportionation
HOMO	Highest Occupied Molecular Orbital
IR	Infrared

LUMO	Lowest Unoccupied Molecular Orbital
Me-PF-Py	Methylated Poly(fluorine-*co*-pyridine)
Mn	Number-Average Molecular Weight
m-SWNTs	Metallic Single Walled Nanotubes
MWNTs	Multi-walled Carbon Nanotubes
NBS	N-bromosuccinimide
NMR	Nuclear Magnetic Resonance
PCPF	Poly(carbazole-*co*-fluorene)
PF-Py	Poly(fluorine-*co*-pyridine)
PL	Photoluminescence
PT	Plasma torch
RBM	Radial Breathing Mode
Sc-SWNTs	Semiconducting Single Walled Nanotubes
SDS	Sodium Dodecyl Sulfate
SEC	Size Exclusion Chromatography
ssDNA	Single Strand DNA Dispersions
SWNTs	Single-walled Carbon Nanotubes
TGA	Thermogravimetric Analysis
THF	Tetrahydrofuran
TLC	Thin Layer Chromatography
Tol	Toluene
UV-vis-NIR	Ultraviolet Visible-Near Infrared

Table of Contents

Abstract iv
Acknowledgements vi
List of Abbreviations viii
List of Tables xii
List of Figures xiii
List of Schemes xviii
Chapter 1: Introduction 1
1.1 Introduction to Carbon Nanotubes 1
1.2 Synthesis Methods of Carbon Nanotubes 2
1.2.1 Arc-Discharge 3
1.2.2 Laser Ablation 3
1.2.3 Chemical Vapour Deposition (CVD) 4
1.2.4 Plasma-Torch 4
1.2.5 High-Pressure Carbon Monoxide Disproportionation (HiPCO) 4
1.3 Carbon Nanotube Electronics 5
1.4 Purification of Carbon Nanotubes 6
1.4.1 Density Gradient Ultracentrifugation 7
1.4.2 Agrose gel Electrophoresis 8
1.4.3 Two-Phase extraction 9
1.4.4 Size Exclusion Chromatography 9
1.4.5 DNA Dispersions 10
1.5 Conjugated Polymers 11
1.5.1 Introduction to Conjugated Polymers 11
1.5.2 Conjugated Polymers and Carbon Nanotubes 12
1.6 Effect of Electron Density on Conjugated Polymer Selectivity 14
1.7 Two-Polymer Sorting 15
1.8 Characterization of Carbon Nanotube Dispersions 17
1.8.1 UV-vis-NIR Absorption Spectroscopy 17
1.8.2 Photoluminescence Mapping 18
1.8.3 Resonance Raman Spectroscopy 19
1.9 Summary and Objectives 21

Chapter 2: Investigation of the Zincke Reaction on Polyfluorene-co-Pyridine 23
2.1 Introduction 23
2.2 Results and Discussion 26
2.3 Conclusion 31
2.4 Experimental 32
2.4.1 General 32
2.4.2 Synthesis of Poly(9,9'-didodecylfluorene-co-pyridine) 32
2.4.3 Zincke Reaction Attempts 39
Chapter 3: Enhancement of the Two-Polymer Extraction Method Using Acetylated PF-Py 43
3.1 Introduction 43
3.2 Results and Discussion 44
3.2.1 Ideal Dispersion Parameter Studies 46
3.2.2 Incorporating A-PF-Py into the Two-Polymer Extraction Method 51
3.3 Conclusion 58
3.4 Experimental 58
3.4.1 General 58
3.4.2 Synthesis 59
3.5 Supporting Information 72
3.5.1 Atomic Force Microscopy (AFM) 72
3.5.2 Additional UV-vis-NIR Absorption Spectra 73
3.5.3 Photographs of Polymers and SWNT Dispersions 77
3.5.4 Thermogravimetric Analysis (TGA) Data 81
Chapter 4: Overall Conclusions and Future Work 83
4.1 General Conclusions 83
4.2 Future Work 84
References 87

List of Tables

Table 1: Reaction conditions for the model Zincke reaction on pyridine including temperature, mass, molar equivalent, reaction time, and yield. 39

Table 2: Reaction conditions for the Zincke reaction on PF-Py including temperature, mass, molar equivalent, molecular weight, concentration, and reaction time. 41

Table 3: Peak absorbance for m-SWNTs (506 nm) and Sc-SWNTs (~1135 nm), ratio of m/sc from Figure 16, the A-PF-Py-SWNTs dispersant solvent study using HiPCO SWNTs. 47

Table 4: Peak absorbance for m-SWNTs (506 nm) and sc-SWNTs (~1135 nm), ratio of m/sc from Figure 17, the A-PF-Py-SWNTs ratio study using HiPCO SWNTs. 48

Table 5: Peak absorbance for m-SWNTs (506 nm) and sc-SWNTs (~1135 nm), ratio of m/sc from Figure 18, the A-PF-Py-SWNTs molecular weight study using HiPCO SWNTs. 49

Table 6: Peak absorbance for m-SWNTs (506 nm) and sc-SWNTs (~1135 nm), ratio of m/sc from Figure 19, the polymer-SWNTs comparison study using HiPCO SWNTs. 50

Table 7: Peak absorbance for m-SWNTs (506 nm) and sc-SWNTs (~1135 nm), ratio of m/sc from Figure 21, the P1-SWNTs extraction study using HiPCO SWNTs. 52

Table 8: Peak absorbance for m-SWNTs (506 nm) and Sc-SWNTs (~1135 nm), ratio of m/Sc from Figure 22, the 0.5:1 A-PF-Py-SWNTs extraction study using HiPCO SWNTs. 54

Table 9: Peak absorbance for m-SWNTs (506 nm) and Sc-SWNTs (~1135 nm), ratio of m/sc from Figure 23, the 0.25:1 A-PF-Py-SWNTs extraction study using HiPCO SWNTs. 55

Table 10: Conductivity measurements for E1P2 and raw HiPCO SWNTs including average conductivity, and sheet resistance. 56

List of Figures

Figure 1: A summary of the unique properties of CNTs with examples of potential applications. Reproduced with permission.[19] Copyright 2020 Multidisciplinary Digital Publishing Institute.... 1

Figure 2: a) Carbon lattice with labeled unit vectors, a_1 and a_2, and zigzag (blue), chiral (purple), and armchair (red) vectors. b) Arm-chair, zigzag and chiral nanotube examples. 2

Figure 3: a) Image of a centrifuge tube containing HiPCO SWNTs sorted by DGU. The distinct coloured bands are layers enriched in different SWNT species. b) Near-infrared absorbance spectra of the marked coloured layer with (n,m) indices labeled. Reproduced with permission.[48] Copyright 2010 Nature Nanotechnology. 8

Figure 4: Separation of SWNTs dispersion in gel by AGE. (a) Sequential photographs showing the progress of separation. (b) Absorption spectra of fractions after AGE. Spectra i and ii correspond to the samples from fractions shown in (a). The bottom black spectrum is for the SWNT dispersion before separation. Reproduced with permission.[49] Copyright 2008 Applied Physics Express..... 9

Figure 5: Time lapse photograph of HiPCO SWNTs dispersed in 1 wt. % SDS in H_2O on a Sephacryl SEC gel. Reproduced with permission.[52] Copyright 2013 American Chemical Society..... 10

Figure 6: Structures of highly researched conjugated polymers..... 12

Figure 7: Outline of the preparation of polymer-SWNT dispersions including sonication, centrifugation, filtration, and redispersion. Prepared using BioRender..... 13

Figure 8: Conjugated polymer sorting extraction system. PCPF (e-rich) shown in blue. Me-PF-Py (e-poor) shown in red. Reproduced with permission. [88] Copyright 2018 American Chemical Society Omega. 16

Figure 9: PL mapping of HiPCO polymer-SWNT dispersions using A) poly(fluorene-*co*-carbazole) B) poly(fluorene-*co*-pyridine). Reproduced with permissions.[88] Copyright 2018 American Chemical Society Omega. 19

Figure 10: Raman Spectrum for HiPCO SWNTs at 633 nm laser power. G-Band labeled in red, RBM labeled in blue. 20

Figure 11: ^{1}H NMR spectrum of 2,7-dibromofluorene in $CDCl_3$. 34

Figure 12: ^{1}H NMR spectrum of 2,7-dibromo-9,9-didodecylfluorene in $CDCl_3$. 35

Figure 13: ^{1}H NMR spectrum of 2,2'-(9,9-didodecylfluorene-2,7-diyl)bis(4,4,5,5-tetramethyl-1,3,2-dioxaborolane) in $CDCl_3$. 37

Figure 14: ^{1}H NMR of Pf-Py in $CDCl_3$. 38

Figure 15: ^{1}H NMR spectrum of model pyridinium salt in C_2D_6OS. 40

Figure 16: UV-vis-NIR absorption spectra for the A-PF-Py-SWNTs dispersant solvent study using HiPCO SWNTs. Spectra are normalized to a local minimum at ~905 nm to show relative m-SWNT and sc-SWNT content. 47

Figure 17: UV-vis-NIR absorption spectra for the A-PF-Py-SWNTs ratio study using HiPCO SWNTs. Spectra are normalized to a local minimum at ~905 nm to show relative m-SWNT and sc-SWNT content. 48

Figure 18: UV-vis-NIR absorption spectra for the A-PF-Py-SWNTs molecular weight study using HiPCO SWNTs. Spectra are normalized to a local minimum at ~905 nm to show relative m-SWNT and sc-SWNT content. 49

Figure 19: UV-vis-NIR absorption spectra for all investigated polymer-SWNT types using HiPCO SWNTs. Spectra are normalized to a local minimum at ~905 nm to show relative m-SWNT and sc-SWNT content. 50

Figure 20: Illustration showing the method of two polymer extraction. P1 (green) is the electron rich PCPF, which is introduced to first extract sc-SWNTs and is repeated for *x* extractions. P2 (black) is the electron poor A-PF-Py and is used as the final dispersant to disperse the remaining m-SWNTs. 51

Figure 21: UV-vis-NIR absorption spectra for the P1-SWNTs extraction study using HiPCO SWNTs. Spectra are normalized to a local minimum at ~905 nm to show relative m-SWNT and sc-SWNT content. 52

Figure 22: UV-vis-NIR absorption spectra for the 0.5:1, A-PF-Py-SWNTs, extraction study using HiPCO SWNTs. Spectra are normalized to a local minimum at ~905 nm to show relative m-SWNT and sc-SWNT content. 53

Figure 23: UV-vis-NIR absorption spectra for the 0.25:1, A-PF-Py-SWNTs, extraction study using HiPCO SWNTs. Spectra are normalized to a local minimum at ~905 nm to show relative m-SWNT and sc-SWNT content. 55

Figure 24: UV-vis-NIR absorption spectra for the polymer-SWNTs dispersion study using plasma-torch SWNTs. Spectra are normalized to a local maximum at ~936 nm to show relative m-SWNT and sc-SWNT content. 57

Figure 25: ^{1}H NMR spectrum of 1-bromo-2-decyl-4-tetradecane in $CDCl_3$. 61

Figure 26: ^{1}H NMR of 2-nitro-4-4'dibromobiphenyl in $CDCl_3$ 62

Figure 27: ^{1}H NMR of 9H-2,7-dibromocarbazole in $CDCl_3$. 63

Figure 28: ^{1}H NMR of N-(2'-decyltetradecane)-2,7-dibromocarbazole in $CDCl_3$. 65

Figure 29: ^{1}H NMR spectrum of Poly(9,9'-didodecylfluorene-co-N-(2'-decyltetradecane)-carbazole) in $CDCl_3$. 67

Figure 30: ^{1}H NMR spectrum of Me-PF-Py in $CDCl_3$. 68

Figure 31: ^{1}H NMR spectrum of acetylated dimethylaminopyridine in $CDCl_3$. 69

Figure 32: ^{1}H NMR spectrum of acetylated PF-Py $CDCl_3$ and D_2O. 71

Figure 33: Atomic force microscopy (AFM) of 0.5:1 A-PF-Py dispersions showing polymer wrapped SWNTs. a) and b) 2 µm scale, c) and d) 5 µm scale. 72

Figure 34: Unnormalized UV-vis-NIR absorption spectra for the A-PF-Py-SWNTs dispersant solvent study using HiPCO SWNTs. 25 kDa Acetylated 1:1 THF diluted 1:20. 25 kDa Acetylated 1:1 THF:Tol diluted 1:20. 73

Figure 35: Unnormalized UV-vis-NIR absorption spectra for the A-PF-Py-SWNTs ratio study using HiPCO SWNTs. 25 kDa Acetylated 1:1 THF:Tol diluted 1:20. 25 kDa Acetylated 0.5:1 THF:Tol undilute. 25 kDa Acetylated 0.25:1 THF:Tol undilute. 73

Figure 36: Unnormalized UV-vis-NIR absorption spectra for the A-PF-Py-SWNTs molecular weight study using HiPCO SWNTs. 47 kDa Acetylated 1:1 THF:Tol diluted 1:10. 25 kDa Acetylated 1:1 THF:Tol 1:10. 13 kDa Acetylated 0.25:1 THF:Tol 1:10. 74

Figure 37: Unnormalized UV-vis-NIR absorption spectra for all polymer-SWNT study using HiPCO SWNTs. 13 kDa Methylated 1:1 THF:Tol Undilute. 25 kDa Acetylated 1:1 THF:Tol 1:10. 13 kDa PF-Py 1:1 THF:Tol 1:4 Dilution, 40 kDa PCPF 1:1 Tol Undilute. 74

Figure 38: Unnormalized UV-vis-NIR absorption spectra for the P1-SWNTs molecular extraction study using HiPCO SWNTs. All 1:4 dilution in 1:1 Toluene. 75

Figure 39: Unnormalized UV-vis-NIR absorption spectra for the 0.5:1, A-PF-Py-SWNTs molecular extraction study using HiPCO SWNTs. All 1:20 dilution in 1:1 THF:Toluene. 75

Figure 40: Unnormalized UV-vis-NIR absorption spectra for the 0.25:1, A-PF-Py-SWNTs molecular extraction study using HiPCO SWNTs. All 1:20 dilution in 1:1 THF:Toluene, except E0P2 which is undilute. 76

Figure 41: Normalized UV-vis-NIR absorption spectra for the E4P2 0.25:1 vs. E0P1 comparison using HiPCO SWNTs. 76

Figure 42: Photograph of polymers dissolved in 1:1 THF:Tol (left to right): PCPF, PF-Py, A-PF-Py, Me-PF-Py. 77

Figure 43: Photograph of PC-PF-SWNT dispersions produced using HiPCO SWNTs (left to right): E0P1, E1P1, E2P1, E3P1. 77

Figure 44: Photograph of PC-PF-SWNT dispersions, diluted 1:2, produced using HiPCO SWNTs (left to right): E0P1, E1P1, E2P1, E3P1. 78

Figure 45: Photograph of A-PF-Py-SWNT dispersions produced using HiPCO SWNTs (left to right): 0.25:1, 0.5:1, 1:1. 78

Figure 46: Photograph of 0.25:1, A-PF-Py-SWNT dispersions produced using HiPCO SWNTs (left to right): E0P2, E1P2, E2P2, E3P2, and E4P2. 79

Figure 47: Photograph of 0.25:1, A-PF-Py-SWNT dispersions, dilute 1:20, produced using HiPCO SWNTs (left to right): E0P2, E1P2, E2P2, E3P2, and E4P2. 79

Figure 48: Photograph of 0.25:1, A-PF-Py-SWNT dispersions, dilute 1:20, produced using HiPCO SWNTs (left to right): E1P2, and E4P2. 80

Figure 49: TGA of raw HiPCO SWNTs. 81

Figure 50: TGA of PC-PF. 81

Figure 51: TGA of residue after dispersion with PCPF:HiPCO SWNTs and rinsed thoroughly with THF. 82

List of Schemes

Scheme 1: Overall reaction of the first step of the Zincke reaction between pyridine and DNCB to form the pyridinium salt (top) and the mechanism (bottom). 23

Scheme 2: Mechanism of the second stage of the Zincke Reaction. The pyridinium salt is reacted with a primary amine to produce the pyridinium ion with an R group attached. 24

Scheme 3: Zincke reaction for addition of amine to wang resin.[106] 25

Scheme 4: Zincke reaction for synthesis of a chiral isoquinolinium salt.[108] 25

Scheme 5: Zincke reaction between PF-Py and 1-chloro-2,5-dinitrobenzene. 26

Scheme 6: Zincke reactions on the 2,5-dibromopyridine monomer, 2-bromopyrdine, and 3-bromopyridine. 31

Scheme 7: Synthesis to form 2,2'-(9,9-didodecylfluorene-2,7-diyl)bis(4,4,5,5-tetramethyl-1,3,2-dioxaborolane). 32

Scheme 8: Reaction to form 2,7-dibromofluorene. 33

Scheme 9: Reaction to form 2,7-dibromo-9,9-didodecylfluorene 34

Scheme 10: Reaction to form 2,2'-(9,9-didodecylfluorene-2,7-diyl)bis(4,4,5,5-tetramethyl-1,3,2-dioxaborolane). 36

Scheme 11: Polymerization to form Poly(9,9'-didodecylfluorene-co-pyridine). 37

Scheme 12: Model Zincke Reaction to form pyridinium salt. 39

Scheme 13: Zincke Reaction on PF-Py. 40

Scheme 14: Zincke reaction on 2,5-dibromopyridine. 41

Scheme 15: Zincke Reaction on 2-bromopyrdine 42

Scheme 16: Zincke Reaction on 3-bromopyrdine. 42

Scheme 17: PF-Py reaction with trifluoroacetic anhydride to generate Acetylated PF-Py (A-PF-Py). 44

Scheme 18: Synthesis to form N(2'decyltetradecane)2,7-dibromocarbazole. 59

Scheme 19: Reaction to form 1-bromo-2-decyl-4-tetradecane. 60

Scheme 20: Reaction to form 2-nitro-4-4'dibromobiphenyl. 61

Scheme 21: Reaction to form 9H-2,7-dibromocarbazole. 62

Scheme 22: Reaction to form N-(2'-decyltetradecane)-2,7-dibromocarbazole. 64

Scheme 23: Synthesis of Poly(9,9'-didodecylfluorene-co-N-(2'-decyltetradecane)-carbazole) (P1). 65

Scheme 24: Synthesis of Methylated PF-Py (Me-PF-Py). 67

Scheme 25: Synthesis of acetylated 4-dimethylaminopyrdine. 68

Scheme 26: Synthesis of Acetylated PF-Py (A-PF-Py). 70

Chapter 1: Introduction

1.1 Introduction to Carbon Nanotubes

Carbon nanotubes (CNTs) have attracted significant research attention due to their unique physical and mechanical properties, since they were first synthesized in 1991.[1,2] The high aspect ratio,[3] tensile strength,[4] electrical and thermal conductivity,[5–8] and optical characteristics[9] of CNTs allow for many potential applications. CNTs can be classified as single-walled carbon nanotubes (SWNTs) or multi-walled carbon nanotubes (MWNTs). Diameters of SWNTs can vary between ~0.4-3.0 nm,[10] whereas the diameters of MWNTs range from ~10-30 nm.[11] SWNTs, the focus of this research, have potential applications in field-effect transistors,[12] sensors,[13] photodetectors,[14] organic photovoltaics,[15] flexible electronics,[16] touch screens,[17] and high-strength nanocomposites.[18]

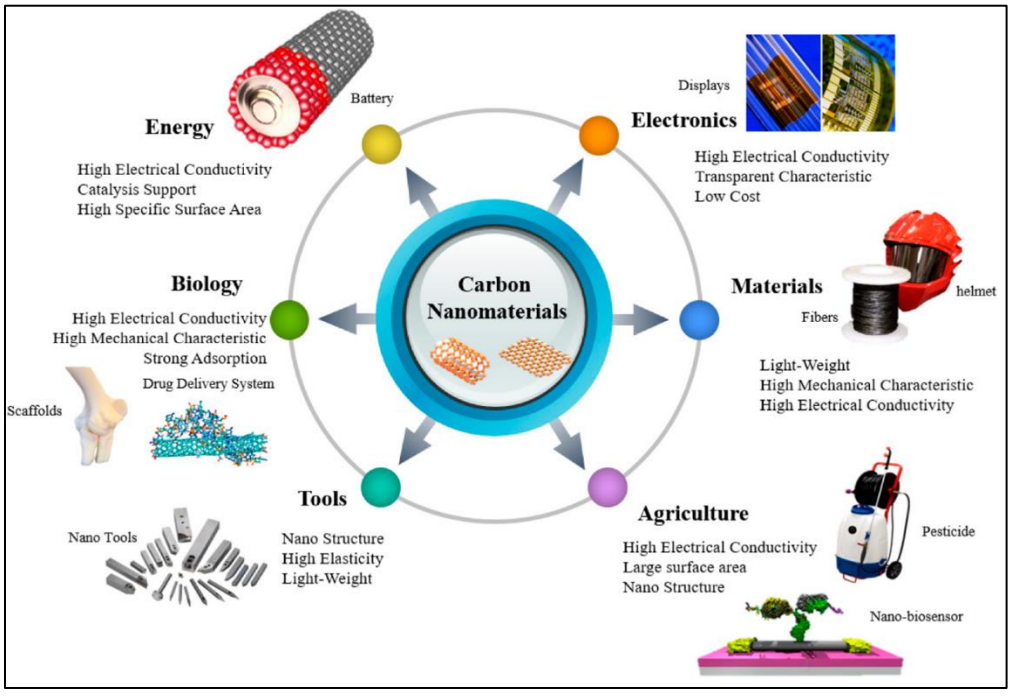

Figure 1: A summary of the unique properties of CNTs with examples of potential applications. Reproduced with permission.[19] Copyright 2020 Multidisciplinary Digital Publishing Institute.

Although not made this way, SWNTs can be idealized as a 2D graphene sheet rolled up into a cylinder. Depending on how the graphene sheet is rolled up, different SWNT species can be visualized (Figure 2). The chiral vector (C_h) represents the circumference of the SWNT species and is the addition of unit vectors a_1 and a_2. The chiral angle (θ) defines the angle between a_1 and C_h.[20] As shown in Equation 1, integer values (n,m) defines the SWNT species associated with C_h. There are three SWNT classes to consider: chiral, zigzag, and armchair. In the zigzag structure, two opposite C-C bonds of each hexagon are parallel to the tube axis (θ=0°), whereas in the armchair conformation the C-C bonds are perpendicular to the axis (θ=30°), in all other arrangements, the opposite C-C bonds lie at an angle to the tube axis, resulting in a nanotube that is chiral (0-30°).[20]

Equation 1: $C_h = na_1 + ma_2 = (n, m)$

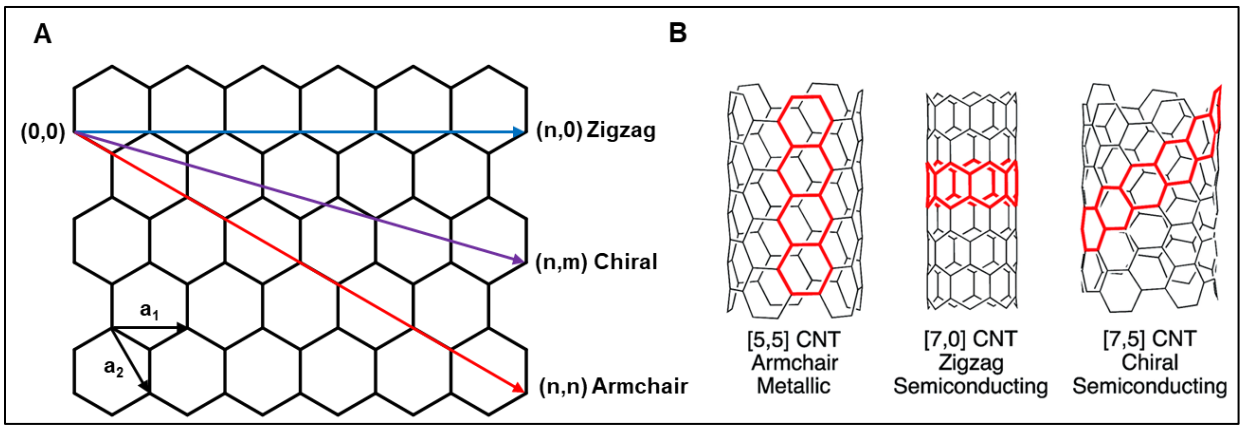

Figure 2: a) Carbon lattice with labeled unit vectors, a_1 and a_2, and zigzag (blue), chiral (purple), and armchair (red) vectors. b) Arm-chair, zigzag and chiral nanotube examples.

1.2 Synthesis Methods of Carbon Nanotubes

CNTs were first synthesized in 1991 using an arc-discharge method, and many techniques have since been developed.[21,22] These techniques include laser ablation,[23] chemical vapour deposition (CVD),[24] plasma-torch growth,[25] high-pressure carbon monoxide disproportionation

(HiPCO),[26] and catalysis using cobalt-molybdenum nanoparticles (CoMoCat).[27] These techniques all offer different advantages and produce various diameter ranges resulting in different internal properties of the nanotubes. Currently, all the mentioned synthesis methods produce a heterogenous mixture of SWNTs and residual impurities from the synthesis.

1.2.1 Arc-Discharge

Arc-discharge produces smaller diameter SWNTs (1.2-1.4 nm) compared to other synthesis methods.[10] A number of variables influence the size and structure of the SWNTs.[28] Arc-discharge occurs within a pressurized chamber filled with an inert gas (argon or helium). Inside the chamber, current is directed between a pair of graphite electrodes while a metal catalyst (iron, cobalt, or nickel) is introduced.[29] Carbon soot is produced between the electrodes and SWNTs begin to grow on the metal catalyst located on the cathode.[29] MWNTs are synthesized similarly but without the use of any metal catalyst.[30] CNTs prepared using arc-discharge result in nanotubes with minimal defects in the carbon lattice.[30]

1.2.2 Laser Ablation

Laser ablation is performed in a high-temperature reactor filled with an inert gas. A graphite target is vaporized using a pulsed laser forming plasma.[23] SWNTs form on cooled areas within the reactor as the vaporized carbon condenses.[23] This method allows for the diameter and length of the SWNTs to be controlled by altering the temperature and metal species used.[23] Laser ablation provides, high quality SWNTs, in higher yields with a narrower size distribution than arc-discharge.[20] One disadvantage of this technique is it is typically more expensive than other synthesis methods.[20]

1.2.3 Chemical Vapour Deposition (CVD)

CVD allows for large quantities of CNTs to be prepared at a high purity.[20] During CVD, a reactor oven containing a catalyst embedded substrate is heated to high temperatures, while a carbon-bearing gas, such as methane, ethylene, or acetylene, and a carrier gas, such as ammonia, nitrogen, or hydrogen, is introduced.[31] As carbon atoms are released from the gas, CNTs begin to grow at the catalyst site. CVD generally provides higher purity and yield of SWNTs than both arc-discharge and laser ablation.[20]

1.2.4 Plasma-Torch

Plasma-torch grown CNTs were first synthesized, in 2000, in Varennes, Canada.[32] Conditions use in arc-discharge and laser ablation are replicated, however, the graphite vapour previously used in these methods, is replaced with a carbon-containing gas. The decomposition of the gas requires 10 times less energy than graphite vaporization.[32] During the growth of plasma torch CNTs, the carbon containing gas (ethylene and ferrocene) is fed into a microwave plasma torch, where the gas is atomized.[32] The SWNTs can then be collected along with some impurities.

1.2.5 High-Pressure Carbon Monoxide Disproportionation (HiPCO)

HiPCO grown CNTs are produced in a high temperature reactor similar to that in CVD.[26] Unlike CVD, however, the catalyst used in HiPCO is in a gaseous state. Within the high-temperature reactor, carbon monoxide and iron pentacarbonyl are added to produce SWNTs continuously. In CoMoCat, a cobalt-molybdenum catalyst is used in place of iron pentacarbonyl.[33] The size distribution of SWNTs produced using CoMoCat is smaller than that of HiPCO SWNTs.[33]

1.3 Carbon Nanotube Electronics

The electronic properties of CNTs may offer the greatest potential of their unique properties for novel applications. Theoretical calculations first predicted that SWNTs could exhibit either metallic or semiconducting behavior depending only on diameter and helicity.[34] This capability to have altered electronic properties without modifying the bonding structure of the material makes SWNTs unique from all other material.[35] The 1D structure of SWNT causes the density of states (DOS) distribution to not be a continuous function of energy, but rather the energy decreases followed by a discontinuous gap. The electrons are confined to van Hove singularities, which are discrete energy levels in the density of states.[36] The energy level barrier, or band gap, between the valence π-band (HOMO) or the conduction π*-band (LUMO) is what makes a SWNT species either semiconducting or metallic.

Electronic band structure calculations predict that the (n,m) indices determine whether a SWNT will be a metal or a semiconductor.[34] In equation 2, if q is any positive whole integer then the SWNT is metallic. Based on this equation all armchair SWNTs where n=m, as well as some chiral SWNTs will exhibit metallic characteristics. For all non armchair (n≠m) there is a band gap between 1-100 meV making these semi-metallic.[37] Despite being semi-metallic these SWNTs exhibit similar electronic characteristics to metallic species and are typically included when referring to metallic SWNTs.[10]

Equation 2: $|n - m| = 3q$

The electronic characteristics of SWNTs allow for potential in a variety of applications. Semiconducting SWNTs (sc-SWNTs) have a useful bandgap and metallic SWNTs (m-SWNTs) have high conductivity.[10] The ability of sc-SWNTs to function as a semiconductor on the nanoscale

makes them advantageous over silicon which is currently used in the majority of semiconducting devices.[6] Also, the high conductivity of m-SWNTs could allow them to replace the use of traditional metals, such as copper, in certain applications.[38] Despite these attractive properties, wide use in commercial devices has yet to come to fruition in large part because CNTs are produced as a mixture of sc-, and m-SWNTs. To be incorporated into applications, the SWNT sample must be purified of all non-nanotube materials and be dispersed to allow for processability. Depending on the application, such as field-effect transistors, isolation of a specific species of SWNT may also be required.

1.4 Purification of Carbon Nanotubes

There are strong Van der Waals interactions present between SWNTs, resulting in self-aggregation and the formation of bundles. The bundling of SWNTs prevents them from being soluble in most solvents, limiting their potential uses. To improve the SWNTs solubility the aggregation must be reduced by individualizing them in dispersing solvents. SWNTs also require purification as the bundles contain both sc- and m-SWNTs. Dispersions that allow for the individualization of SWNTs can be achieved by covalent or non-covalent functionalization.

CNT sidewalls can be chemically functionalized to assist with dispersion of CNTs in organic solvents.[39] For example, SWNTs can be sonicated with a strong acid to allow functional groups such as carboxylic acids or esters to form at defect sites and tube ends of the SWNTs.[40] Solubilizing groups can be added to these functional groups, to allow for solubilization in a desired solvent. The disadvantage of chemically functionalizing the sidewalls of CNTs is that the conjugated network of the SWNTs is perturbed by the addition of these functional groups and can interfere with the properties of the SWNTs.[41] In some cases, the reactions can be thermally reversed, so that the properties of the pristine m- or sc-SWNTs can be recovered.[42] Exposing the

SWNTs to these extreme conditions can also prevent their use in mechanical applications as it has been shown that the lengths of SWNTs can be shortened.[43] Sc-SWNTs have shown more residence to oxidization than m-SWNTs and this discovery has allowed m-SWNTs to be selectively modified under covalent functionalization conditions. [44,45]

An alternative to covalent functionalization is non-covalent functionalization. Non-covalent functionalization allows for the unique electronic, optical, and physical properties of SWNTs to be maintained.[46] Through sonication the bundles are broken apart allowing for the dispersant to directly interact with the surface of the SWNTs through non-covalent mechanisms. Dispersant types that can non-covalently functionalize SWNTs include surfactants, small molecules, and conjugated polymers.

Nanotube purity is a challenge because all current commercial synthetic methods produce a mixture of both sc-SWNTs and m-SWNTs. The differences in the exploitable properties used to separate the electronic types are small, making the separation extremely difficult. Despite this, there have been many techniques developed that are capable of separating SWNTs including density gradient ultracentrifugation (DGU), agarose gel electrophoresis (AGE), two-phase extraction, size exclusion chromatography (SEC), and single strand DNA dispersions (ssDNA).

1.4.1 Density Gradient Ultracentrifugation

Applying density gradient ultracentrifugation (DGU) for the purification of SWNTs was first employed by Hersam and co-workers.[47]. Prior to this, DGU was used in biology for separating subcellular components with differing buoyant densities.[48] Generally, the technique involves adding samples to a centrifuge tube containing liquid mixtures and centrifuging at high speeds which separates the mixture based on density. Applying this technique to SWNTs, Hersam added surfactant-SWNT dispersions into a density gradient media.[47] They then centrifuged the samples

up to 250,000 *g* for 18 hours or more.[48] The technique allowed for the separation of different SWNT species based on their densities, producing distinct coloured bands enriched in different SWNT species (Figure 3).[48]

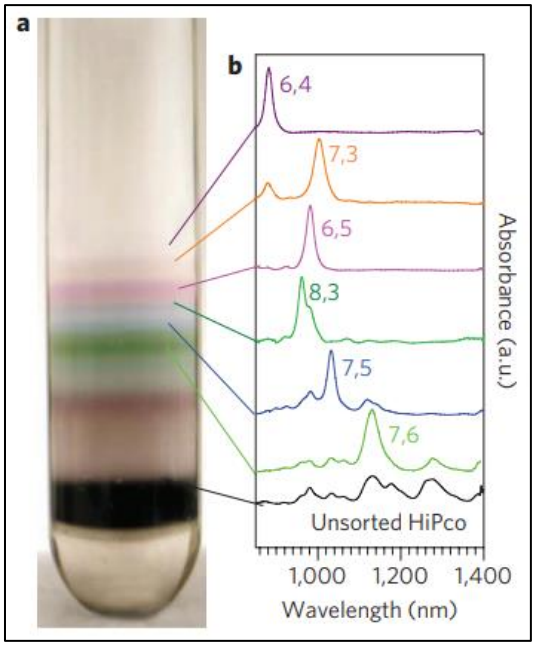

Figure 3: a) Image of a centrifuge tube containing HiPCO SWNTs sorted by DGU. The distinct coloured bands are layers enriched in different SWNT species. b) Near-infrared absorbance spectra of the marked coloured layer with (n,m) indices labeled. Reproduced with permission.[48] Copyright 2010 Nature Nanotechnology.

1.4.2 Agrose gel Electrophoresis

Tanaka *et. al*[49] discovered that the separation of m- and sc-SWNTs occurs during electrophoresis of SWNTs in an agarose gel. Agarose gel electrophoresis (AGE) is widely employed in biology for the separation of DNA. The SWNT-containing gel can be prepared by dispersing SWNTs in a sodium dodecyl sulphate (SDS) solution, and then gelling the mixture with liquid agarose.[49] In electrophoresis, the application of a constant direct current to the gel causes most of the metallic SWNTs to migrate in solution out of the starting gel, leaving the sc-SWNTs in the gel itself. This method has been improved to allow for samples containing up to 70%

metallic species by a modification of the technique that involved first adsorbing the SWNT-SDS mixture to the agarose and squeezing the gel to isolate the m-SWNTs.[50]

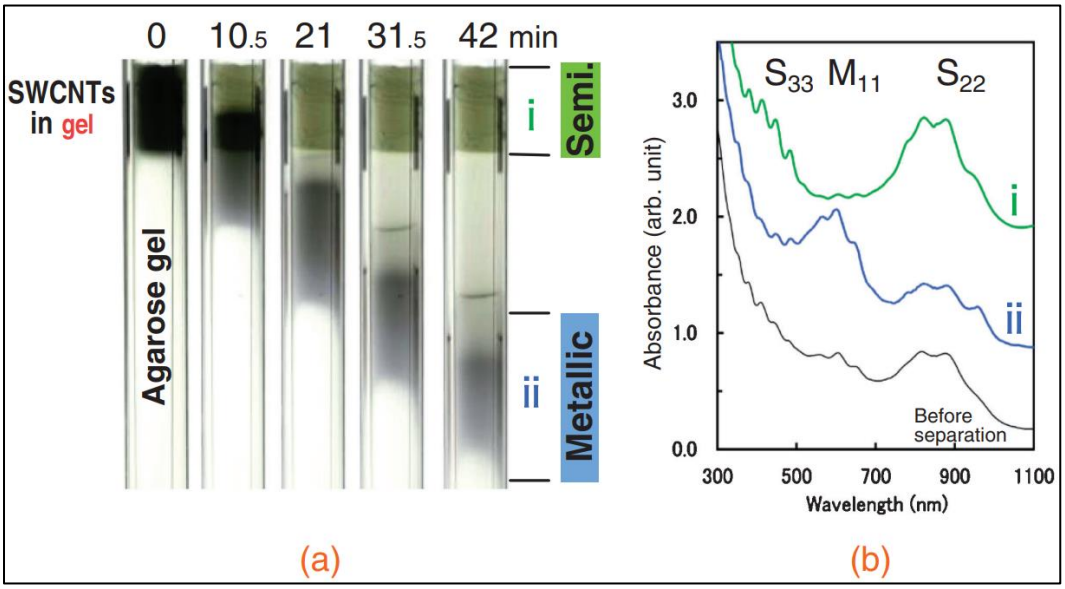

Figure 4: Separation of SWNTs dispersion in gel by AGE. (a) Sequential photographs showing the progress of separation. (b) Absorption spectra of fractions after AGE. Spectra i and ii correspond to the samples from fractions shown in (a). The bottom black spectrum is for the SWNT dispersion before separation. Reproduced with permission.[49] Copyright 2008 Applied Physics Express.

1.4.3 Two-Phase extraction

Two-phase extraction can also be used to purify SWNTs by separation into two phases. In this technique two aqueous phases contain different polymers, which are typically poly(ethylene glyol) (PEG) and Dextran. Adding certain surfactant-SWNT dispersions to this two-phase system causes certain SWNT types to partition between the phases. This partitioning is due to the differences in the diameters and the electronic nature of the SWNTs. This technique is not straight forward and is difficult to perform on large scale.

1.4.4 Size Exclusion Chromatography

Another separation technique developed by Moshammer *et al.*[51] uses Sephacryl (allyl dextran/*N,N'*-methylene bisacrylamine cross-linked polymer) media for size exclusion

chromatography (SEC) and is the most straightforward and highest throughput method of separation.[52] By choosing an appropriate column medium, particle size, gel porosity, and eluent composition, it is possible to run the SEC column as a filter, with the sc-SWNTs becoming trapped on the gel and the smaller m-SWNTs being eluted with a 1 wt.% SDS solution.[52] Trapped sc-SWNTs were then removed from the gel by eluent exchange to 1 wt.% SChol. [52]

Figure 5: Time lapse photograph of HiPCO SWNTs dispersed in 1 wt. % SDS in H_2O on a Sephacryl SEC gel. Reproduced with permission.[52] Copyright 2013 American Chemical Society.

1.4.5 DNA Dispersions

SWNTs have been dispersed and purified with DNA by using π-π stacking between the DNA and the SWNT surface.[53] Zheng *et. al*[54] reported that single-stranded DNA (ssDNA) wraps around CNTs to form a stable DNA-CNT complex that disperses CNTs. Zheng *et. al*[55] also discovered that anion exchange chromatography provides a separation method based on electronic type of DNA-SWNT complexes.[55] Also, a library of specific single-stranded DNA types was generated that when dispersed with SWNTs are selectivity isolated down the specific (n,m) species for sc-SWNTs.[53]

Although these purification methods have been shown to be successful on a small scale, scalability is limited, preventing use on an industrial stage. A more scalable purification approach is conjugated polymer sorting, which has shown selectivity for both m- and sc-SWNTs.

1.5 Conjugated Polymers

1.5.1 Introduction to Conjugated Polymers

Conjugated Polymers (CPs) are organic macromolecules characterized by a backbone of alternating single and double bonds. CPs have a delocalized π system throughout the polymer chain due to the overlapping p orbitals. The delocalization of the π-electrons in CPs allow them to behave both as electron transport materials and as chromophores.[56] The unique properties of CPs accommodate a variety of applications including light-emitting diodes (LEDs), energy-storage materials, and field-effect transistors (FETs).[56] CPs can be embedded into materials like packaging, coatings, and fabric.[56] CPs facilitate revolutionary improvements in these applications, allowing them to be more light-weight and stretchable.[56]

There is large variability in the structure of CPs, resulting in an intense research interest in modifying their properties. The most studied CPs include polythiophene, poly(p-phenylene), poly(p-phenylene vinylene), polyfluorene, and polycarbazole (Figure 3).[56] The structure of the CPs can be modified to include heteroatoms in the backbone structure and copolymers of different monomer structures can be combined creating a large library of possibilities.

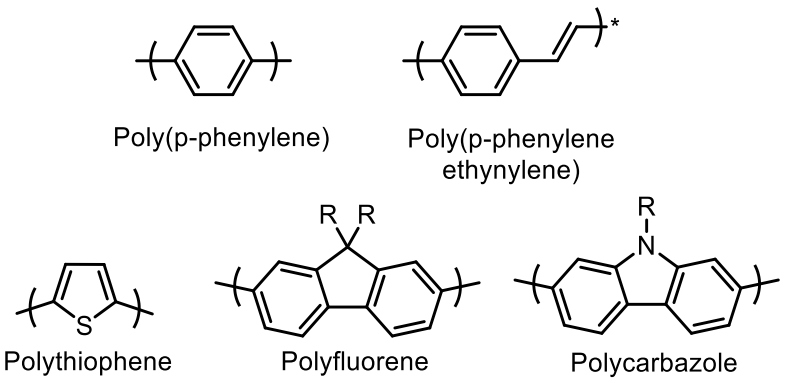

Figure 6: Structures of highly researched conjugated polymers.

1.5.2 Conjugated Polymers and Carbon Nanotubes

The use of conjugated polymers to selectively disperse specific SWNT species is the most promising method for nanotube purification, when addressing the issue of scalability. Initial studies showed that conjugated structures such as pyrene derivatives[57] can increase the dispersibility of SWNTs. Specific CPs, such as poly(phenylene vinylene), were also found to produce dispersions with SWNTs.[58–61] When dissolved in a solvent, CPs enhance the dispersibility of SWNTs in that solvent by wrapping around the SWNT using π-π stacking.[59] Wrapping the SWNT also avoids self-aggregation by preventing Van der Waals interactions.

In addition, CPs have been investigated to produce selective SWNT dispersions of specific electronic species. Nicholas *et. al.*[62] showed that selective dispersions of certain SWNT species were possible using CPs, such as poly(9,9-di-n-octylfluorene) (PFO). This report laid the groundwork for studies investigating CP-SWNT interactions and have progressed to the point where the selective dispersions of sc-SWNTs with purities up to 99.9% is possible.[63]

CPs are difficult to remove from the nanotube surface once wrapped. However, there have been reports that have removed the polymer from the SWNTs surface after purification. Typically, these techniques remove CPs through either conformational changes of the polymer[61] or backbone

depolymerization.[64–66] The high yields attainable on a large scale for CPs makes conjugated polymer sorting the most viable technique for the large scale purification of SWNTs.

Typically, preparing a polymer-SWNT dispersion involves sonication, centrifugation, and filtration. Every combination of polymer and SWNT requires tuning of specific parameters that can dramatically impact dispersions including sonication time and power,[67] temperature,[68,69] polymer:SWNT mass ratio,[70,71] solvent choice,[72–74] and centrifugation speed. Specifically, the polymer:SWNT ratio can have a significant impact on both selectivity and concentration of the dispersion. In most cases, increasing the relative amount of polymer will allow for increased concentrations of dispersions but can decrease the selectivity.

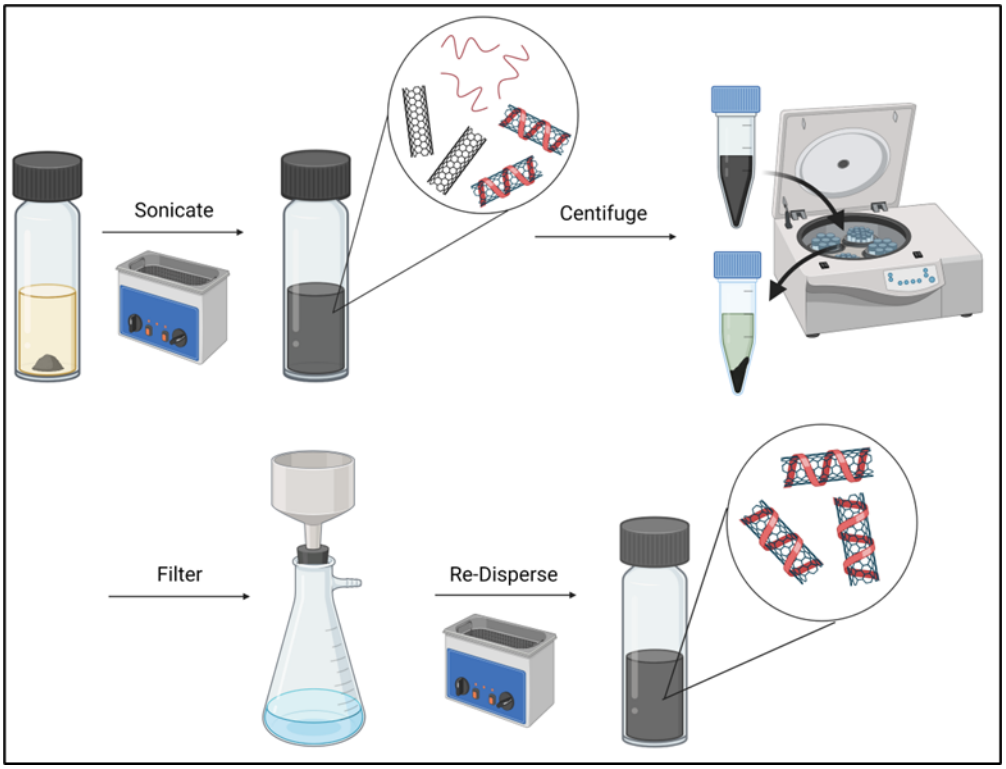

Figure 7: Outline of the preparation of polymer-SWNT dispersions including sonication, centrifugation, filtration, and redispersion. Prepared using BioRender.

Of the dispersion parameters, solvent choice is one of the most important considerations when preparing a SWNT-polymer dispersion. Dispersion solvents must have a density less than

1.3 g/mL, which is the buoyant density of a SWNT bundle.[75] Also, solvent parameters such as polarity,[72] viscosity,[73] and dielectric constant[74] can affect how SWNTs are dispersed. Common solvents for the selective dispersion of sc-SWNTs include toluene, THF, xylene, tetralin and decalin.

A benefit of CPs is the ability to tune the structure for the selectivity toward different SWNTs species. Altering the CPs architecture, like molecular weight, side-chain length, back-bone rotational flexibility, and electron-density, the selectivity can be tuned. Polyfluorenes,[71,62] polycarbazoles,[76–78] and polythiophenes[68,79] all show selectivity toward sc-SWNTs. Similarly, poly(phenylene vinylene)s[80] and poly(phenylene ethynylene)s[81,82] show selectively toward different SWNT diameters.[78]

1.6 Effect of Electron Density on Conjugated Polymer Selectivity

The CPs that have shown selectivity toward sc-SWNTs all possess electron-rich π-systems. There is a hypothesis that the interaction between the electron rich polymers and SWNTs is due to the electron-poor π-system of sc-SWNTs.[10] Conversely, m-SWNTs are relatively easy to oxidize[83,84] and are more polarizable[72] than sc-SWNTs indicating m-SWNTs have more electron-rich π-systems. This has sparked research investigating whether a CP with an electron-deficient π-system could be used for the selective dispersion of m-SWNTs. The foundation of this idea stems from studies involving electron-poor small molecules preferentially adsorbing to m-SWNT species.[85] These studies found that there were higher binding energies to m-SWNTs by electron-poor molecules than electron-rich molecules.[85]

Wanting to expand this idea to CPs, Rice et al.[86] synthesized two poly(fluorene-*co*-phenylene) derivatives, one with an electron-rich *p*-dimethoxyphenyl component, and one with an

electron-poor *p*-dinitrophenyl component.[86] It was found that the electron rich polymer produced significantly more concentrated metallic dispersions compared to the electron poor polymer. These findings further confirmed the hypothesis as the electron poor polymer was more selective toward m-SWNTs.[86] Building on this further, Fong *et al.*[87] synthesized an electron rich poly(fluorene-*co*-pyridine) (PF-Py) and then methylated the pyridines to produce an electron poor methylated-PF-Py. This allowed for direct comparison of an electron-poor and electron-rich polymer while maintaining the same degree of polymerization. As expected, the electron-poor polymer dispersed m-SWNTs more efficiently than the unmethylated electron-rich polymer. Despite the dispersion being enriched in m-SWNTs there remained a significant amount of sc-SWNTs. Thus, a system was necessary that would allow both the removal of the sc-SWNT and the dispersion of the m-SWNTs.

1.7 Two-Polymer Sorting

Building on the selectivity of electron-poor conjugated polymers compared to electron-rich, Bodnaryk *et Al.*[88] developed a new technique to enrich samples with metallic character. A two-polymer system was developed using an electron-rich conjugated polymer, poly(carbazole-*co*-fluorene) (PCPF) to first extract sc-SWNTs, and subsequently an electron-poor polymer, Me-PF-Py, to disperse the remaining m-SWNTs (Figure 8). Repeated extraction of the SWNT sample with the electron-rich polymer enabled removal of a substantial proportion of the sc-SWNTs. This residue could then be dispersed with an electron-poor polymer, producing a m-SWNT dispersion up to ~70% in metallic character as determined using UV-vis-NIR absorption spectroscopy (Figure 8).[88] To demonstrate the potential scalability of this technique, the scale was increase to 100 mg of SWNTs, a ~10^5 fold increase in scale relative to purification by DGU.[88]

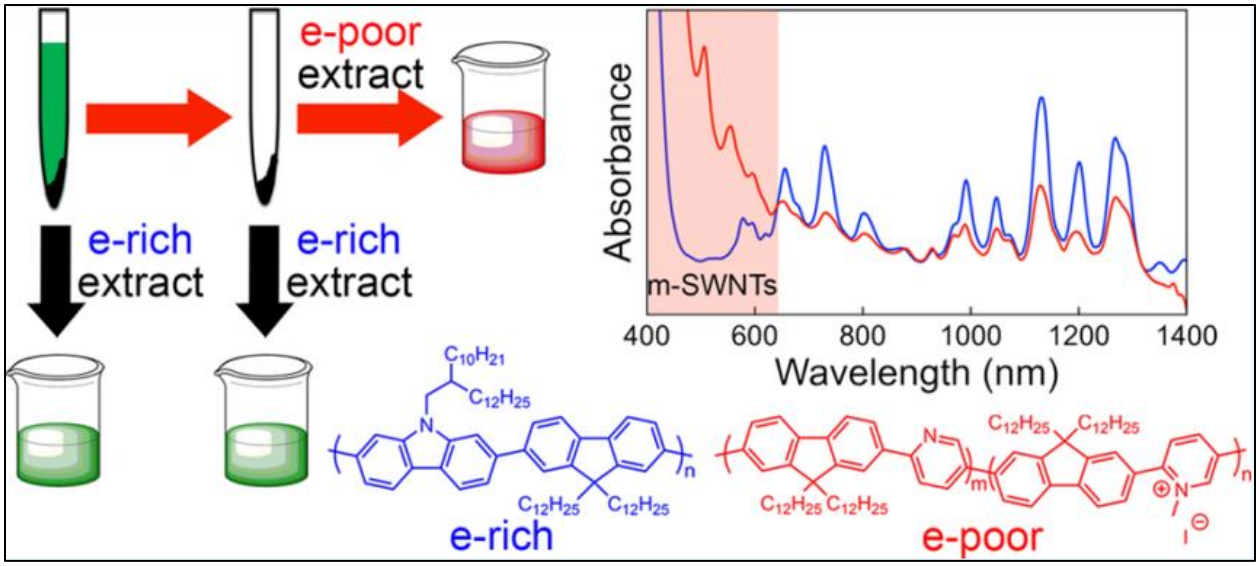

Figure 8: Conjugated polymer sorting extraction system. PCPF (e-rich) shown in blue. Me-PF-Py (e-poor) shown in red. Reproduced with permission. [88] Copyright 2018 American Chemical Society Omega.

This technique provided the most enriched m-SWNT dispersion that has ever been observed using conjugated polymer dispersion methods.[10] Despite this achievement this technique can be further optimized to generate closer to the desired 100% isolation of m-SWNTs. Specially improvement on the electron-poor polymer may be possible by the addition of a more electron withdrawing functional group. As previously mentioned, electron deficient polymers disperse m-SWNTs more efficiently so it is reasonable to hypothesize that a more electron withdrawing functional group will result in an increase in m-SWNT selectivity. Another limitation of the methylation is that it only had a ~50% conversion on the polymer backbone. Furthermore, the solubility of the methylated polymer is a concern as higher molecular weights greater than 13 kDa are insoluble in THF. With these limitations in mind, the addition of a more electron withdrawing functional group will be explored. Specifically, the addition of a dinitrobenzene and a trifluoroacetyl moiety onto the PF-Py polymer are investigated.

1.8 Characterization of Carbon Nanotube Dispersions

The characterization of the electronic nature of SWNTs can be accomplished using a combination of characterization methods. The main characterization methods typically used for qualitative and quantitative analysis of the electronic nature of SWNT dispersions are UV-vis-NIR spectroscopy, photoluminescence mapping, Raman spectroscopy, atomic force microscopy, transmission electron microscopy, scanning electron microscopy and conductivity techniques.

1.8.1 UV-vis-NIR Absorption Spectroscopy

The electronic transitions are unique for each SWNT subset which allows for characterization through techniques like UV-vis-NIR absorption spectroscopy (UV-vis).[89] UV-vis is a relatively simple technique to perform and allows for the determination of electronic purity of polymer-SWNT dispersions. The absorption spectrum of SWNTs exhibits many peaks as a result of the different SWNT types present and due to the differences in the density of states (DOS), sc- and m- species are able to be observed in different regions.[90] The diameter of the SWNT also has an impact on the appearance of the peaks in the absorption spectrum. HiPCO absorption spectra have four characteristic regions: one metallic (M_{11} at 440-645 nm), and three semiconducting regions (S_{11} at 830-1600 nm, S_{22} at 600-800 nm, and S_{33} 350-500 nm).[91] The slight overlap between the S_{22} and M_{11} regions prevents UV-vis of HiPCO SWNTs from providing an exact ratio of sc- to m-SWNTs. Also, since the CPs that are wrapping the SWNTs typically have an absorbance in a similar region to S_{33}, this region is not a good indicator of sc-SWNTs present in the dispersion. Plasma torch absorption spectra also have four characteristic regions: one metallic (M_{11} at 600-750 nm) and three semiconducting regions (S_{11} at 1400-1900 nm, S_{22} at 750-1150 nm, and S_{33} at 420-580 nm).[71] Plasma torch does allow for the exact ratio of the sc- to m-SWNT to be determined because there is no overlap between the their regions. However, this

ratio assumes that the molar extinction coefficient for all SWNT species wrapped in polymer are the same.[10]

A qualitative indication that a sample contains m-SWNTs or SWNT bundles, is a broad exponential background throughout the absorption spectrum. This phenomenon is a result of π and plasmon absorbance.[92]

1.8.2 Photoluminescence Mapping

Photoluminescence (PL) spectroscopy is specifically useful for the characterization of sc-SWNTs due to their unique fluorescence ability.[89] Sc-SWNTs have a band gap between their conduction and valance bands and electrons can be excited to a higher energy level. When this electron relaxes a photon of characteristic wavelength is emitted, producing fluorescence.[89] The same fluorescence is not observed in m-SWNTs as they do not possess a band gap. In addition, PL spectroscopy allows for the characterization of specific types of sc-SWNTs present in a dispersion. This is accomplished by using multiple excitation wavelengths to generate a PL map that indicates the maximum PL for all sc-SWNT species in the sample. This PL map can then be compared with a reference PL map outlining the PL maxima of all sc-SWNTs.[93]

The qualitative presence of m-SWNTs can also be characterized using PL mapping. In a sample containing both m- and sc-SWNTs, when an electron relaxes to a lower energy level in a sc-SWNTs a nearby m-SWNT can accept the electron which quenches the fluorescence.[94] SWNT aggregates also contain m-SWNTs and therefore their presence can cause quenching of fluorescence. Thus, qualitative comparison of the presence of m-SWNTs can only be performed for samples of completely individualized SWNTs. The lower the PL maxima, the more m-SWNTs

present in the sample. Comparison of PL mapping for evaluation of m-SWNT content has been performed by Rice *et al.*[86], Fong *et al.*[87], and Bodnaryk *et al.*[88] (Figure 9).

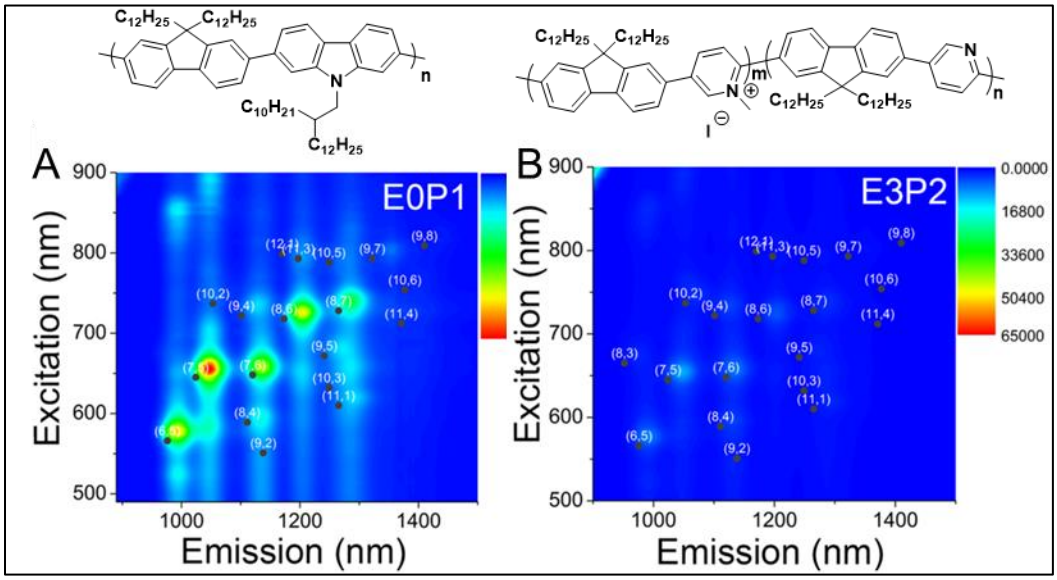

Figure 9: PL mapping of HiPCO polymer-SWNT dispersions using A) poly(fluorene-*co*-carbazole) B) poly(fluorene-*co*-pyridine). Reproduced with permissions.[88] Copyright 2018 American Chemical Society Omega.

1.8.3 Resonance Raman Spectroscopy

In resonance Raman spectroscopy (RRS), Raman scattering is measured. Generally, the enhancement of the Raman signal occurs when the incident wavelength is in resonance with the sample.[95–97] Applying RRS to SWNTs allows for signal enhancement by tuning the laser excitation wavelength to be in resonance with the electronic transitions of the desired SWNT species. Due to the large variations in the electronic nature of different types of SWNTs it is not possible to be in resonance with all SWNTs using one laser excitation wavelength. Since m- and sc-SWNTs are in resonance at different wavelengths RRS can probe either m- or sc-SWNT species by altering the laser excitation wavelength allowing for the degree of purification to be detmermined.[98–100]

When analyzing the Raman spectrum of a SWNT sample there are four main regions of interest. These regions include the radial breathing mode (RBM), the D-band, the G-band and the G'-band ranging from ~100-400 cm^{-1}, ~1250-1450 cm^{-1}, ~1550-1595 cm^{-1}, and ~2500-2900 cm^{-1}, respectively.[98]

The regions that provide the most information for SWNT samples include the RBM and G-bands. For HiPCO SWNTs using a 633 nm excitation wavelength both m- (175-230 cm^{-1}) and sc-SWNTs (240-300 cm^{-1}) are in resonance and can be compared using the RBM.[101] For SWNTs, the G-band has two different modes the G^- and G^+ bands at (1550-1585 cm^{-1}) and ~1590 cm^{-1}, respectively. A qualitative indication of the presence of m-SWNTs is the broad asymmetric feature of the G^- band. [102]

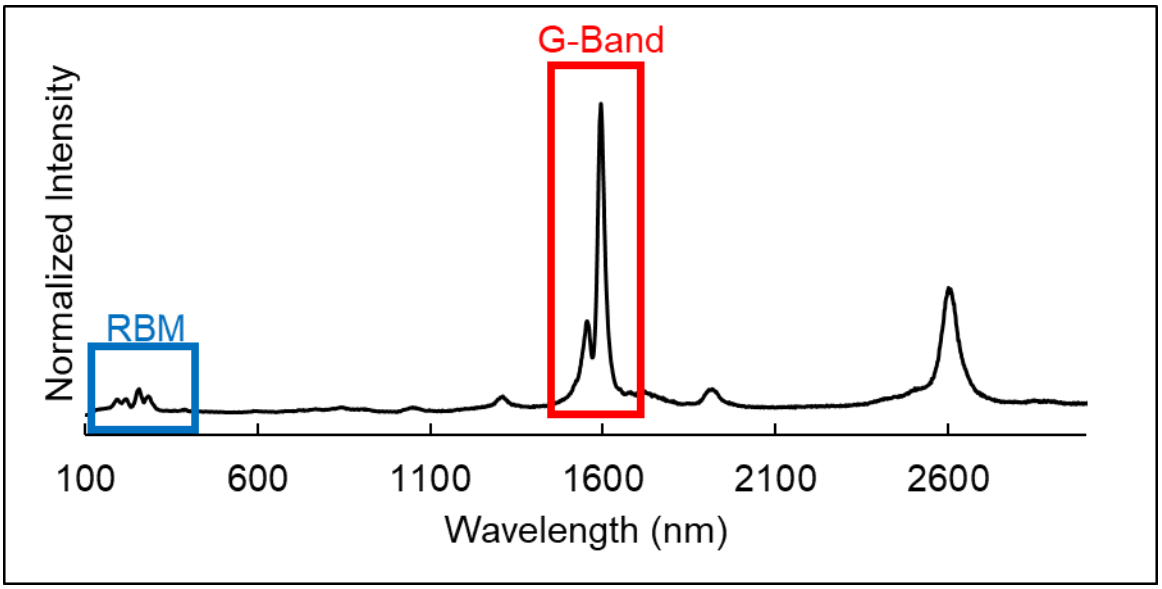

Figure 10: Raman Spectrum for HiPCO SWNTs at 633 nm laser power. G-Band labeled in red, RBM labeled in blue.

For complete characterization of the purity of sc- and m- SWNTs in a sample, a combination of RRS, UV-vis, and PL mapping, must be implemented. Both the G-band and RBM region can be analysed using multiple laser excitations wavelengths in RRS. All regions can be

analysed in UV-vis-NIR spectroscopy, and the fluorescence maxima can be compared using PL mapping.

1.9 Summary and Objectives

SWNTs possess exceptional properties and incorporation into various applications has the potential to provide revolutionary improvements. Unfortunately, when initially produced SWNTs are insoluble, and comprise a heterogenous mixture of sc- and m-SWNTs. All current methods previously outlined lack scalability resulting in prohibitively high costs for high purity SWNTs in many applications. One scalable alternative for the purification of SWNTs exists in the form of conjugated polymer sorting. The use of conjugated polymers has allowed for the isolation of sc-SWNTs with purities up to 99.9% but has been less successful in the enrichment of m-SWNTs.[63] The CPs that show selectivity toward sc-SWNTs, like polythiophenes, polyfluorenes, and polycarbazoles are all electron-rich. Conversely, electron poor conjugated polymers have shown selectivity toward m-SWNTs, but initial dispersions have a significant quantity of sc-SWNTs remaining. To further enrich samples in m-SWNTs, a two-conjugated-polymer system was developed using an electron-rich conjugated polymer to remove sc-SWNTs, and an electron-poor polymer to disperse the remaining m-SWNTs.[88] However, m-SWNTs were not completely isolated, and the electron-poor polymer used required improvement.

In this Thesis, I examine how the structure of the electron-poor conjugated polymer can be modified to better disperse m-SWNTs. The objective is to add a more electron withdrawing functional group than the previously investigated methyl group. The first reaction investigated was the addition of a dinitrobenzene moiety using the Zincke reaction. The Zincke reaction was chosen since the addition of the dinitrobenzene moiety is highly electron withdrawing and may also allow for further reaction with a primary amine to generate a library of different functional groups.

Although this reaction was successful on pyridine, the reaction post polymerization was unsuccessful under the reaction conditions attempted. A variety of different reaction conditions were explored including, temperature, solvent, molecular weight, reaction concentration, and reaction time. The reaction was also attempted on a series of brominated pyridines to determine if functionalization prior to polymerization was possible and to investigate the effects of sterics on the Zincke reaction. None of these reactions were successful and an alternative reaction to functionalize the pyridine required exploration.

In Chapter 3, I explore the possibility of the addition of a trifluoroacetyl group. The synthesis allows for a more straightforward functionalization of the pyridine in the conjugated polymer and had a 100% conversion compared to only 50% for the methylated polymer. I also investigate how the newly discovered acetylated PF-Py (A-PF-Py) disperses SWNTs. Finally, I incorporate the A-PF-Py into the two-polymer extraction system and successfully show that it is possible to produce highly concentrated enriched m-SWNTs dispersions. Characterization was performed using UV-vis-NIR spectroscopy, and conductivity measurements.

Chapter 2: Investigation of the Zincke Reaction on Polyfluorene-co-Pyridine

2.1 Introduction

The Zincke reaction was named after Theodor Zincke who first discovered the reaction in 1904.[103] The first step involves the conversion of a pyridine into a pyridinium salt by reaction with 2,4-dintiro-chlorobenzene (DNCB) (Scheme 1). This reaction is an S_N2 reaction as there is a nucleophilic substitution where a bond is broken, and another is formed synchronously. The pyridine acts as the nucleophile with the lone pair attacking the partial positive charge that is generated on the carbon attached to the chlorine molecule. The chlorine anion acts as the leaving group in this reaction generating a pyridinium salt (Scheme 1).

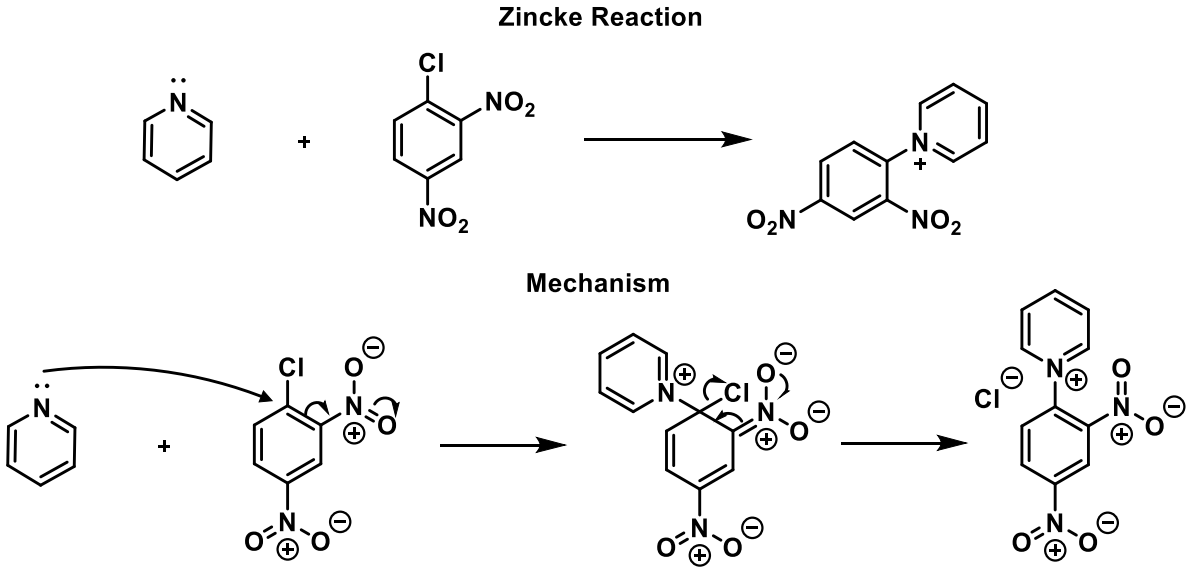

Scheme 1: Overall reaction of the first step of the Zincke reaction between pyridine and DNCB to form the pyridinium salt (top) and the mechanism (bottom).

Once the pyridinium salt is purified it can also be further reacted upon by heating with a primary amine. The overall mechanism is an example of an ANRORC mechanism, a nucleophilic addition, ring opening, and ring closing (Scheme 2). The addition of the amine leads to the opening

of the pyridinium ring (3), and a second addition of an amine leads to the displacement of 2,4-dinitroaniline (4). It is thought that the König salt (5a&5b) transforms by either sigmatropic rearrangement or nucleophilic addition of a zwitterionic intermediate to reform the cyclic ring (6).[104] This has been suggested to be the rate-determining step.[105] After the addition of a proton to the amine (7) followed by the amines elimination, the pyridinium ion is generated (8).

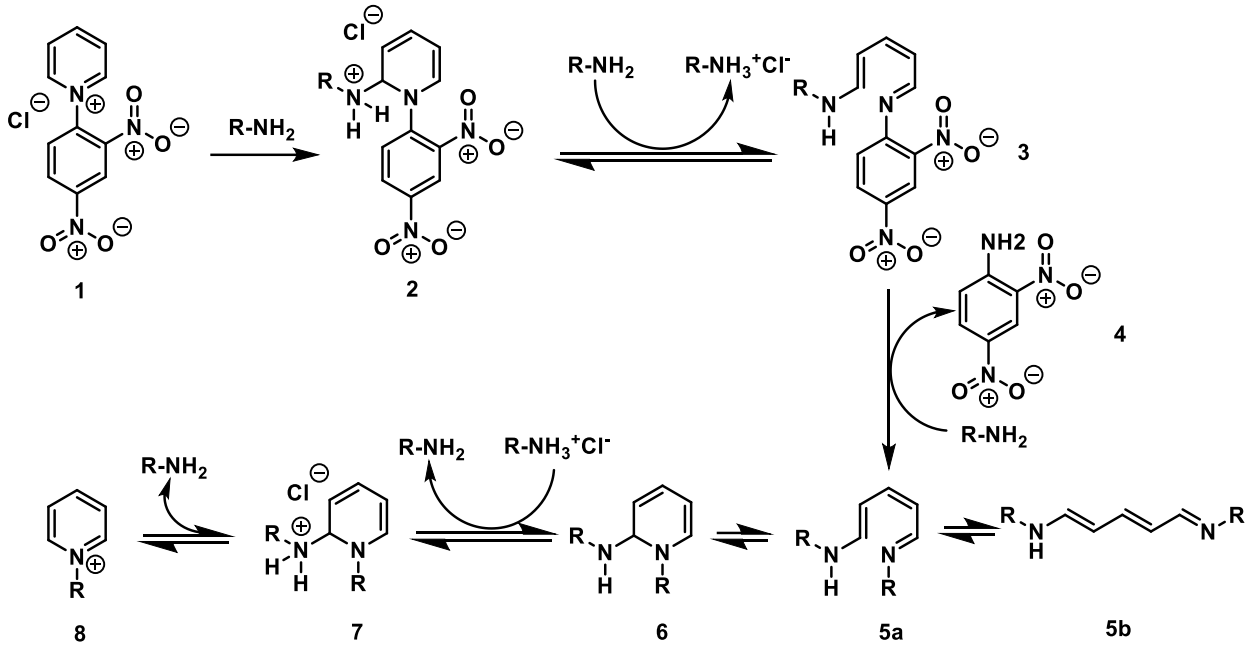

Scheme 2: Mechanism of the second stage of the Zincke Reaction. The pyridinium salt is reacted with a primary amine to produce the pyridinium ion with an R group attached.

The Zincke reaction is an attractive reaction as it can generate an aromatic, quaternary ammonium salt.[106] Recent interest in this old reaction mainly focused on mechanistic determination. Less research has been performed on the synthetic potential of the Zincke reaction largely due to the difficulty with purification of the pyridinium ion from dinitroaniline and other intermediates in the reaction since they are highly polar.[107] Another challenge with the Zincke reaction is that the pyridinium salt is difficult to solubilize in many organic solvents and the chloride counter anion can cause decomposition of the salt due to its nucleophilicity in the second stage of the Zincke reaction.[108] An approach to solve these issues was reported by Marazano *et.*

al.[108,109] Specifically, it was reported that the use of a lipophilic dodecyl sulfate counteranion, instead of chloride, minimizes nucleophilic attack on the pyridinium salt and has improved solubility in organic solvents.

One synthetic application of the Zincke reaction involves the addition of an amine to a wang resin (Scheme 3).[106] This addition was aimed at the discovery of a new small molecule to act as a cystic fibrosis transmembrane conductance regulator that contains a quaternary nitrogen, a lipophilic component, and a hydroxyl moiety (Scheme 3).[106] Another example is the synthesis of a chiral isoquinolinium salt (Scheme 4).[108]

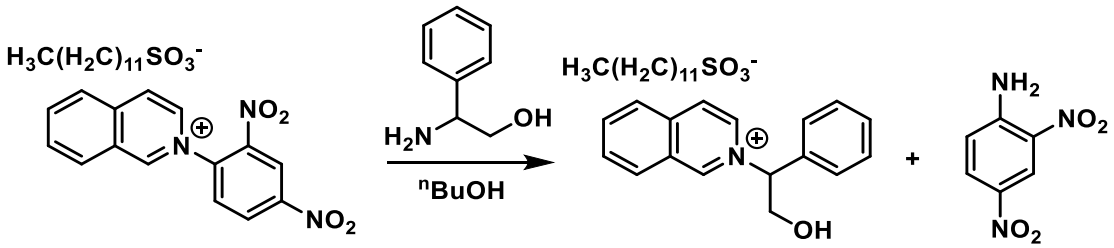

Scheme 3: Zincke reaction for addition of amine to wang resin.[106]

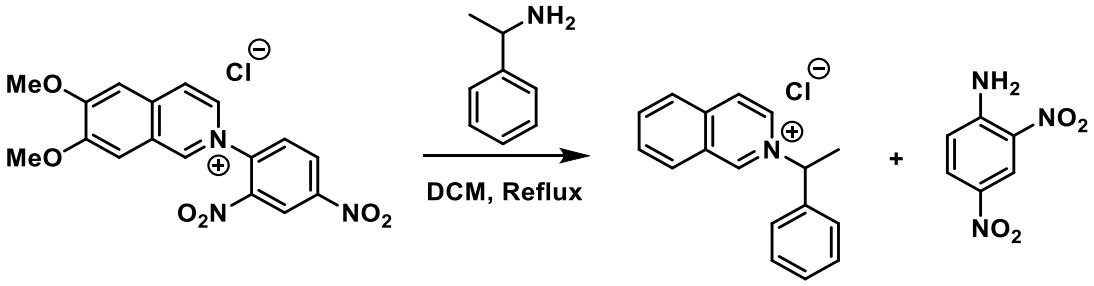

Scheme 4: Zincke reaction for synthesis of a chiral isoquinolinium salt.[108]

The Zincke reaction has proven to be an effective way of producing a quaternary nitrogen with a very electron withdrawing functional group, dinitrobenzene, attached. Applying the Zincke reaction to poly(fluorene-*co*-pyridine) (PF-Py) (Scheme 5) would add an electron withdrawing moiety that could pull electron density from the polymer backbone. This would produce an overall polymer that is relatively electron poor when compared to the unfunctionalized polymer. This

reaction is especially interesting to explore as further reactions with primary amines may be possible and a library of potential functional groups could be investigated. If necessary, this reaction would also allow for further modification of the counteranion to increase solubility in desired organic solvents, such as toluene or THF. For these reasons, the Zincke reaction is an interesting candidate to produce an electron poor conjugated polymer for incorporation into the two-polymer conjugated polymer sorting system.

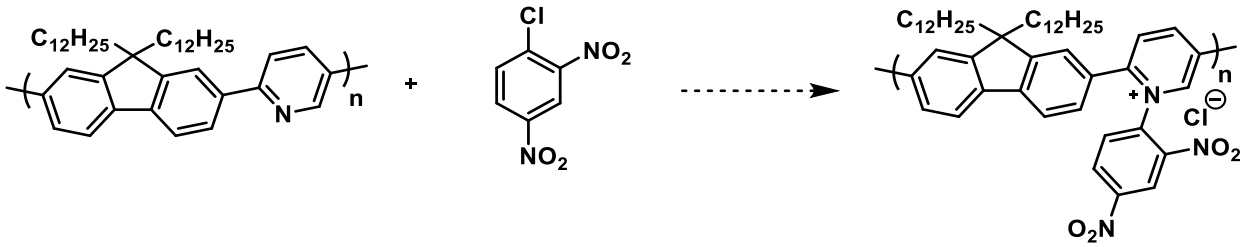

Scheme 5: Zincke reaction between PF-Py and 1-chloro-2,5-dinitrobenzene.

2.2 Results and Discussion

The fluorene monomer was synthesized by first brominating commercially available fluorene with N-bromosuccinimide (NBS), followed by alkylation with 1-bromododecane, and the addition of boronate groups with bis(pinacolato)diboron by Miyaura Borylation (Scheme 7). Next, the fluorene monomer and commercially available 2,5-dibromopyridine underwent Suzuki polycondensation polymerization, to produce poly(fluorene-*co*-pyridine) PF-Py (Scheme 11). This polymerization was repeated to produce a variety of different molecular weights. Using GPC analysis, the PF-Py synthesized had a number-average molecular weight (M_n) of 8 kDa, 13 kDa, 25 kDa, 47 kDa, and 73 kDa, and a dispersity (Đ) of 1.8, 2.2, 2.6, 3.4, and 2.4, respectively.

When designing the ideal conditions for the Zincke reaction to be applied to PF-Py it is useful to first investigate the Zincke reaction on the model system with pyridine (Scheme 12). The reaction was first attempted in a 1 to 1 molar ratio between pyridine and 1-chloro-2,4-

dinitrobenzene (CDNB) in acetone and the reaction mixture was refluxed for 21 hours. Due to the increased polarity of the pyridinium salt, the product precipitated out of solution. The synthesis of the pyridinium salt was also repeated in tetrahydrofuran (THF) and toluene at reflux to demonstrate that the reaction was successful in these solvents and reaction temperatures.

The Zincke reaction was first attempted under the same reaction conditions that the model reaction was successful under. The reaction was attempted in a minimum of THF and heated to reflux with a condenser attached, while stirring. The reaction was not possible to monitor by thin layer chromatography (TLC) because the polymer streaked and the CDNB was added in excess. After 22 hours nothing had precipitated out of solution. Visual indications that the reaction was proceeding would have included formation of precipitate and a colour change (likely to a dark red/black). The reaction was monitored using infrared (IR) spectroscopy, in an attempt to see a shift in the nitro group peaks. An IR was taken prior to the reaction and after 22 hours, with no observable differences in the IR spectra. The primary approach to monitoring the progression of the reaction was done using ^{1}H nuclear magnetic resonance (NMR) spectroscopy. After functionalization, an increase in chemical shift of the existing aromatic peaks and the addition of three hydrogens would be expected in the ^{1}H NMR spectrum. To isolate the polymer a drop of the reaction mixture was precipitated into chilled methanol. Yellow product was collected after precipitation and a ^{1}H NMR was taken of the sample. There was no visible difference in the ^{1}H NMR of the PF-Py starting polymer and the polymer after reaction indicating that the reaction had failed to successfully functionalize the polymer to any extent.

While the initial attempt at the Zincke reaction did not proceed there were still many reaction variables that could be modified to push the reaction forward. The variables that were

investigated include, temperature, solvent, molecular weight, reaction concentration, and reaction time. Table 2 summarizes the reaction conditions for the nine sets of reaction conditions attempted.

The solvents that were possible were limited by the solubility of PF-Py, as the polymer was only soluble in a limited number of solvents. The solvents attempted were chloroform, THF, toluene, 1,2-Dichlorobenzene, and dimethylsulfoxide at temperatures of 60°C, 66°C, 85°C, 180°C, and 189°C, respectively. The reaction is an S_N2 reaction and therefore a polar aprotic solvent will enhance the rate of the S_N2 process by raising the energy of the nucleophile thereby giving a smaller activation energy. Therefore, all solvents chosen were aprotic solvents and as polar as possible while maintaining good solubility of both reagents. Also, the chosen solvents were aimed at reaching high reaction temperatures to provide the energy required to overcome the activation barrier of the reaction. All solvent and temperature adjustments were unsuccessful at driving the reaction forward.

Altering the molecular weight of the PF-Py polymer was also investigated. The reaction was attempted on PF-Py with low Mn (8 kDa, 13 kDa) and a high Mn (73 kDa). The reactions were attempted both in THF and 1-2dichlorobenzene. All attempts resulted in no reaction as confirmed by ^{1}H NMR. This study indicated that the alteration of the Mn of the polymer alone was insufficient to allow the reaction to proceed.

The next reaction variable that was investigated was the molar ratio and concentration of the reaction mixture. Le Chatelier's principle states that if a dynamic equilibrium is disturbed by changing the conditions, the position of equilibrium shifts to counteract the change to re-establish an equilibrium. Therefore, increasing the amount of either starting material may increase the rate of functionalization of the polymer. With the PF-Py being in much more limited supply the amount

of CDNB was increased. The molar ratio between PF-Py:CDNB was altered between 1:4, 1:10, and 1:87. Despite increasing the amount of CDNB the reaction still did not proceed.

The next reaction condition that was altered was reaction time. In most attempts, the reaction was left for 16-22 hours before monitoring by ^{1}H NMR. It was hypothesised that with the increase in steric hinderance of PF-Py compared to the pyridine, there may be fewer collisions with the correct orientation for reaction, thus requiring a longer reaction time. An experiment was set up and monitored every 22 hours in 1,2-dichlorobenzene, for a total of 80 hours. After the entirety of the reaction attempt there was no change in the ^{1}H NMR.

In every reaction attempt there was a colour change of the solution to dark red. To determine the cause of this colour change, a control with only CDNB dissolved in dichlorobenzene was run alongside a regular reaction containing all reactants, both heating to 180°C. Both reactions changed colour to the dark red solution indicating the colour change was a result of heating CDNB and not an indication of functionalization of PF-Py.

Another hypothesis was that the pyridinium polymer product was soluble in the methanol when precipitating and only unfunctionalized PF-Py was precipitating out. This was investigated by evaporating off all solvent instead of precipitating and taking a ^{1}H NMR of the crude mixture. We also attempted to precipitate in a non-polar solvent, hexane, which would allow for all products including the expectedly polar pyridinium polymer product, to precipitate. Only starting material was observed in the ^{1}H NMR, for both attempts.

The rate of an S_N2 reaction is greatly impacted by steric hindrance. For example, a tertiary alkyl halide undergoing an S_N2 process is typically so slow that it is assumed to be inert. In the polymer structure the nitrogen is sterically hindered by the neighbouring fluorene molecule.

Although it is possible that the reaction may proceed in small undetectable quantities the polymer is required to be highly functionalized to be useful as an electron poor polymer.

The Zincke reaction directly on the polymer was not successful even after altering the reaction conditions previously discussed. An alternative way to achieve the same polymer structure would be to perform the Zincke reaction on the 2,5-dibromopyridine (DBP) monomer prior to polymerization (Scheme 6). The reaction between CDNB and DBP was attempted in both THF and acetone but neither reaction indicated that a new pyridinium salt was formed by either the formation of precipitate or by monitoring with TLC. The failure of this reaction is another indication that the Zincke reaction does not proceed with substituents in the ortho or meta positions to the nitrogen.

To further investigate the effects steric hinderance has on the Zincke reaction, reaction with monobrominated pyridines was investigated in the ortho and meta positions (Scheme 6). It was hypothesised that the ortho position would be unable to react despite the bromine being an ortho director as there is too much steric bulk for the nucleophile to attack. The reaction on 2-bromopyridine was unsuccessful, with no reaction observed after 24 hours. This indicates that steric hinderance can have an influence on the Zincke reaction.

The Zincke reaction was also attempted on meta substituted 3-bromo-pyridine (Scheme 6). Although this position is less sterically hindered the bromine is deactivating in the meta position resulting in this reaction being unsuccessful. This indicates that if there is a deactivating group the nitrogen will not be nucleophilic enough to allow for the reaction to proceed. Overall, the Zincke reaction was deemed an unsuitable method for the functionalization of the polymer backbone.

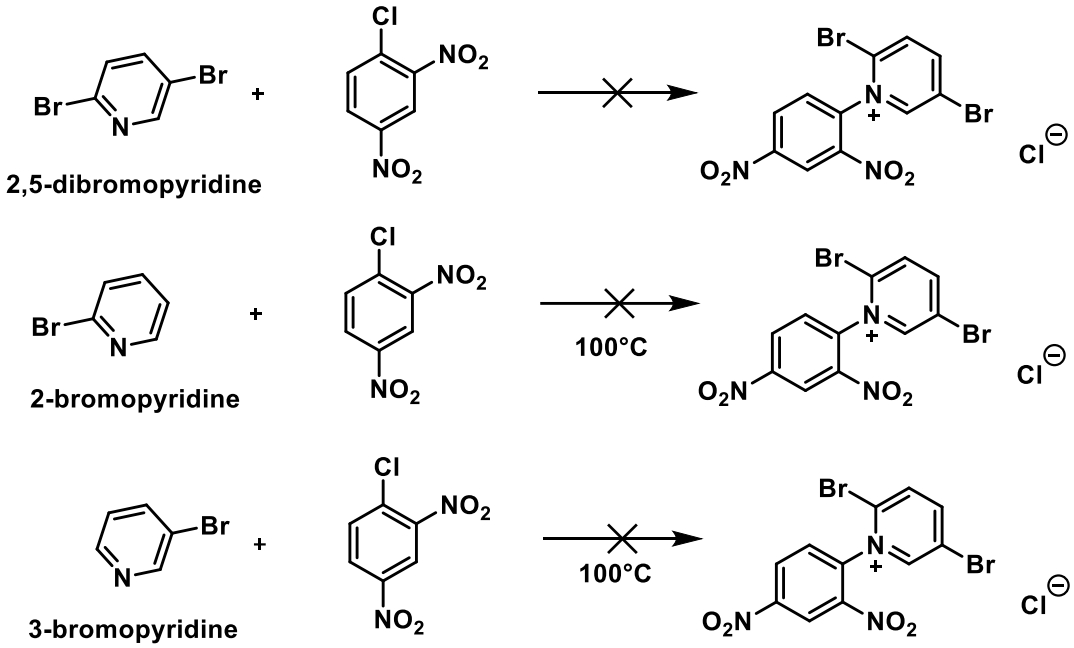

Scheme 6: Zincke reactions on the 2,5-dibromopyridine monomer, 2-bromopyrdine, and 3-bromopyridine.

2.3 Conclusion

The application of the Zincke reaction on the PF-Py to generate a more electron-poor polymer has been explored. The reaction variables that were investigated include, temperature, solvent, molecular weight, concentration, and reaction time. The reaction was monitored using ^{1}H NMR and there were no detectable changes in the aromatic regions for any of the reaction attempts. The Zincke reaction was also attempted on the monomer, DBP, to investigate the possibility of functionalization prior to polymerization. This reaction did not proceed for all reaction attempts. To further investigate the effects of that steric hinderance had on this reaction monobromated pyridine in the ortho and meta positions were investigated. The ortho position was unsuccessful suggesting that steric hinderance can impact the Zincke reaction; the meta position was unsuccessful despite being less sterically hindered indicating the bromine resulted in a decrease in nucleophilicity of the nitrogen. These results demonstrate that the Zincke reaction is not a

possibility for generating a more electron poor polymer when applied to PF-Py under the attempted reaction conditions.

2.4 Experimental

2.4.1 General

All reagents were purchased from commercial chemical suppliers and used as received. Flash chromatography was performed using an Intelliflash 280 by AnaLogix. All compounds were monitored using a variable wavelength detector at 254 nm. Columns were prepared in Biotage® SNAP KP-Sil cartridges using 40-63 µm silica or 25-40 µm silica purchased from Silicycle. ^{1}H NMR spectra were recorded on Bruker Avance 600 MHz spectrometers and shift-referenced to the residual solvent resonance. Polymer molecular weights and dispersities were analyzed, relative to polystyrene standards, by gel permeation chromatography (GPC) using a Waters 2695 Separations Module equipped with a Waters 2412 refractive index detector and a Tosoh TSKgel SuperHZM-N multi-pore GPC column with dimensions of 4.6 mm internal diameter, length of 15 cm, and 3µm particle size. THF with 2% acetonitrile was used as the eluent at a flow rate of 0.3 mL/min.

2.4.2 Synthesis of Poly(9,9'-didodecylfluorene-co-pyridine)

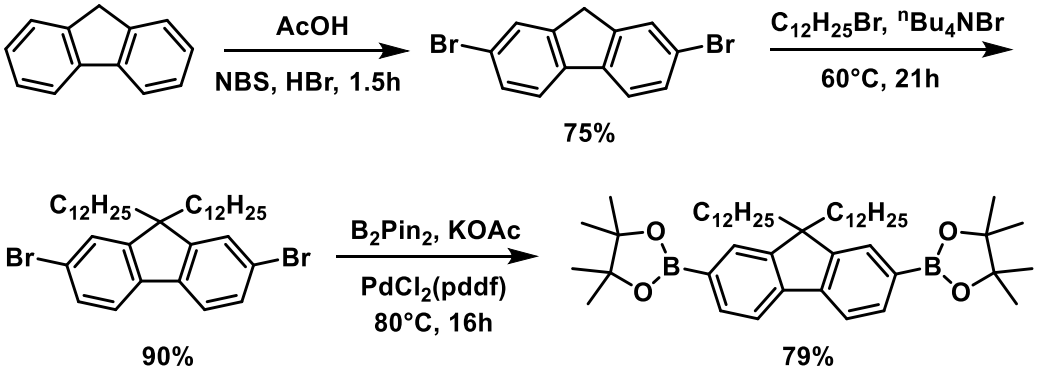

Scheme 7: Synthesis to form 2,2'-(9,9-didodecylfluorene-2,7-diyl)bis(4,4,5,5-tetramethyl-1,3,2-dioxaborolane).

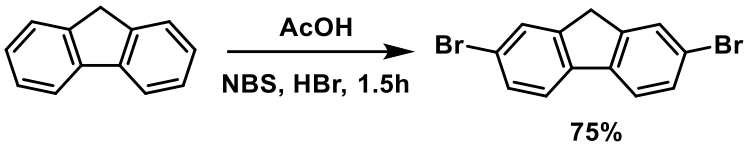

Scheme 8: Reaction to form 2,7-dibromofluorene.

2,7-dibromofluorene (Adapted from reference 110)

A 250 mL round bottom flask equipped with a magnetic stir bar was charged with fluorene (5.096 g, 30 mmol), N-bromosuccinimide (10.084 g, 57 mmol), and acetic acid (60 mL). To the reaction mixture, concentrated hydrogen bromide (1.5 mL) was added dropwise. The reaction mixture was stirred at room temperature for 1.5 hours, and then distilled water (30 mL) was added and the resulting suspension was filtered to obtain an orange solid. The crude product was recrystallized from a 2.5:1 mixture of ethanol:acetone (~250 mL total volume), then the mother liquor was concentrated *in vacuo* and recrystallized using the same solvent mixture (~25 mL total volume). The fractions were combined to afford 2,7-dibromofluorene as a white solid (7.47 g, 75%). ^{1}H NMR (600 MHz; $CDCl_3$): δ = 7.67 (d, 2H), 7.61 (d, 2H), 7.52-7.50 (m, 2H), 3.88 (s, 2H).

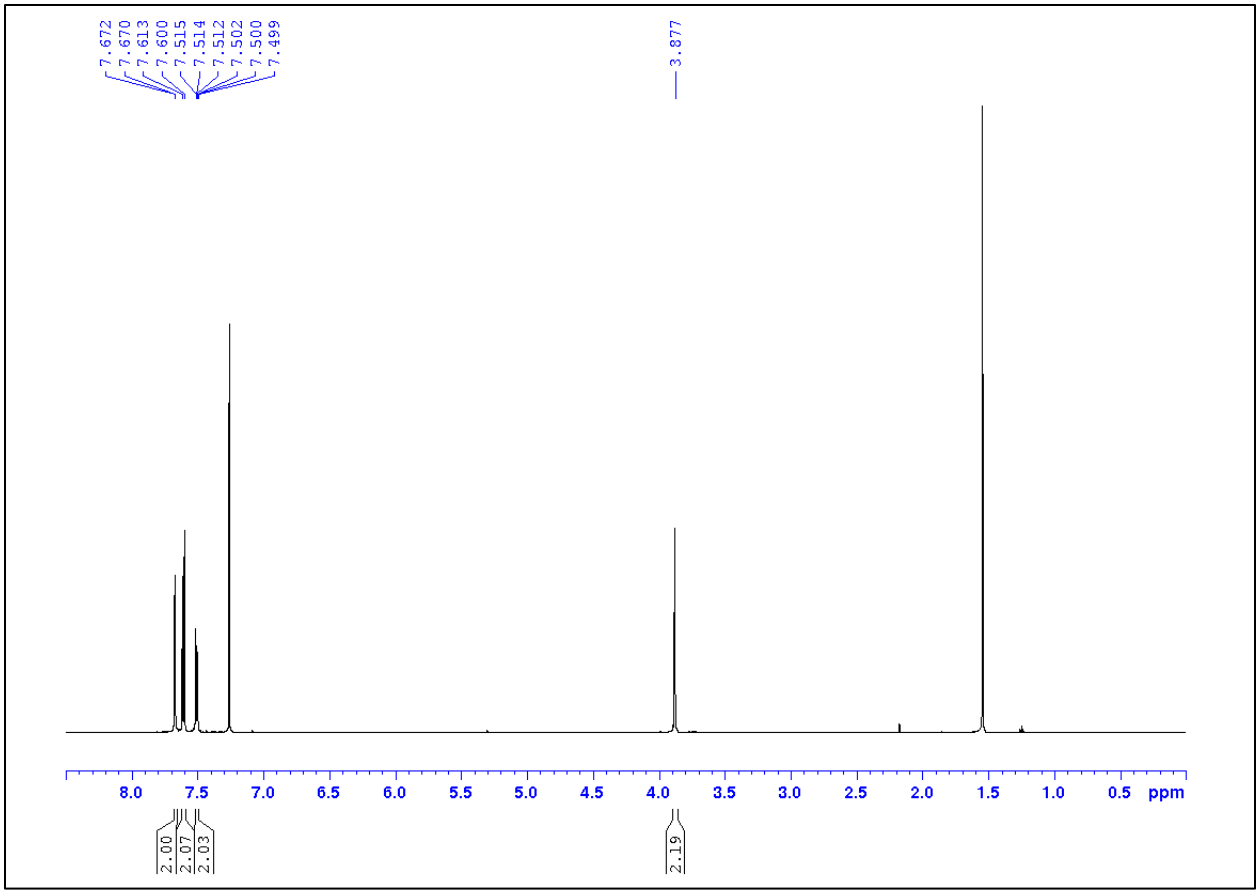

Figure 11: ^{1}H NMR spectrum of 2,7-dibromofluorene in $CDCl_3$.

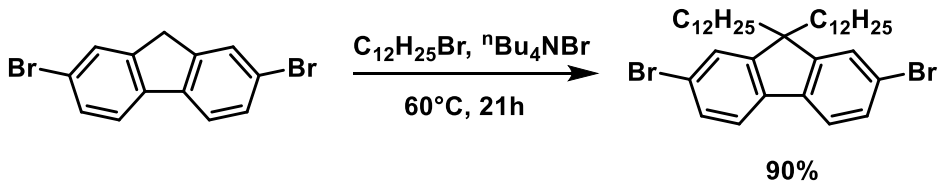

Scheme 9: Reaction to form 2,7-dibromo-9,9-didodecylfluorene.

2,7-dibromo-9,9-didodecylfluorene (Adapted from reference 87 and 88)

A 250 mL round bottom flask equipped with a magnetic stir bar was charged with 1-bromododecane (14 mL, 58 mmol), toluene (45 mL), and saturated potassium hydroxide (90 mL). The biphasic mixture was sparged with nitrogen for 1 hour, and then 2,7-dibromofluorene (7.55 g, 23 mmol) and tetrabutylammonium bromide (1.5 g, 5 mmol) were added. The mixture was stirred at 60°C under an inert atmosphere for 21 hours. The organic phase was separated using liquid-

liquid extraction 2x with 110 mL diethyl ether. The crude product was then filtered through a silica plug, eluting the product using hexanes. The product was concentrated in vacuo and 100 mL of 3:1 methanol:acetone was added and stirred at high speeds to precipitate the product. The product was then filtered and washed with 2x portions of 100 mL 3:1 methanol:acetone solution to afford 2,7-dibromo-9,9-didodecylfluorene as a colourless crystalline solid (13.80 g, 90%). ^{1}H NMR (600 MHz; $CDCl_3$): δ 7.51 (s, 2H), 7.46- 7.44 (m, 4H), 1.92-1.89 (m, 4H), 1.28-1.04 (m, 36H), 0.87 (t, 6H), 0.58 (s, 4H).

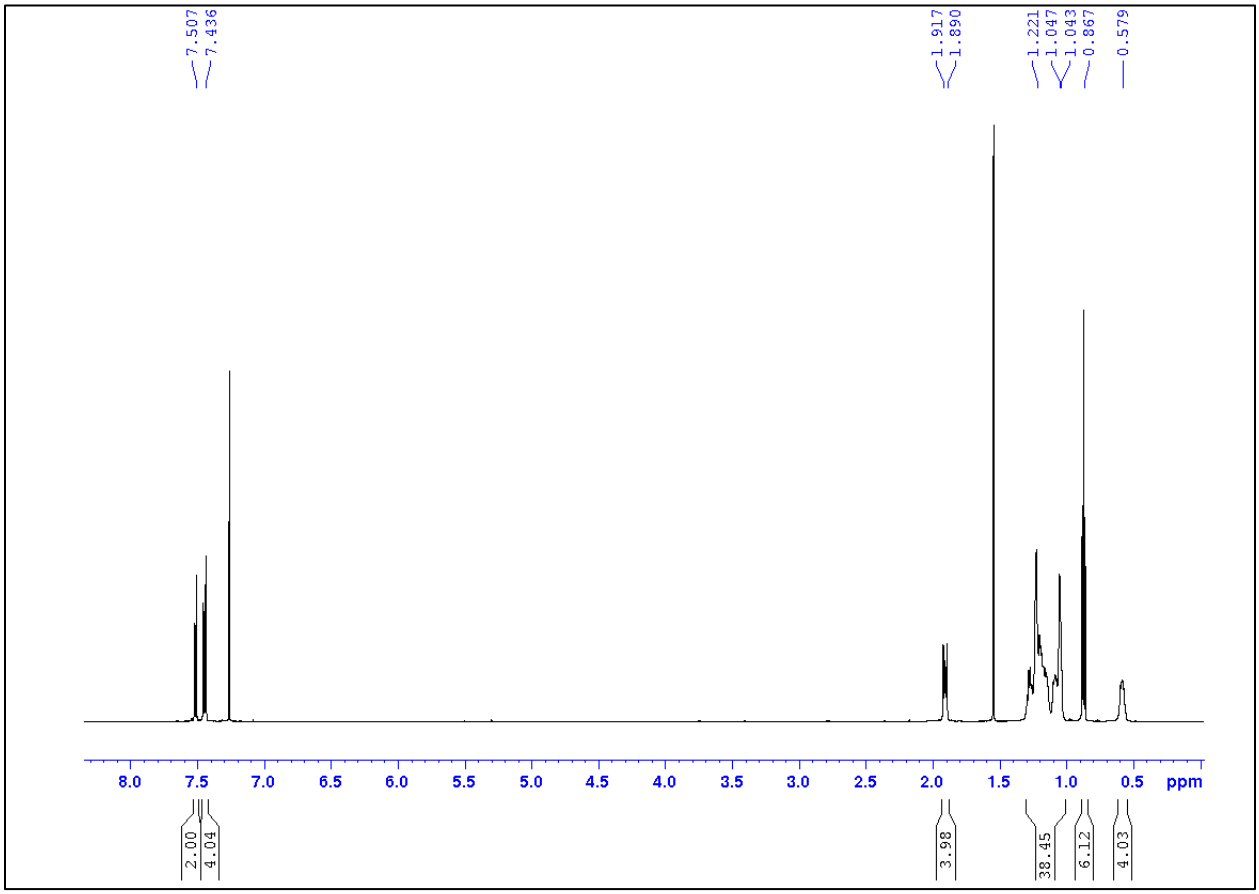

Figure 12: ^{1}H NMR spectrum of 2,7-dibromo-9,9-didodecylfluorene in $CDCl_3$.

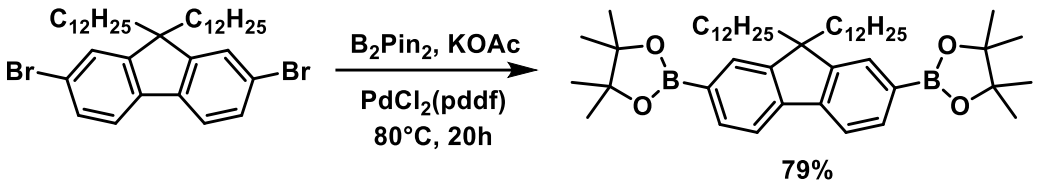

Scheme 10: Reaction to form 2,2'-(9,9-didodecylfluorene-2,7-diyl)bis(4,4,5,5-tetramethyl-1,3,2-dioxaborolane).

2,2'-(9,9-didodecylfluorene-2,7-diyl)bis(4,4,5,5-tetramethyl-1,3,2-dioxaborolane) (Adapted from reference 87 and 88)

A 300 mL round bottom flask equipped with a magnetic stir bar was charged with 2,7-dibromo-9,9-didodecylfluorene (6.78 g, 10.3 mmol), bis(pinacolato)diboron (7.81 g, 30.8 mmol), potassium acetate (4.03 g, 41 mmol), and dioxane (100 mL) and sparged with nitrogen for 1 hour. $Pd(dppf)_2Cl_2$ (676 mg, 923 µmol) was added and then the reaction mixture was stirred at 80°C for 20 hours. The reaction mixture was partitioned with 100 mL water and extracted twice with 50 mL portions of dichloromethane (DCM). The organic extracts were then washed with brine twice with 50 mL portions. The organic phase was then dried over magnesium sulphate and concentrated *in vacuo*. The crude brown oil was then passed through a silica plug and the product was eluted with 350 mL 1:1 hexanes/DCM. The liquid was then concentrated *in vacuo* to yield a yellow oil, and 100 mL of a 4:1 methanol:acetone solution was added to yield a solid yellow product. The solid was then stirred rapidly with an additional 200 mL of a 4:1 methanol:acetone solution until only fine white powder remained. The white powder was then filtered to afford 2,2'-(9,9-didodecylfluorene-2,7-diyl)bis(4,4,5,5-tetramethyl-1,3,2-dioxaborolane) as a white solid (6.12 g, 79%). ^{1}H NMR (600 MHz; $CDCl_3$): δ 7.80 (dd, 2H), 7.74 (s, 2H), 7.72 (d, 2H), 1.99 (dt, 4H), 1.39 (s, 24H), 1.26-1.00 (m, 36H), 0.86 (t, 6H), 0.55 (s, 4H).

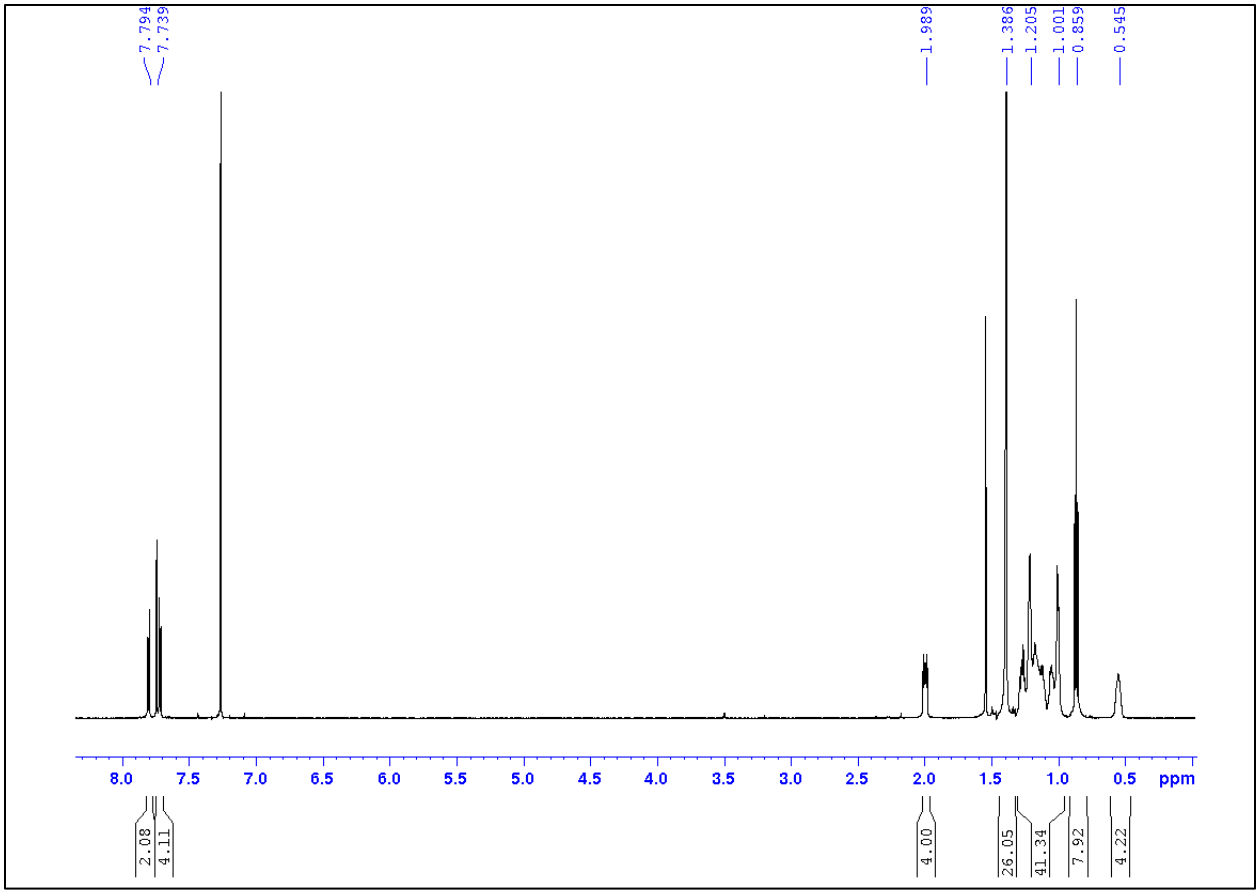

Figure 13: ^{1}H NMR spectrum of 2,2'-(9,9-didodecylfluorene-2,7-diyl)bis(4,4,5,5-tetramethyl-1,3,2-dioxaborolane) in $CDCl_3$.

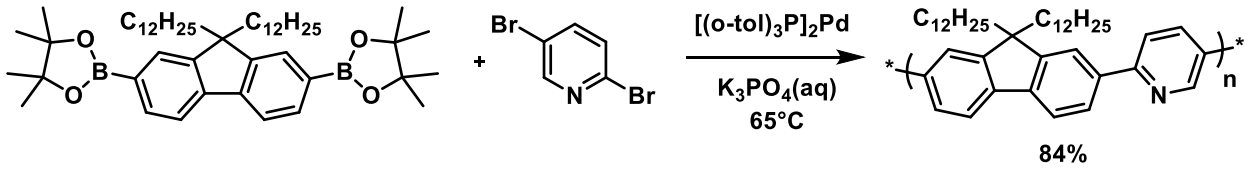

Scheme 11: Polymerization to form Poly(9,9'-didodecylfluorene-co-pyridine).

Poly(9,9'-didodecylfluorene-co-pyridine) (Adapted from reference 87 and 88)

A Schlenk tube equipped with a magnetic stir bar was charged with 2,2'-(9,9-didodecylfluorene-2,7-diyl)bis(4,4,5,5-tetramethyl-1,3,2-dioxaborolane) (1.5 g, 1.99 mmol), 2,5-dibromopyridine (0.471 g, 1.99 mmol), tetrahydrofuran (THF) (8 mL), and 3 M tripotassium phosphate (8 mL) and the mixture was degassed by three freeze-pump-thaw cycles. The biphasic mixture was frozen under liquid nitrogen and $[(o\text{-tol})_3P]_2Pd$ (71 mg, 90 µmol) was added under a

positive pressure of nitrogen. The Schlenk tube was evacuated and backfilled with nitrogen four times and then the reaction mixture was vigorously stirred at 65 °C for 2 hours. The phases were allowed to separate, and the organic layer was isolated then filtered through a celite and neutral alumina plug (1:1 composition). The plug was thoroughly washed with THF and the filtrate was concentrated *in vacuo*. The crude polymer was precipitated into rapidly stirring chilled methanol (350 mL) and then filtered to afford PF-Py as a yellow solid. Repeated the celite/alumina plug and reprecipitated in 300 mL chilled methanol to remove additional impurities. ^{1}H NMR (600 MHz; $CDCl_3$): δ 9.07 (1H, m), 8.60- 7.66 (8H, m), 2.11 (4H, m), 1.20 (40H, m), 0.84 (6H, s).

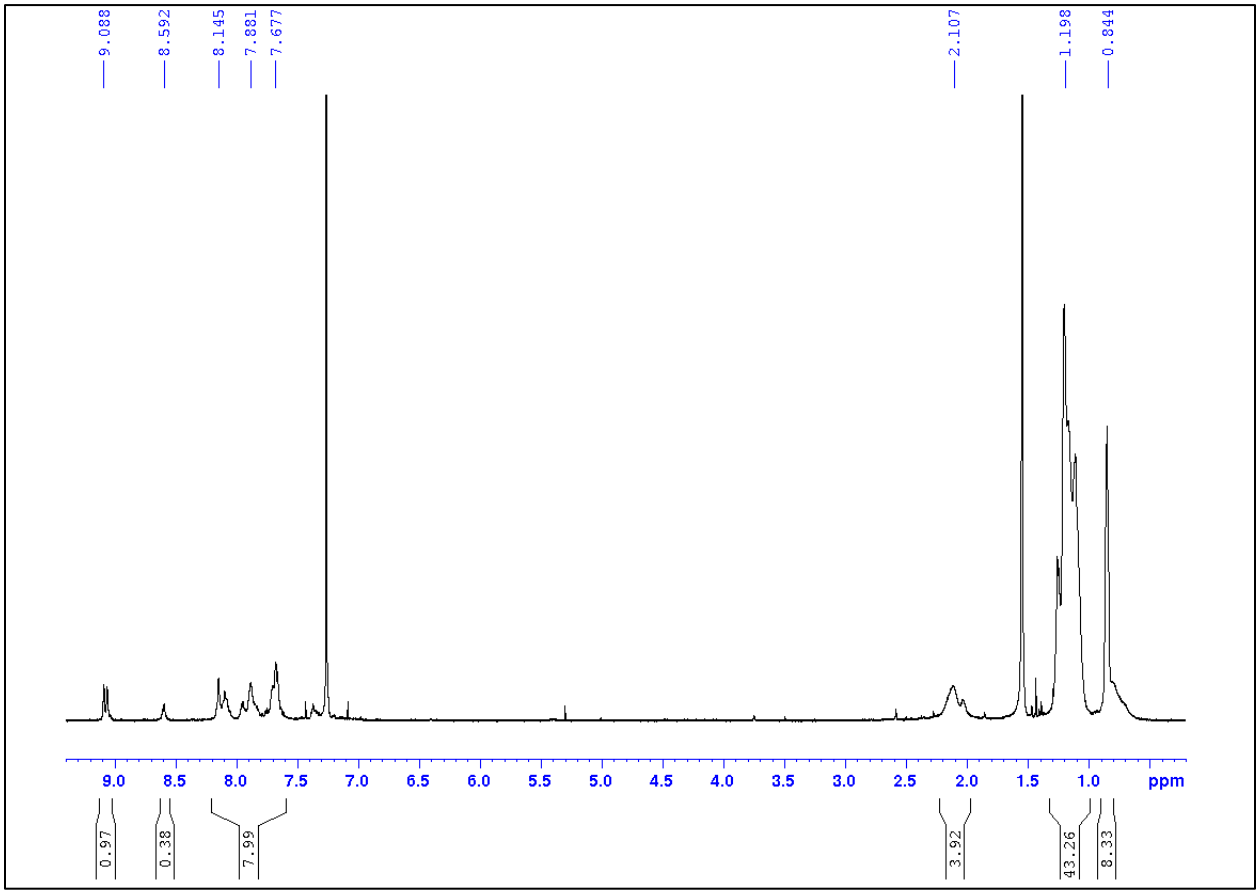

Figure 14: ^{1}H NMR of Pf-Py in $CDCl_3$.

2.4.3 Zincke Reaction Attempts

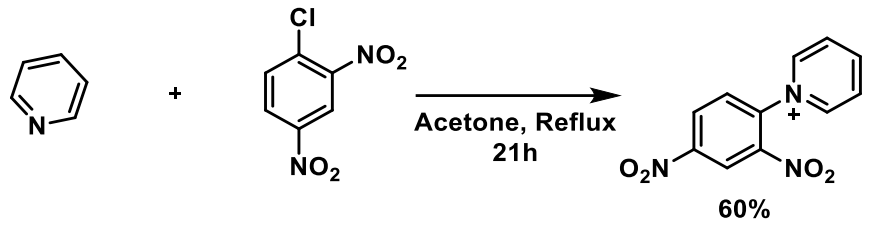

Scheme 12: Model Zincke Reaction to form pyridinium salt.

Pyridinium salt

A 10 mL round bottom flask equipped with a magnetic stir bar was charged with 1-chloro-2,4-dinitrobenzene (0.5 g, 2.5 mmol), and pyridine (0.200 µL, 2.5 mmol), and 3 mL acetone. The mixture was stirred at 56°C, solution first turned dark red and then white precipitate began forming after 3 hours; the reaction was run for 22 hours. The product was then collected by filtration and washed with hexanes and acetone while crushing the product up to eliminate any residue starting material. The pyridinium salt was then collected as a white powder (0.415 g, 60%). ^{1}H NMR (600 MHz; C_2D_6OS): δ 9.42 (d, 2H), 9.17 (d, 4H), 9.01 (m, 2H), 8.470 (m, 3H).

Table 1: Reaction conditions for the model Zincke reaction on pyridine including temperature, mass, molar equivalent, reaction time, and yield.

Solvent	Temperature (°C)	1-Chloro-2,4-Dinitrobenzene	Pyridine	Molar Equivalent	Reaction Time (Hours)	Yield (%)
Acetone (3 mL)	56	0.5 g 2.50 mmol	0.200 mL 2.50 mmol	1:1	22	60
THF (1 mL)	66	0.5 g 2.50 mmol	0.200 mL 2.50 mmol	1:1	22	55
Toluene (1 mL)	66	0.25 g 1.25 mmol	0.100 mL 1.25 mmol	1:1	22	50

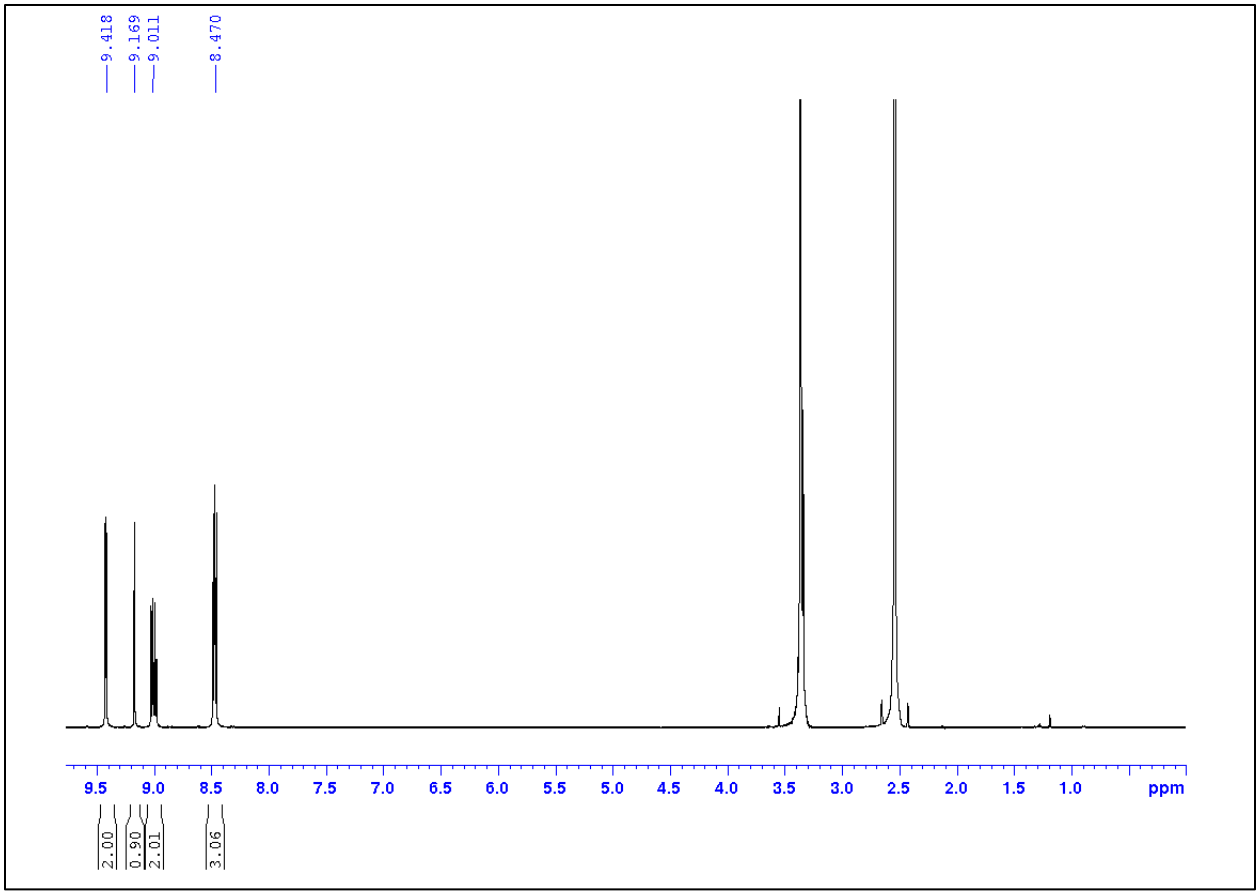

Figure 15: ^{1}H NMR spectrum of model pyridinium salt in C_2D_6OS.

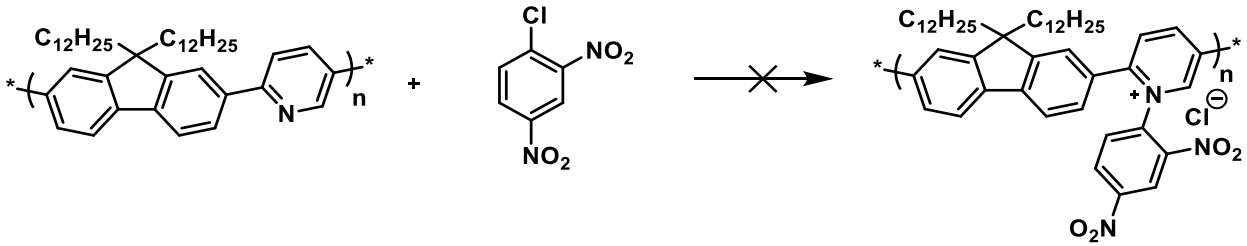

Scheme 13: Zincke Reaction on PF-Py.

Zincke Reaction Attempts on PF-Py

The Zincke reaction on PF-Py was attempted nine times while varying the solvent, temperature, molar equivalent ratios, molecular weight of PF-Py, concentration, and the reaction time. A summary of the reaction conditions for these nine reaction attempts are listed in Table 2. The general setup of the Zincke reaction involved using a 5 mL round bottom flask equipped with

a magnetic stir bar and a condenser charged with 1-chloro-2,4-dinitrobenzene, and PF-Py, and a solvent. The mixture was stirred while heating, for varying lengths of times and monitored by precipitating into either chilled methanol, or hexanes, or by evaporating to dryness followed by ^{1}H NMR.

Table 2: Reaction conditions for the Zincke reaction on PF-Py including temperature, mass, molar equivalent, molecular weight, concentration, and reaction time.

Solvent	Temperature (°C)	CDB	PF-Py	Molar Equivalent	Molecular Weight (kDa)	Concentration (mol/L)	Time (Hours)
$CHCl_3$ (1mL)	60	0.167 g 0.83 mmol	0.048 g 0.083 mmol	1:10	73	0.90	8
THF (1 mL)	66	0.014 g 0.069 mmol	0.01 g 0.017 mmol	1:4	8	0.09	22
THF (1 mL)	66	0.328 g 1.62 mmol	0.094 g 0.16 mmol	1:10	8	1.78	22
THF (1 mL)	66	0.572 g 2.82 mmol	0.164 g 0.28 mmol	1:10	13	3.11	27
Toluene (1 mL)	85	0.167 g 0.83 mmol	0.048 g 0.083 mmol	1:10	73	0.90	8
1-4-DCB (2 mL)	130	1.49 g 7.33 mmol	0.048 g 0.083 mmol	1:87	73	3.71	16
1-4-DCB (1 mL)	130	0.436 g 2.15 mmol	0.025 g 0.043 mmol	1:50	13	2.20	24
1-4-DCB (1 mL)	180	0.167 g 0.83 mmol	0.048 g 0.083 mmol	1:10	73	0.90	80
DMSO (2 mL)	189	0.167 g 0.83 mmol	0.048 g 0.083 mmol	1:10	73	0.45	7

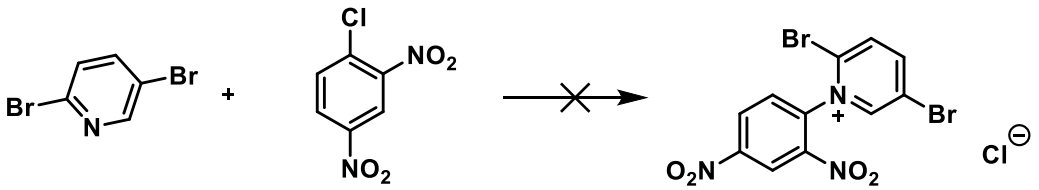

Scheme 14: Zincke reaction on 2,5-dibromopyridine.

Zincke reaction attempt on 2-5-dibromopyridine

A 5 mL round bottom flask equipped with a magnetic stir bar and a condenser was charged with 1-chloro-2,4-dinitrobenzene (0.427 g, 2.11 mmol), 2,5-dibromopyridine (0.5 g, 2.11 mmol),

and 1 mL THF. The mixture was stirred at 67°C for 15 hours and no precipitate had formed, and no product spot appeared on the TLC. Reaction was abandoned.

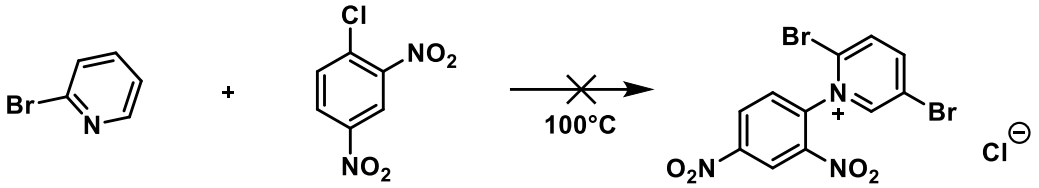

Scheme 15: Zincke Reaction on 2-bromopyrdine

Zincke reaction attempt on 2-bromopyridine

A 5 mL round bottom flask equipped with a magnetic stir bar and a condenser was charged with 1-chloro-2,4-dinitrobenzene (0.15 g, 0.75 mmol), and 3-bromopyridine (0.14 mL, 1.5 mmol). The mixture was stirred at 100°C for 24 hours and no precipitate had formed, and no product spot appeared on the TLC. Reaction was abandoned.

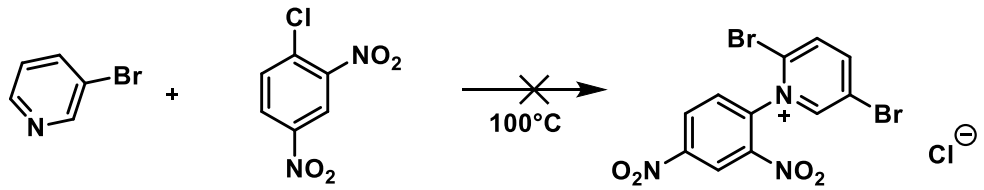

Scheme 16: Zincke Reaction on 3-bromopyrdine.

Zincke reaction attempt on 3-bromopyridine

A 5 mL round bottom flask equipped with a magnetic stir bar and a condenser was charged with 1-chloro-2,4-dinitrobenzene (0.15 g, 0.75 mmol), and 2-bromopyridine (0.14 mL, 1.5 mmol). The mixture was stirred at 100 °C for 24 hours and no precipitate had formed, and no product spot appeared on the TLC. Reaction was abandoned.

Chapter 3: Enhancement of the Two-Polymer Extraction Method Using Acetylated PF-Py

3.1 Introduction

When initially synthesized, SWNT samples contain approximately one third m-SWNTs and two thirds sc-SWNTs. This heterogenous mixture of SWNT species prevents immediate device incorporation and a purification method is required. Although there are many techniques currently capable of separating individual SWNT species, scalability is limited. A promising alternative and scalable method is conjugated polymer sorting.[75,88,111] Conjugated polymer properties can be altered such as side chain, polymer backbone, and molecular weight, to selectively disperse different species of SWNTs. The molecular properties of conjugated polymers have been modified and derivatives of polyfluorene,[62] polycarbazole,[88] polythiophene,[68] and others have been used to produce enriched sc-SWNT samples. However, a polymer that is completely selective for the isolation of m-SWNT has yet to be discovered.

To allow for the enrichment of specifically m-SWNT Bodnaryk *et al.*[88] recently developed a two polymer enrichment system. An electron rich conjugated polymer produces enriched sc-SWNT dispersions that biases the initial metallic to semiconducting ratio toward m-SWNTs and then a second polymer dispersant can be used to disperse the residual m-SWNTs. In their work they performed a series of sc-SWNT extractions using poly(carbazole-*co*-fluorene) (PCPF), and then dispersed the resulting m-SWNT enriched residue using methylated poly(fluorene-*co*-pyridine) (Me-PF-Py). It was determined that the amount of dispersed m-SWNTs is improved through the combination of initial sc-SWNT removal followed by use of an electron-poor conjugated polymer as the final dispersant.

While the poly carbazole was successful at dispersing nearly exclusively sc-SWNTs, the selective dispersion of m-SWNTs with the electron poor polymer was not as efficient. The methylation reaction only functionalized ~50% of the pyridine units along the polymer backbone which limits the increase in electron deficiency of the polymer. The solubility of Me-PF-Py is also an issue as it is insoluble in toluene, a common dispersing solvent for SWNT-polymer dispersions. With these limitations in mind, the addition of a more electron withdrawing functional group will be explored. Specifically, the addition of a trifluoroacetyl moiety to PF-Py is investigated (Scheme 17).

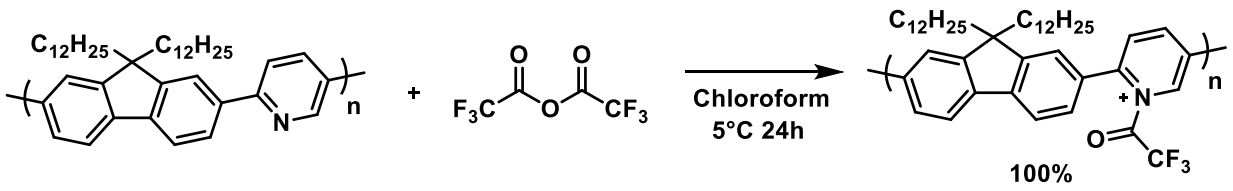

Scheme 17: PF-Py reaction with trifluoroacetic anhydride to generate Acetylated PF-Py (A-PF-Py).

3.2 Results and Discussion

The initial focus of the project was the synthesis of the required polymers. We first prepared the electron-rich poly(carbazole-*co*-fluorene) conjugated polymer, the electron-poor acetylated poly(fluorene-*co*-pyridine), and the electron-poor methylated poly(fluorene-*co*-pyridine). The carbazole monomer was prepared starting with commercially available 4,4'dibromobiphenyl and nitrating it to add a nitro group, followed by Cadogan ring closure to form the carbazole. Also, phase transfer alkylation was performed to attach the branched alkyl side chain to enhance solubility (Scheme 18). The fluorene monomer was synthesized as shown in Chapter 2 (Scheme 7). The fluorene and carbazole monomers were then polymerized using Suzuki polycondensation polymerization to afford P1 (Scheme 23). The fluorene monomer and commercially available 2,5-dibromopyrdine were similarly polymerized to generate poly(fluorene-co-pyridine) (PF-Py)

(Scheme 11). This PF-Py could then either be acetylated with trifluoroacetic anhydride or methylated using methyl iodide to produce A-PF-Py and Me-PF-Py, respectively. GPC analysis showed that P1 had a number-average molecular weight (Mn) of 40 kDa, and a dispersity (Đ) of 2.26. GPC analysis showed that A-PF-Py had a Mn of 13 kDa, 25 kDa, 47 kDa, and 73 kDa with a dispersity of 2.16, 2,61, 3.48, and 2.36, respectively. Me-PF-Py had a Mn of 13 kDa, with a dispersity of 2.16. Higher molecular weights of Me-PF-Py were attempted but found to be insoluble in both THF and toluene.

With our polymers in hand, dispersions between the polymers and raw HiPCO SWNTs were prepared following literature procedures.[88] Generally, raw SWNTs were added to an optimal ratio of polymer and dissolved in 10mL of dispersing solvent. The sample was sonicated for 2 hours in an ice-chilled bath sonicator, followed by centrifugation at 8,346 *g* for 30 minutes. The supernatant was carefully removed while the residue in the centrifuge tube was sonicated in 10 mL of THF for 10 min, then filtered through a 0.2 µm pore-diameter Teflon membrane to remove excess polymer.

To characterize the resulting polymer-SWNT complexes, we first performed UV-vis-NIR absorption spectroscopy (UV-vis). The variety of absorption peaks in the UV-vis spectrum are a result of the different SWNT species in the dispersion. For HiPCO SWNTs, there are three different regions in the spectrum, one metallic region, M_{11} (440-645 nm) and two semiconducting regions, S_{11} (830-1600 nm) and S_{22} (600-800 nm).[88] The UV-vis absorption spectra were normalized to the local minimum at 905 nm to demonstrate the differences in m- and sc- SWNT content for the dispersions. It is not possible to quantify the exact amount of sc- and m-SWNTs using UV-vis for HiPCO SWNTs due to the overlap between the M_{11} and S_{22} regions. Despite this, an approximate ratio (m/sc) can be determined by comparing the peak absorbance of the metallic

region at 506 nm and the semiconducting region at ~1135 nm. A higher m/sc peak ratio indicates a larger amount of m-SWNTs present in the sample. Unnormalized spectra are provided in Supporting Information 3.5.2.

3.2.1 Ideal Dispersion Parameter Studies

First, we evaluated different dispersion solvents and polymer to nanotube mass ratios for the A-PF-Py polymer. The solvents studied were THF, toluene (tol), and a 1:1 THF:Tol mixture. Toluene alone was not a suitable solvent as only the 13 kDa A-PF-Py polymer was completely soluble. It was determined that a 1:1 THF:Toluene dispersing solvent for A-PF-Py was ideal as it provided the best selectivity toward metallic nanotubes. The m/sc peak ratios were compared for the dispersions in THF vs. 1:1 THF:Tol to determine which was more selective toward m-SWNTs. The dispersions in THF and 1:1 THF:Tol gave a m/sc peak ratio of 0.96 and 1.03, respectively. Although the concentration of dispersion was determined to be higher in THF than THF:Tol as indicated in the unnormalized UV-vis data, (Figure 34), the difference was marginal and selectivity toward m-SWNTs was preferable. The remaining studies involving A-PF-Py were all performed in a 1:1 THF:Tol solvent mixture.

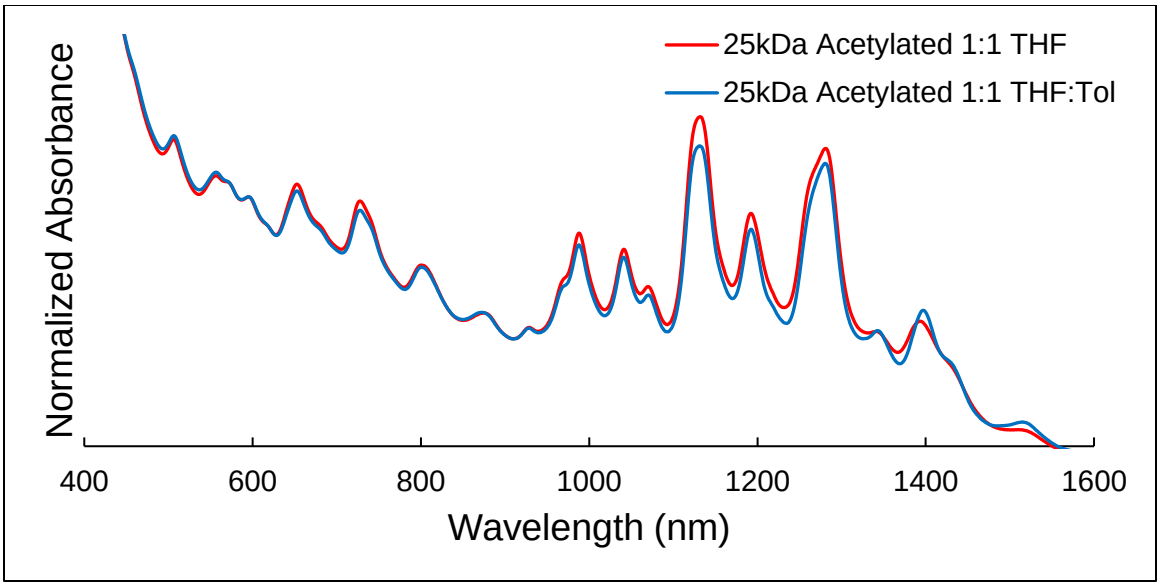

Figure 16: UV-vis-NIR absorption spectra for the A-PF-Py-SWNTs dispersant solvent study using HiPCO SWNTs. Spectra are normalized to a local minimum at ~905 nm to show relative m-SWNT and sc-SWNT content.

Table 3: Peak absorbance for m-SWNTs (506 nm) and Sc-SWNTs (~1135 nm), ratio of m/sc from Figure 16, the A-PF-Py-SWNTs dispersant solvent study using HiPCO SWNTs.

Sample Name	Metallic Peak Absorbance (506 nm)	Semiconducting Peak Absorbance (~1135 nm)	Ratio (m/sc)
25kDa Acetylated 1:1 THF	1.92	2.00	0.96
25kDa Acetylated 1:1 THF:Tol	1.93	1.87	1.03

Next, a polymer:SWNT ratio study was performed to determine the optimal ratio for SWNT dispersions with A-PF-Py. Although the dispersion of A-PF-Py showed that a 1:1, polymer:SWNT ratio, provides higher concentration of nanotube dispersions, 0.5:1 had the highest selectivity for m-SWNTs. The m/sc ratio for 1:1, 0.5:1, and 0.25:1 were 1.03, 1.33, and 1.27, respectively. This indicates that A-PF-Py has a greater selectivity to m-SWNTs at lower concentrations and increasing concentration compromises metallic selectivity. To confirm that the polymer was successfully wrapping the surface of the SWNTs atomic force microscopy (AFM) of a 0.5:1 dispersion was performed (Figure 33). The sample was spin coated onto a silicon wafer at

3000 RPMs for 30 seconds. The AFM showed polymer surrounding the SWNTs indicating that at 0.5:1 the polymer is interacting with the surface of the SWNTs.

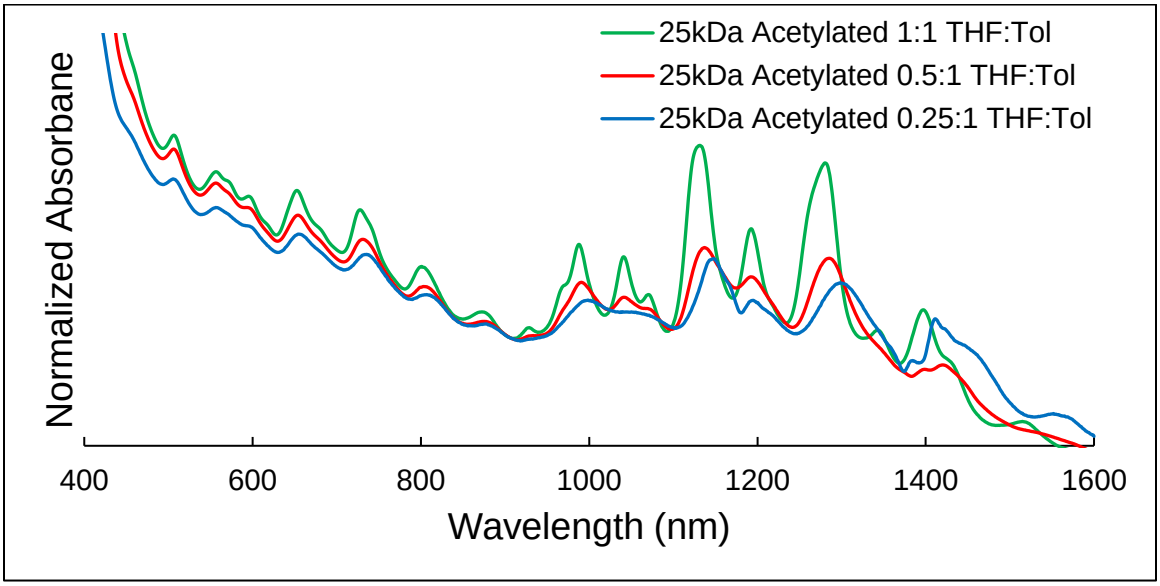

Figure 17: UV-vis-NIR absorption spectra for the A-PF-Py-SWNTs ratio study using HiPCO SWNTs. Spectra are normalized to a local minimum at ~905 nm to show relative m-SWNT and sc-SWNT content.

Table 4: Peak absorbance for m-SWNTs (506 nm) and sc-SWNTs (~1135 nm), ratio of m/sc from Figure 17, the A-PF-Py-SWNTs ratio study using HiPCO SWNTs.

Sample Name	Metallic Peak Absorbance (506 nm)	Semiconducting Peak Absorbance (~1135 nm)	Ratio (m/sc)
25kDa Acetylated 1:1 THF:Tol	1.93	1.87	1.03
25kDa Acetylated 0.5:1 THF:Tol	1.87	1.41	1.33
25kDa Acetylated 0.25:1 THF:Tol	1.73	1.36	1.27

Next, a molecular weight study was performed to investigate how molecular weight affects both dispersion concentration and selectivity for the A-PF-Py polymer. The molecular weights that were investigated were 13 kDa, 25 kDa, 47 kDa, and 73 kDa. The 73 kDa polymer was determined to be partially insoluble in the 1:1 THF:Tol mixture and a dispersion with SWNTs was not possible. Dispersions with SWNTs were prepared with the remaining molecular weights and the concentration of the dispersions decreased with increasing molecular weight. The m/sc peak ratios

were 0.99, 1.03, and 1.03 for 13 kDa, 25 kDa, and 47 kDa, respectively. The slight differences between peak absorbance indicate that the selectivity is only minimally impacted by molecular weight. Although the selectivity for the 25 kDa and 47 kDa polymers were identical, the 25 kDa polymer provided a more concentrated dispersion (Figure 36). Therefore, 25 kDa was deemed to provide the optimal concentration while providing the best selectivity toward m-SWNTs.

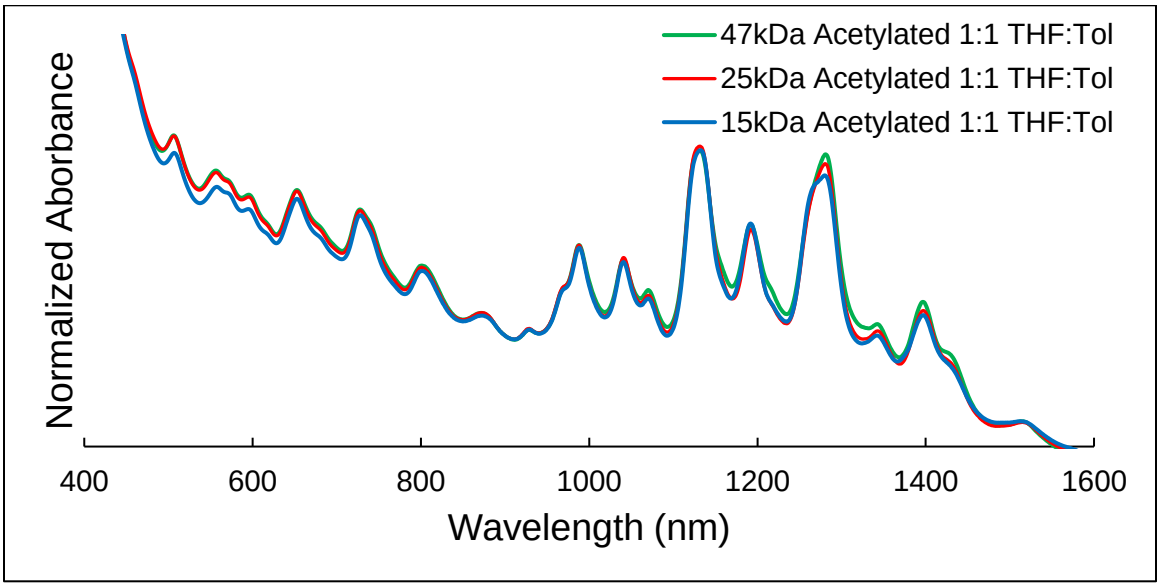

Figure 18: UV-vis-NIR absorption spectra for the A-PF-Py-SWNTs molecular weight study using HiPCO SWNTs. Spectra are normalized to a local minimum at ~905 nm to show relative m-SWNT and sc-SWNT content.

Table 5: Peak absorbance for m-SWNTs (506 nm) and sc-SWNTs (~1135 nm), ratio of m/sc from Figure 18, the A-PF-Py-SWNTs molecular weight study using HiPCO SWNTs.

Sample Name	Metallic Peak Absorbance (506 nm)	Semiconducting Peak Absorbance (~1135 nm)	Ratio (m/sc)
13kDa A-PF-Py 1:1 THF:Tol	1.85	1.87	0.99
25kDa A-PF-Py 1:1 THF:Tol	1.93	1.87	1.03
47kDa A-PF-Py 1:1 THF:Tol	1.93	1.87	1.03

With the preliminary mass ratio and dispersing solvent studies complete the A-PF-Py could then be compared with the other polymer types. The purpose of this study was to determine whether A-PF-Py offers greater selectivity toward m-SWNTs and can be used as the final metallic

dispersant in the two-polymer conjugated polymer sorting system. The A-PF-Py, Me-PF-Py, PF-Py, and PC-PF produced m/sc ratios of 1.03, 0.94, 0.50, and 0.28, respectively. The A-PF-Py provided the best selectivity toward m-SWNTs. The concentration of the A-PF-Py's dispersions were also much more concentrated than any of the other polymer types indicating it is more efficient at dispersing SWNTs.

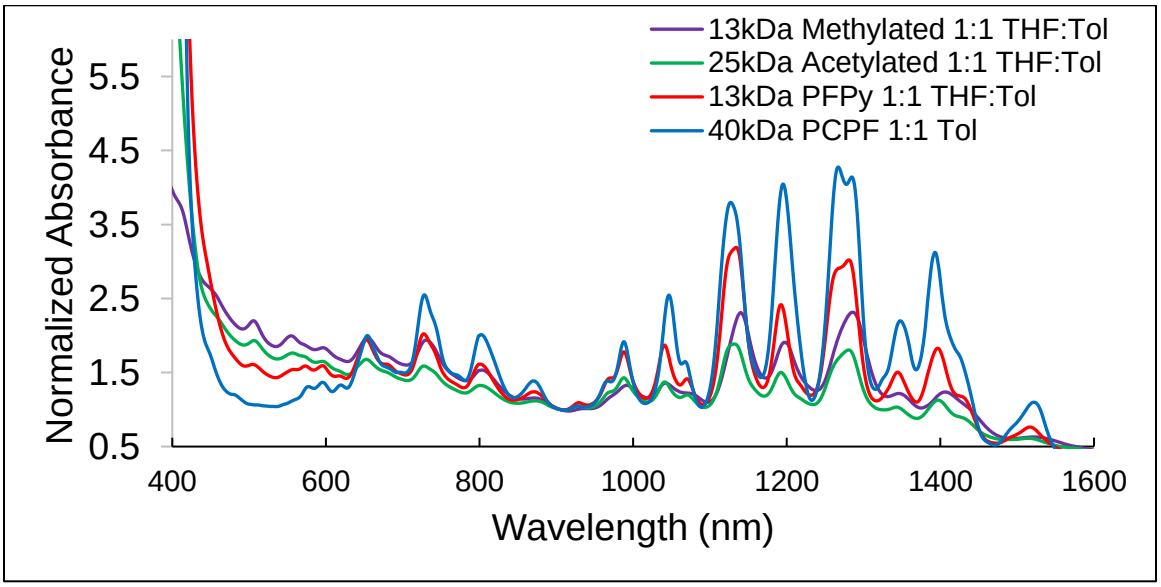

Figure 19: UV-vis-NIR absorption spectra for all investigated polymer-SWNT types using HiPCO SWNTs. Spectra are normalized to a local minimum at ~905 nm to show relative m-SWNT and sc-SWNT content.

Table 6: Peak absorbance for m-SWNTs (506 nm) and sc-SWNTs (~1135 nm), ratio of m/sc from Figure 19, the polymer-SWNTs comparison study using HiPCO SWNTs.

Sample Name	Metallic Peak Absorbance (506 nm)	Semiconducting Peak Absorbance (~1135 nm)	Ratio (m/sc)
40kDa PCPF 1:1 Tol	1.06	3.80	0.28
13kDa PF-Py 1:1 THF:Tol	1.61	3.19	0.50
25kDa A-PF-Py1:1 THF:Tol	1.93	1.87	1.03
13kDa Me-PF-Py 1:1 THF:Tol	2.20	2.33	0.94

3.2.2 Incorporating A-PF-Py into the Two-Polymer Extraction Method

With the initial studies of the A-PF-Py polymer indicating that it provides the greatest concentration of nanotubes and optimal selectivity toward m-SWNTs, it was deemed a suitable candidate to be used as the final dispersant (P2) in the conjugated polymer sorting system. First, 5mg of raw SWNTs were added to a solution of 5 mg of P1 dissolved in 10mL of toluene. After sonication and centrifugation, the supernatant was removed and the residue in the centrifuge tube was washed of excess polymer. As demonstrated in Figure 20, the residue could then be redispersed using either 5 mg of P1 (to further extract sc-SWNTs) or 2.5 mg of A-PF-Py (P2) (to disperse m-SWNTs). In this study the nomenclature used follows the format of ExPy, where x indicates the number of extractions (0-4), and y indicates the polymer used to redisperse the residue (1 or 2). Using this process, we first produced seven polymer-SWNT dispersions, which were evaluated for sc- and m-SWNT using UV-vis.

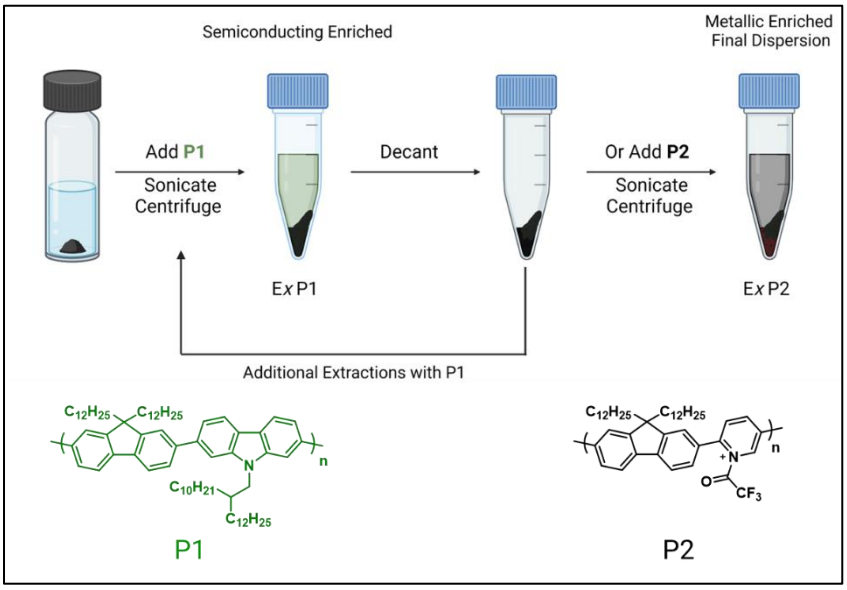

Figure 20: Illustration showing the method of two polymer extraction. P1 (green) is the electron rich PCPF, which is introduced to first extract sc-SWNTs and is repeated for *x* extractions. P2 (black) is the electron poor A-PF-Py and is used as the final dispersant to disperse the remaining m-SWNTs.

As shown in Figure 21, the intensity of the M_{11} region increases after each extraction step in the P1-SWNT dispersion series. The m/sc peak ratios for E0P1, E1P1, E2P1, and E3P1 were 0.25, 0.36, 0.52, and 0.74, respectively. This suggests that sc-SWNT discrimination is diminished as the m-:sc-SWNT ratio is biased toward m-SWNTs, or as the polymer:SWNT mass ratio increases because the total amount of SWNTs decreases with each extraction.

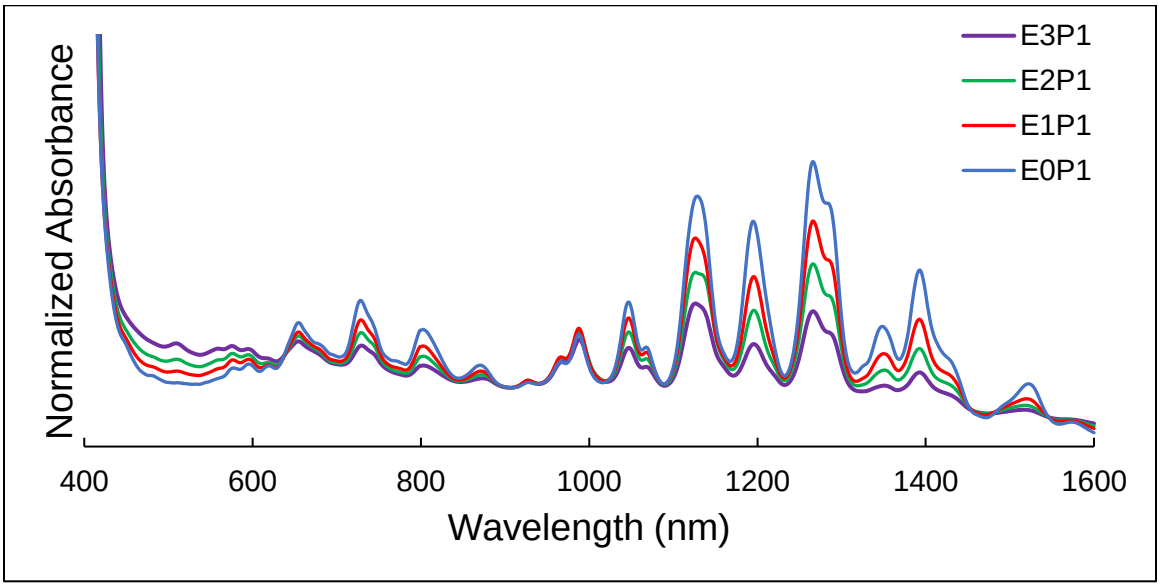

Figure 21: UV-vis-NIR absorption spectra for the P1-SWNTs extraction study using HiPCO SWNTs. Spectra are normalized to a local minimum at ~905 nm to show relative m-SWNT and sc-SWNT content.

Table 7: Peak absorbance for m-SWNTs (506 nm) and sc-SWNTs (~1135 nm), ratio of m/sc from Figure 21, the P1-SWNTs extraction study using HiPCO SWNTs.

Sample Name	Metallic Peak Absorbance (506 nm)	Semiconducting Peak Absorbance (~1135 nm)	Ratio (m/sc)
E3P1	1.81	2.43	0.74
E2P1	1.55	2.96	0.52
E1P1	1.28	3.54	0.36
E0P1	1.08	4.26	0.25

Similarly, the intensity of the M_{11} region also increases for the P2-SWNT dispersion series as a function of extraction count, except E0P2 (Figure 22). The m/sc peak ratio for the P2 extractions with a mass ratio of 0.5:1, were 1.33, 0.98, 1.15, and 1.36 for E0P2, E1P2, E2P2, and

E3P2. Despite the m/sc ratio being high in E0P2 the concentration of this dispersion is far more dilute than all other extractions (Figure 39). As expected, the electron-poor P2 disperses more m-SWNTs than the electron-rich P1. This is illustrated in the m/sc ratios as all P2 extractions are higher values than the P1 extractions. This trend reveals that the use of A-PF-Py as an electron-poor conjugated polymer is beneficial in dispersing significant amounts of m-SWNTs, especially when compared to using only P1 as both the sc-SWNT extraction agent and as the final m-SWNT dispersant. In addition, qualitative colour analysis of the polymer-SWNT dispersion agree with the UV-vis analysis. For HiPCO samples, a green colour was observed for the P1-SWNT dispersion, indicating sc-SWNT enrichment, while a black colour was observed for the A-PF-Py-SWNT dispersions, indicating m-SWNT enrichment. Photographs of the dispersions are provided in the supporting information.

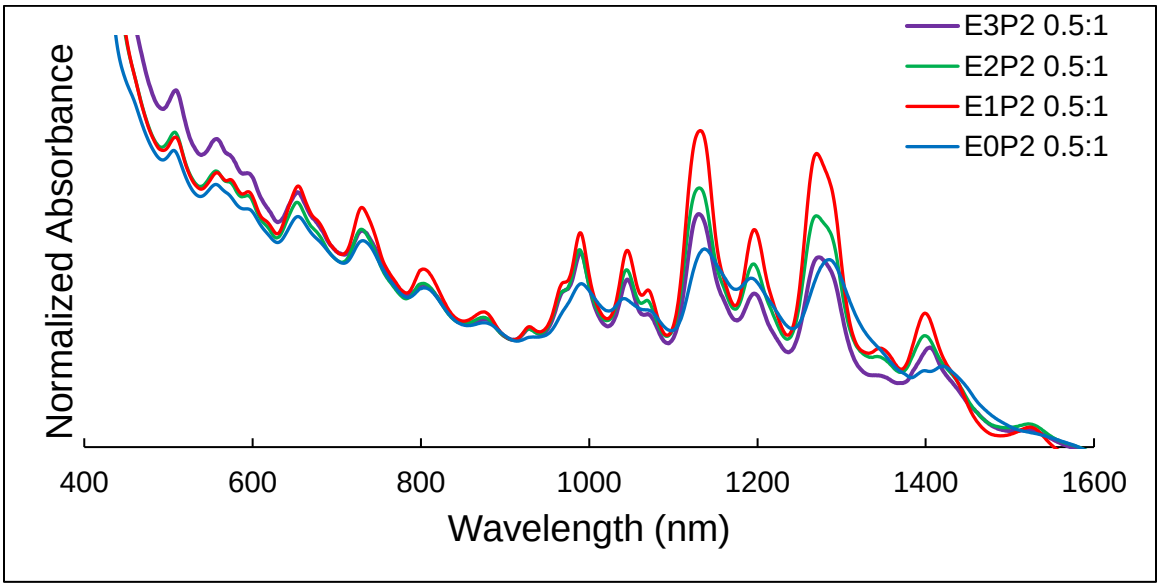

Figure 22: UV-vis-NIR absorption spectra for the 0.5:1, A-PF-Py-SWNTs, extraction study using HiPCO SWNTs. Spectra are normalized to a local minimum at ~905 nm to show relative m-SWNT and sc-SWNT content.

Table 8: Peak absorbance for m-SWNTs (506 nm) and Sc-SWNTs (~1135 nm), ratio of m/Sc from Figure 22, the 0.5:1 A-PF-Py-SWNTs extraction study using HiPCO SWNTs.

Sample Name	Metallic Peak Absorbance (506 nm)	Semiconducting Peak Absorbance (~1135 nm)	Ratio (m/sc)
E3P2	2.14	1.57	1.36
E2P2	1.95	1.69	1.15
E1P2	1.92	1.96	0.98
E0P2	1.87	1.41	1.33

Another study was performed reattempted the conjugated polymer sorting using 1.2 mg (0.25:1) of P2 instead of 2.5 mg (0.5:1) of P2. Reduction of the polymer used was investigated because of the significant increase in dispersion concentration after one extraction with P1. The molar ratio study demonstrated that increased polymer concentration can result in a decrease in selectivity toward metallics so the reduction to 0.25:1 was aimed at greater selectivity. The m/sc ratio for E0P2, E1P2, E2P2, E3P2, and E4P2, were 1.27, 1.06, 1.11, 1.37, and 1.59, respectively. The selectivity and concentration did not seem to be largely affected by using less A-PF-Py. Minimizing polymer use is ideal, thus 0.25:1 was determined to be the ideal mass ratio for A-PF-Py after at least one extraction with P1.

Intriguingly, despite both 0.5:1 and 0.25:1 initially producing dilute dispersions of SWNTs after one extraction with P1 these dispersions were much more concentrated. The large increase in concentration is likely due to an increase in polymer:SWNT mass ratio because the total amount of SWNTs decreases with each extraction. There is also unremovable partially wrapped P1 still remaining on the surface of the nanotubes, even after thorough rinsing, which may aid in dispersion. The residual P1 was confirmed by thermogravimetric analysis (TGA) by analyzing HiPCO SWNTs, PCPF, and the residue after one extraction. As seen in Figure 51, there is a change in mass from 90-75% ranging from 350-500°C in the TGA of the residue. A similar mass loss is

present in the TGA of PCPF from 90-30% at 350-500°C, while no similar mass loss is observed in raw HiPCO SWNTs. These results indicate that there is residual polymer in the residue that is unable to be removed during the rinsing process.

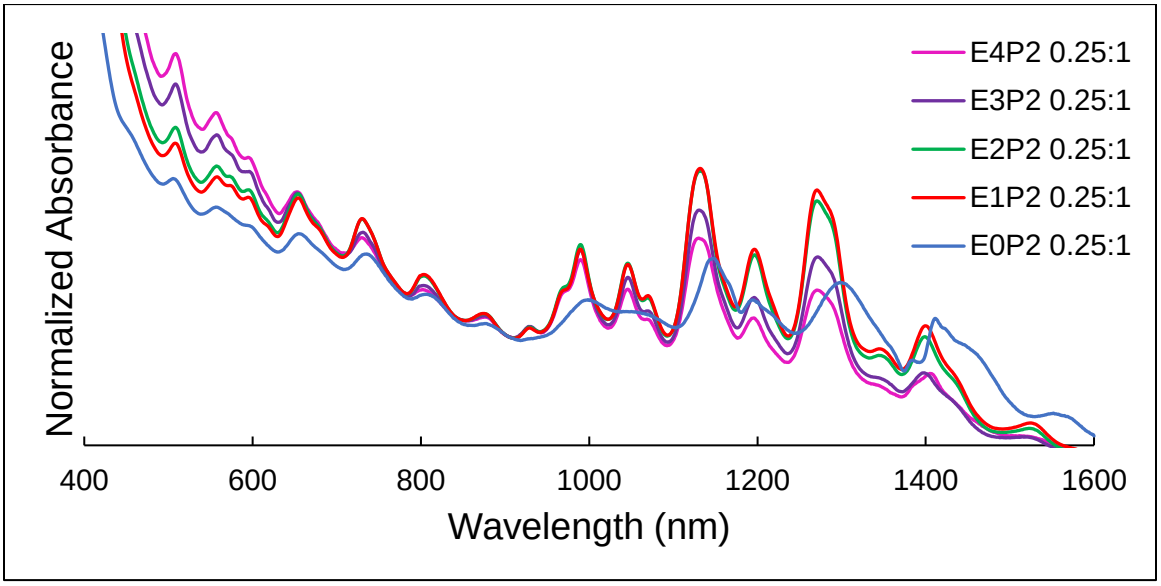

Figure 23: UV-vis-NIR absorption spectra for the 0.25:1, A-PF-Py-SWNTs, extraction study using HiPCO SWNTs. Spectra are normalized to a local minimum at ~905 nm to show relative m-SWNT and sc-SWNT content.

Table 9: Peak absorbance for m-SWNTs (506 nm) and Sc-SWNTs (~1135 nm), ratio of m/sc from Figure 23, the 0.25:1 A-PF-Py-SWNTs extraction study using HiPCO SWNTs.

Sample Name	Metallic Peak Absorbance (506 nm)	Semiconducting Peak Absorbance (~1135 nm)	Ratio (m/sc)
E4P2	2.30	1.45	1.59
E3P2	2.16	1.58	1.37
E2P2	1.96	1.76	1.11
E1P2	1.89	1.78	1.06
E0P2	1.73	1.36	1.27

Lastly, we characterized a SWNT sample using electrical conductivity measurements using a four-point probe method. We first prepared a circular thin film of E1P2 (prepared with a molar ratio of 0.25:1) with a diameter of 18 mm and a thickness of 0.031 µm. The thin film was prepared by filtering the polymer-SWNT dispersion through a Teflon filtration membrane having a 0.2 µm

pore diameter. The thin film was dried by vacuum suction overnight and then resistance was measured by direct contact with four platinum probes placed in the middle of the circular thin film. The measurements were performed on three separate locations on the thin film. The average sheet resistance (R_s) was calculated to be 127±8 Ω/sq and the average conductivity was measured to be 256 ± 16 S/m for E1P2. These measurements are encouraging as the R_S of the E4P2 thin film previously reported for the Me-PF-Py was (2 ± 1) x 10^6 Ω/sq. The R_s difference of four orders of magnitude indicate that the A-PF-Py allows for much higher conductivity when wrapping the nanotubes compared to Me-PF-Py. The conductivity of raw HiPCO SWNTs were also taken with the average sheet resistance (R_s) being 1.98±0.01 Ω/sq and the average conductivity was measured to be 1685 ± 10 S/m. A lower conductivity of the polymer-SWNT thin film was expected as the polymer acts as an insulator reducing conductivity. The conductivity was only one order of magnitude higher in the raw SWNTs. The high conductivity of the A-PF-Py could allow for implementation in some applications without the removal of the polymer.

Table 10: Conductivity measurements for E1P2 and raw HiPCO SWNTs including average conductivity, and sheet resistance.

Sample	Average Conductivity (S/m)	Sheet resistance (Ω/sq)
E1P2 0.25:1	256 ± 16	127 ± 8
HiPCO SWNTs	1685 ± 10	1.98 ± 0.01

Encouraged by these results, we investigated our methodology using plasma-torch SWNTs, which have a higher average diameter, with tube diameter of 1.1-1.5 nm. Dispersions were prepared with plasma-torch (PT) grown SWNTs according to literature procedures.[88] For plasma-torch SWNTs, there are four regions of interest in the absorption spectrum: one metallic region, M_{11} (600-750 nm) and three semiconducting regions, including S_{11} (1400-1900 nm), S_{22} (750-1150 nm), and S_{33} (420-580 nm). The spectra were normalized to a local maximum at ~936

nm to highlight the differences in m-/sc-SWNT content. There is an increase in the metallic region for the A-PF-Py compared to the PCPF which has no visible peak in the m-SWNT region. This suggests that PCPF is also selective for sc-SWNT for PT SWNTs and the A-PF-Py is capable of dispersing m-SWNTs. These preliminary results indicate that the use of A-PF-Py can also be implemented in the polymer sorting system using PT SWNTs.

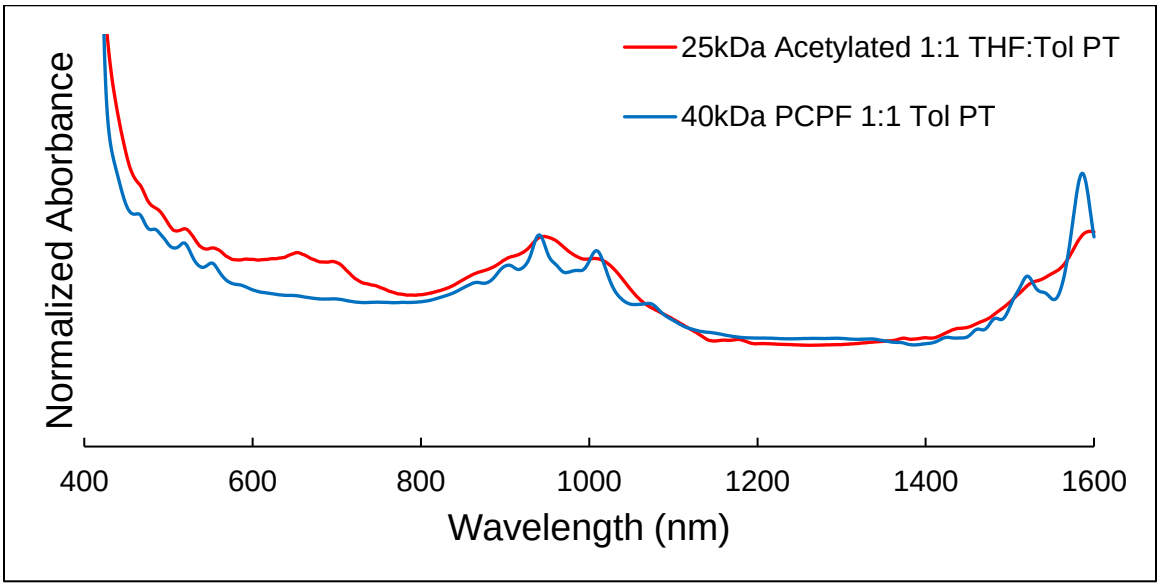

Figure 24: UV-vis-NIR absorption spectra for the polymer-SWNTs dispersion study using plasma-torch SWNTs. Spectra are normalized to a local maximum at ~936 nm to show relative m-SWNT and sc-SWNT content.

Overall, there are many advantages of the newly discovered A-PF-Py over the previously investigated Me-PF-Py. The advantages start during the synthesis as the acetylation reaction proceeds to complete functionalization of the pyridine while Me-PF-Py only allows for ~50% functionalization. The Me-PF-Py also is insoluble in common dispersing solvents, such as THF and toluene, when the molecular weight is greater than 13 kDa. Also, the dispersions produced with A-PF-Py are much more concentrated than the dispersions with Me-PF-Py. The A-PF-Py allows for highly concentrated dispersions enriched with m-SWNTs.

3.3 Conclusion

The improvement of the two-polymer m-SWNT enrichment method has been explored. Using an electron-rich conjugated polymer that is selective toward sc-SWNT, the initial m/sc SWNT ratio can be biased toward m-SWNTs. Ensuing dispersions of the residue using an electron-poor conjugated polymer produces dispersions that are more enriched in m-SWNTs than possible using only the electron-rich polymer. Characterization of HiPCO polymer-SWNT samples using UV-vis-NIR indicate that P2-SWNT samples possessed more m-SWNTs than P1-SWNT samples. The A-PF-Py also showed the greatest selectivity toward m-SWNTs when compared to Me-PF-Py, PF-Py and PCPF. Electrical conductivity measurements were also performed demonstrating that dispersions with A-PF-Py had higher conductivity and lower sheet resistance than samples prepared with Me-PF-Py. These results demonstrate an alternative dispersant for m-SWNTs in the m-SWNT enrichment system.

3.4 Experimental

3.4.1 General

Raw HiPCO SWNTs were purchased (HR37-033) and used without further purification. Plasma-torch SWNTs were purchased from Raymor Industries Inc. (RNB-661-120-X466) and were also used without further purification. All reagents were purchased from commercial chemical suppliers and used as received. Dr. Daryl Fong, a former student in the group, synthesized the 73 kDa PF-Py polymer. Flash chromatography was performed using an Intelliflash 280 by AnaLogix. All compounds were monitored using a variable wavelength detector at 254 nm. Columns were prepared in Biotage® SNAP KP-Sil cartridges using 40-63 μm silica or 25-40 μm silica purchased from Silicycle. ^{1}H NMR spectra were recorded on Bruker Advance 600 MHz spectrometers and shift-referenced to the residual solvent resonance. Polymer molecular weights

and dispersities were analyzed (relative to polystyrene standards) via GPC using a Waters 2695 Separations Module equipped with a Waters 2412 refractive index detector and a Tosoh TSKgel SuperHZM-N multi-pore GPC column with dimensions of 4.6 mm internal diameter, length of 15 cm, and 3 µm particle size. THF with 2% acetonitrile was used as the eluent at a flow rate of 0.3 mL/min. Sonication was performed in a Branson Ultrasonic B2800 bath sonicator. Centrifugation of the polymer-SWNT samples was performed using a Sorvall Legend X1R centrifuge. UV-vis-NIR absorption spectra were recorded on a Cary 5000 spectrometer in dual beam mode using twin 3.5 mL quartz cuvettes with a 1 cm pathlength. AFM images were acquired on a Bruker Dimension iCon AFM in ScanAsyst mode with a ScanAsyst-Air tip.

3.4.2 Synthesis

Synthesis of N(2'decyltetradecane)2,7-dibromocarbazole

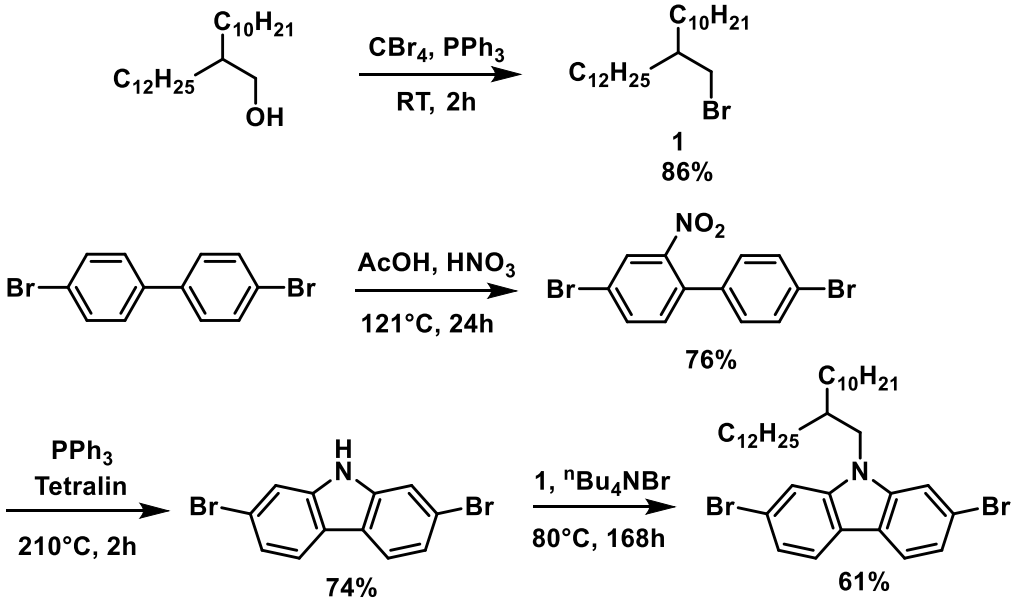

Scheme 18: Synthesis to form N(2'decyltetradecane)2,7-dibromocarbazole.

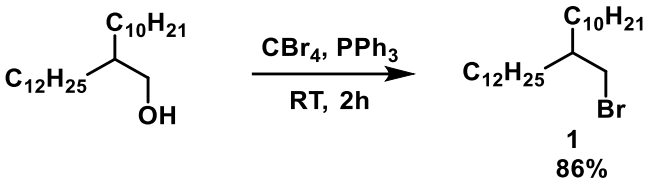

Scheme 19: Reaction to form 1-bromo-2-decyl-4-tetradecane.

1-bromo-2-decyl-4-tetradecane (Adapted from reference 88)

A 100 mL round bottom flask equipped with a magnetic stir bar was charged with 2-decyl-1-tetradecanol (6 mL, 14.1 mmol), triphenylphosphine (4.44 g, 16.9 mmol), and DCM (7.5 mL). The mixture was cooled to 0°C using an ice bath and then the carbon tetrabromide (5.6 g, 16.8 mmol) powder was added portion-wise. The reaction mixture was warmed to room temperature and stirred for 2 hours. The crude mixture was filtered through a silica plug and hexanes was used to elute the product. The filtrate was concentrated in vacuo to afford 1-bromo-2-decyl-4-tetradecane as a colourless oil (5.06 g, 86%). ^{1}H NMR (600 MHz; $CDCl_3$): δ 3.45 (d, 2H), 1.59 (m, 1H), 1.37-1.26 (m, 40H), 0.88 (m, 6H).

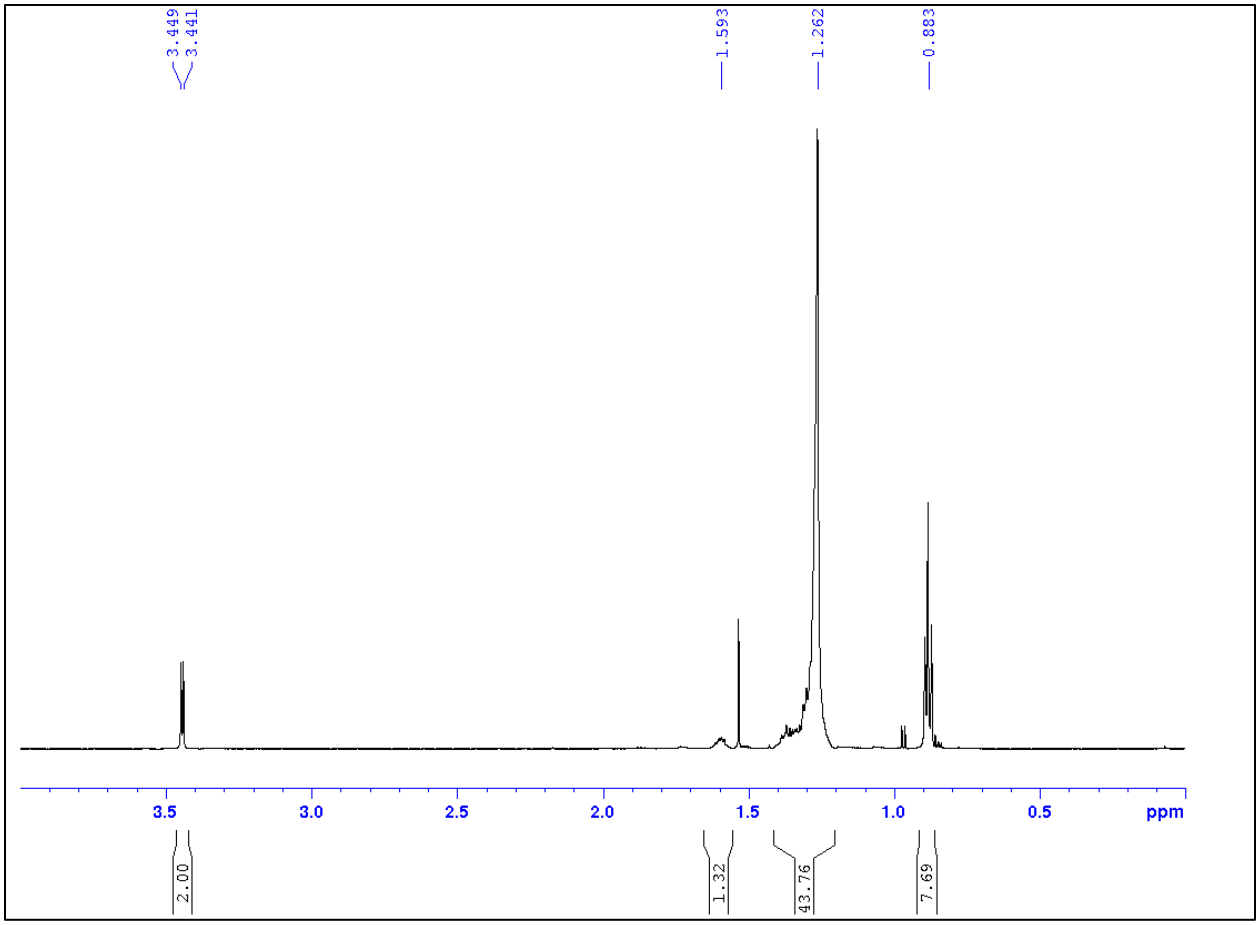

Figure 25: ^{1}H NMR spectrum of 1-bromo-2-decyl-4-tetradecane in $CDCl_3$.

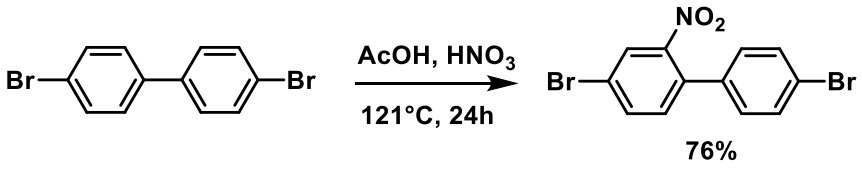

Scheme 20: Reaction to form 2-nitro-4-4'dibromobiphenyl.

2-nitro-4-4'dibromobiphenyl (Adapted from reference 88)

A 250 mL round bottom flask equipped with a magnetic stir bar was charged with 4,4'-dibromobiphenyl (2.0 g, 6.4 mmol), glacial acetic acid (24 mL), and concentrated nitric acid (8 mL). The reaction mixture was heated to 121°C for 24 hours and then precipitated into ice water to produce yellow crystals. The slurry was filtered and rinsed with chilled water. The yellow crude product was then recrystallized in a minimum of ethanol (37 mL) and crystals were allowed to

from slowly at room temperature overnight. The product was then filtered to yield 2-nitro-4-4'dibromobiphenyl as a yellow solid (1.73 g, 76%). ^{1}H NMR (600 MHz; $CDCl_3$): δ 8.03 (d, 1H), 7.76 (dd, 1H), 7.56 (d, 2H), 7.29 (d, 1H), 7.16 (d, 2H).

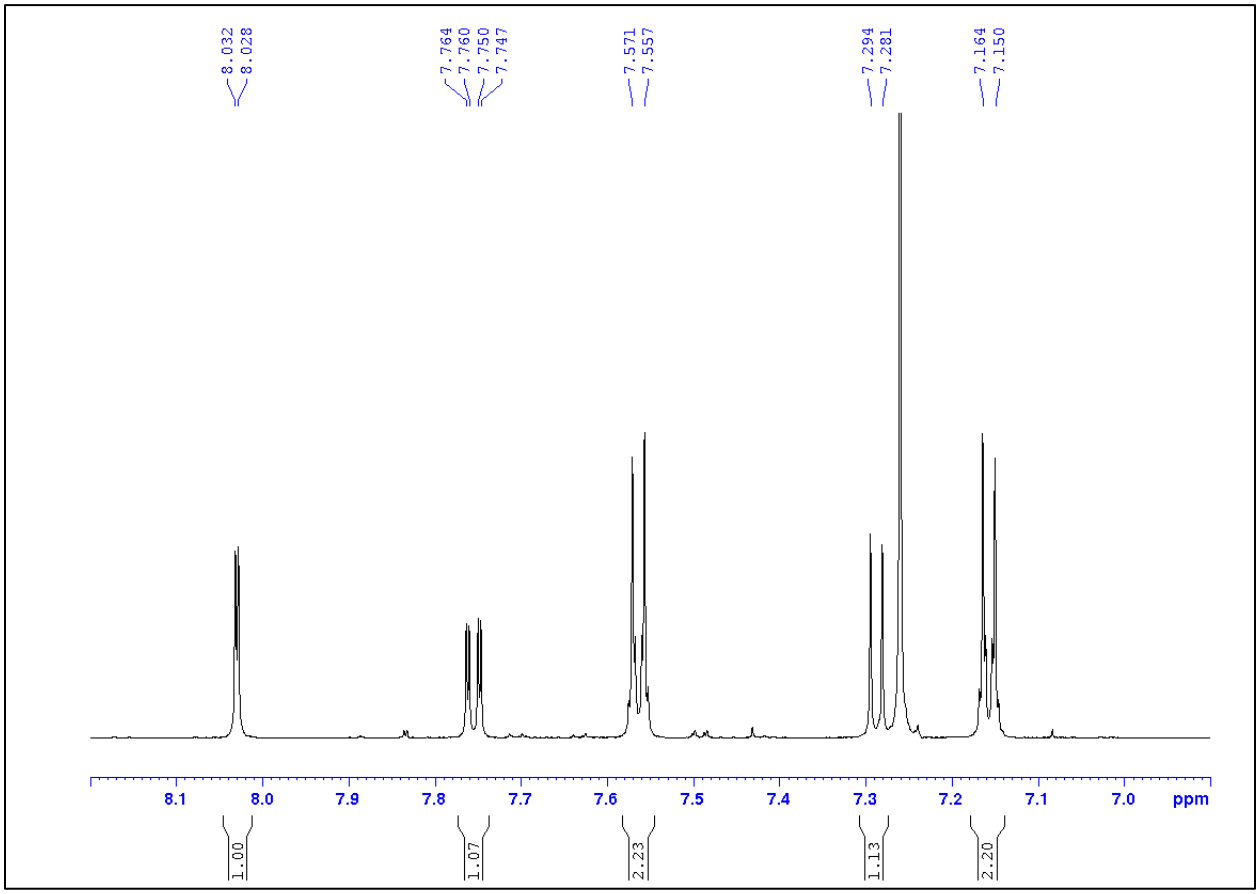

Figure 26: ^{1}H NMR of 2-nitro-4-4'dibromobiphenyl in $CDCl_3$.

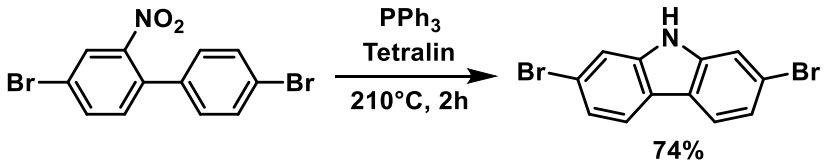

Scheme 21: Reaction to form 9H-2,7-dibromocarbazole.

9H-2,7-dibromocarbazole (Adapted from reference 88)

A 250 mL round bottom flask equipped with a magnetic stir bar and condenser was charged with 2-nitro-4,4'-dibromobiphenyl (2.68 g, 7.5 mmol), triphenylphosphine (4.92 g, 18.8 mmol),

and tetralin (16 mL). The reaction mixture was heated to 210°C with a nitrogen balloon attached for 2hrs. The crude residue was purified by flash chromatography (12 g column, 5% to 50% DCM in hexanes) to afford 9H-2,7-dibromocarbazole as brown solid (1.79 g, 74%). ^{1}H NMR (600 MHz; $CDCl_3$): δ 8.06 (s, 1H), 7.88 (d, 2H), 7.59 (d, 2H), 7.37-7.35 (dd, 2H).

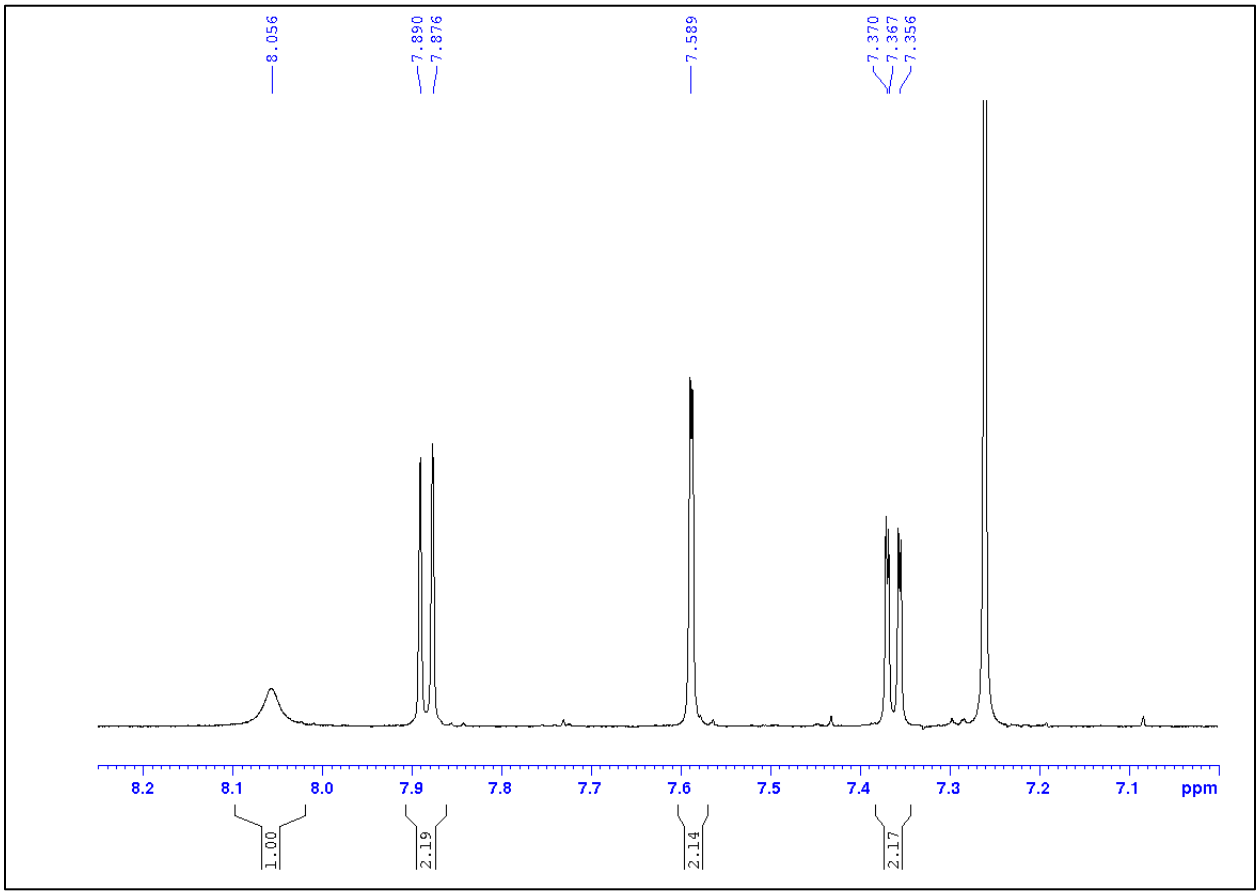

Figure 27: ^{1}H NMR of 9H-2,7-dibromocarbazole in $CDCl_3$.

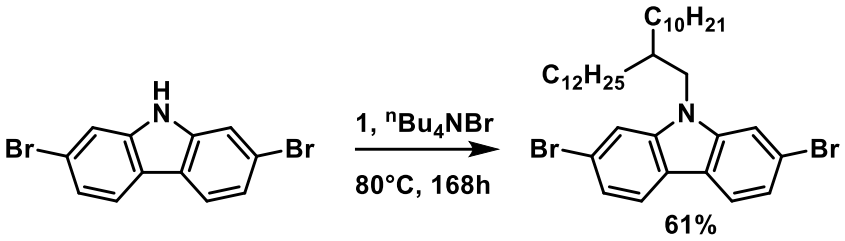

Scheme 22: Reaction to form N-(2'-decyltetradecane)-2,7-dibromocarbazole.

N-(2'-decyltetradecane)-2,7-dibromocarbazole (Adapted from reference 88)

A 250 mL round-bottom flask equipped with a magnetic stir bar was charged with 1-bromo-2-decyl-4-tetradecane (2.27 g, 5.4 mmol), toluene (10 mL), and sat. KOH (14 mL). The biphasic mixture was sparged with nitrogen for 1 hour, and then 9H-2,7-dibromocarbazole (1.60 g, 5.0 mmol) and tetrabutylammonium bromide (0.31 g, 0.97 mmol) were added. The reaction mixture was heated to 80 °C under an inert atmosphere for 168 hours. The organic phase was isolated using liquid-liquid extraction using three extractions of 100 mL diethyl ether. The black organic phase was then concentrated in vacuo to produce a thick black oil. The crude product was then purified using flash chromatography (120 g fine silica column 100% hexanes). The pure fractions were combined and concentrated but remained a liquid due to residual alkyl chains. The product was then precipitated by adding a 3:1 mixture of methanol:acetone and cooled to -20°C. The product was then filtered to afford *N*-(2'-decyltetradecane)-2,7-dibromocarbazole as a white solid (1.99 g, 61%). ^{1}H NMR (600 MHz; $CDCl_3$): δ 7.88 (d, 2H), 7.50 (d, 2H), 7.34 (dd, 2H), 4.06 (d, 2H), 2.08 (m, 1H), 1.37-1.21 (m, 40H), 0.88 (t, 6H).

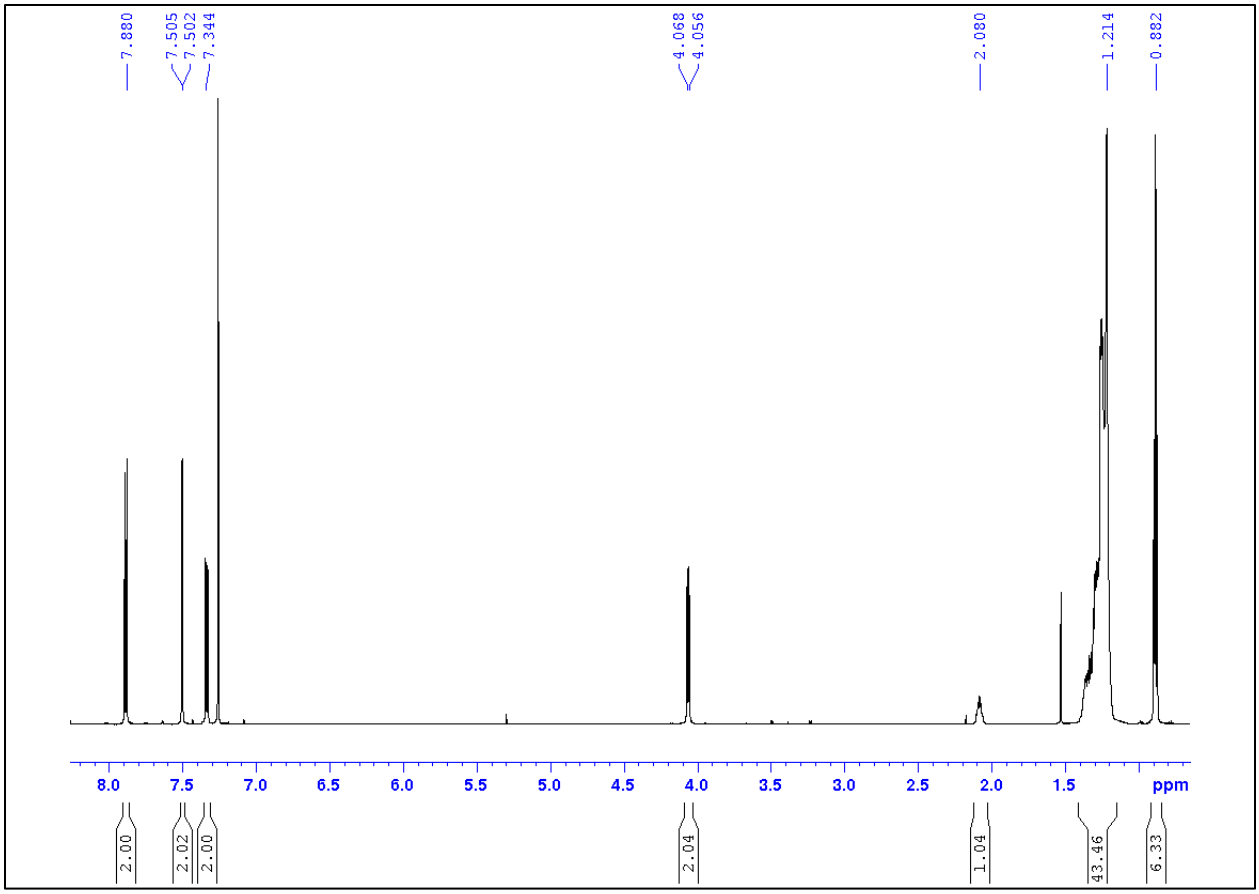

Figure 28: ^{1}H NMR of N-(2'-decyltetradecane)-2,7-dibromocarbazole in $CDCl_3$.

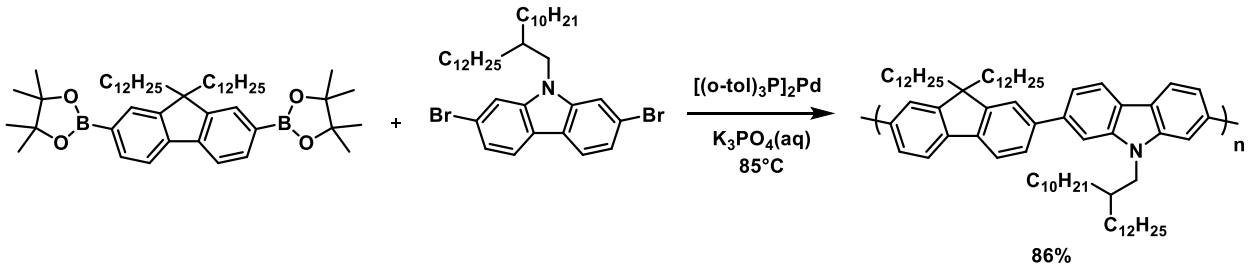

Scheme 23: Synthesis of Poly(9,9'-didodecylfluorene-co-N-(2'-decyltetradecane)-carbazole) (P1).

Poly(9,9'-didodecylfluorene-co-N-(2'-decyltetradecane)-carbazole) (P1) (Adapted from reference 88)

A 25 mL Schlenk tube was equipped with a magnetic stir bar and charged with *N*-(2'-decyltetradecane)-2,7-dibromocarbazole (200 mg, 0.30 mmol), 2,2'-(9,9-didodecylfluorene-2,7-diyl)bis(4,4,5,5-tetramethyl-1,3,2-dioxaborolane) (226 mg, 0.30 mmol), toluene (2.5 mL), and 3M

K_3PO_4 (2.5 mL) and the reaction mixture was degassed via three freeze-pump-thaw cycles. The biphasic mixture was frozen under liquid nitrogen, then $((o\text{-}tol)_3P)_2Pd$ (11 mg, 7.5 µmol) was added under a positive pressure of nitrogen. The Schlenk tube was evacuated and backfilled with nitrogen three times, and the reaction mixture was vigorously stirred at 85 °C for 2 hours. The phases were allowed to separate, and the organic layer was pipetted off. The organic layer was filtered through a plug of 1:1 celite and neutral alumina. The plug was washed with THF until the flow-through no longer fluoresced and the filtrate was concentrated in vacuo. The crude polymer was precipitated into chilled methanol (150 mL) and then filtered to afford P1 as a yellow solid (260 mg, 86%). ^{1}H NMR (600 MHz; $CDCl_3$): 8.21 (m, 2H), 7.85 (m, 2H), 7.74 (m, 4H), 7.70 (m, 2H), 7.60 (m, 2H), 4.34 (m, 2H), 2.31 (m, 1H), 2.13 (m, 4H), 1.24 (m, 80H), 0.84 (m, 12H).

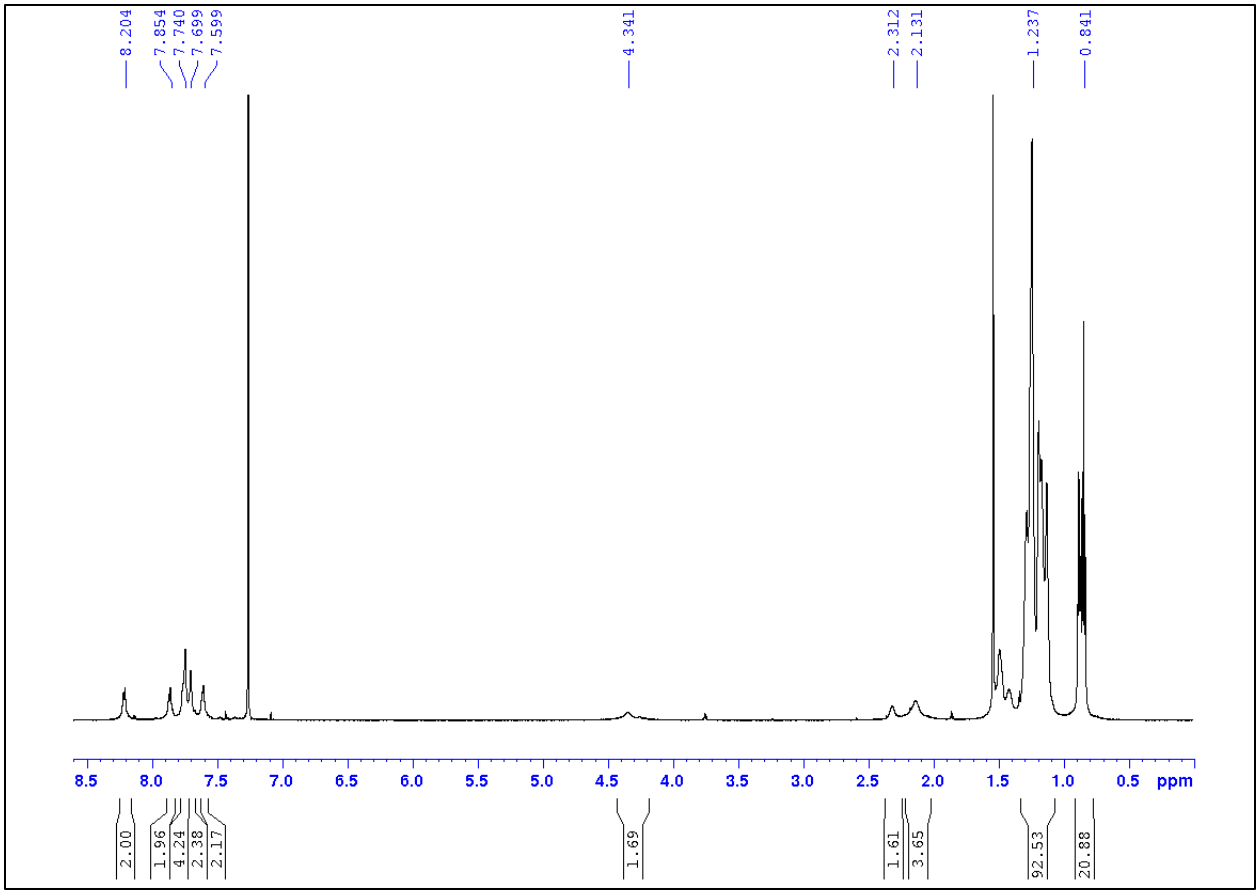

Figure 29: ^{1}H NMR spectrum of Poly(9,9'-didodecylfluorene-co-N-(2'-decyltetradecane)-carbazole) in $CDCl_3$.

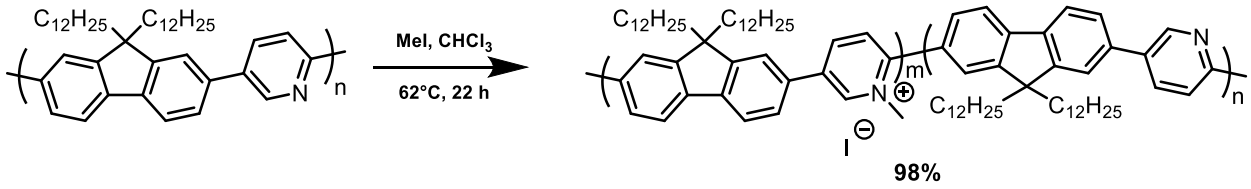

Scheme 24: Synthesis of Methylated PF-Py (Me-PF-Py).

Methylated PF-Py (Me-PF-Py) (Adapted from reference 88)

A Schlenk tube equipped with a magnetic stir bar was charged with PF-Py (50 mg, 87 µmol, Mn 13 kDa), MeI (1080 µL, 17 mmol), and chloroform (5 mL) and the reaction mixture was heated to reflux for 22 hours. The reaction mixture was then transferred to a pre-weighed glass vial and the solvent was removed by passing a stream of nitrogen over the vial, followed by drying

the sample under high vacuum overnight. Me-PF-Py was isolated as a red solid (63 mg, 98%). ^{1}H NMR (600 MHz; $CDCl_3$): δ 9.09-7.68 (m), 4.72 (m), 2.15-2.12 (m), 1.25-0.85 (m).

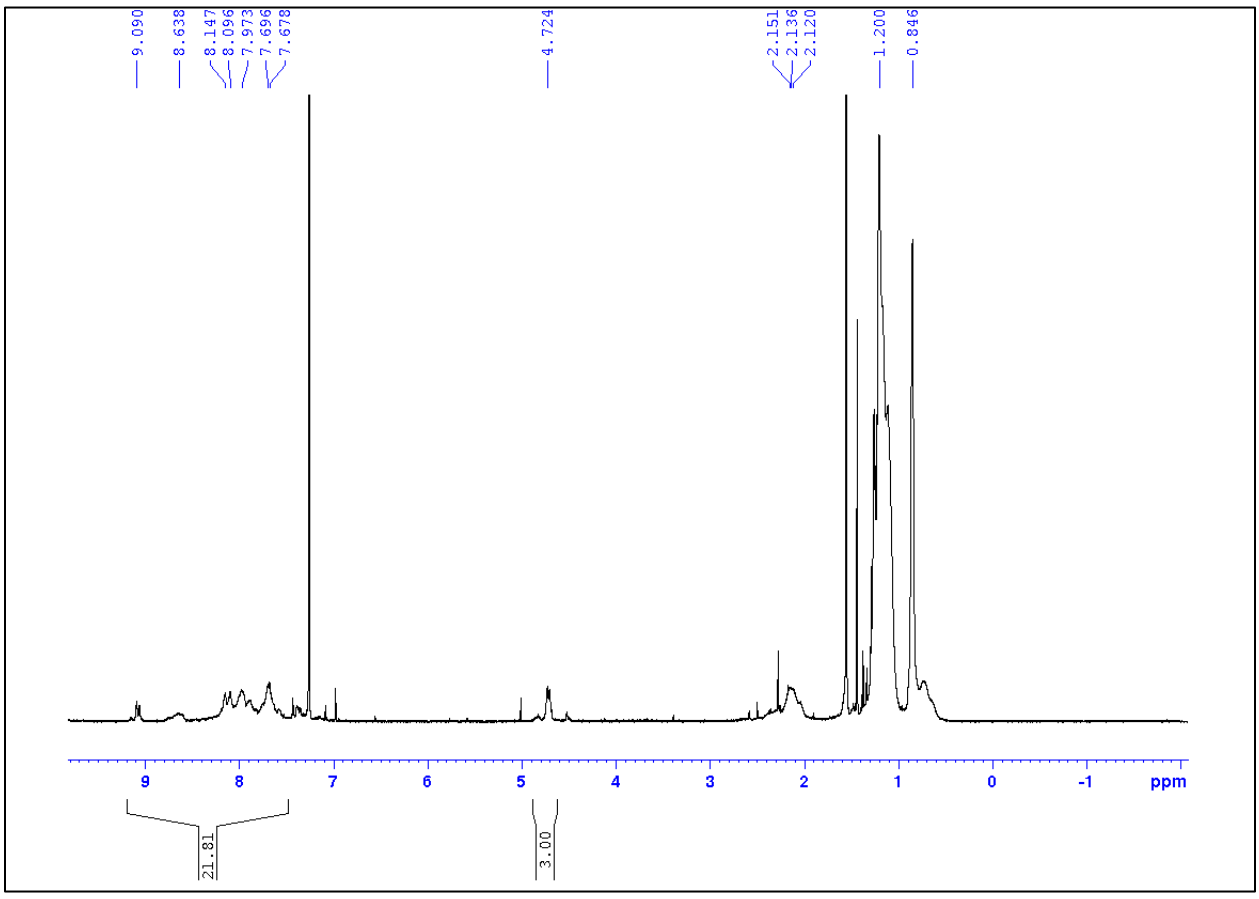

Figure 30: ^{1}H NMR spectrum of Me-PF-Py in $CDCl_3$.

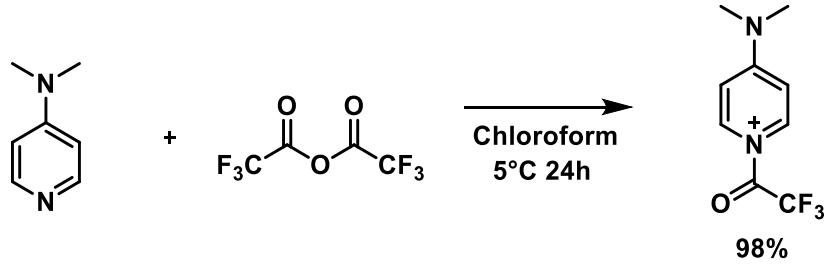

Scheme 25: Synthesis of acetylated 4-dimethylaminopyrdine.

Acetylated dimethylaminopyrdine

A 5 mL round bottom flask equipped with a magnetic stir bar and condenser was charged with 4-Dimethylaminopyidine (0.439 g, 3.6 mmol), and DCM (2 mL). The reaction mixture was cooled to 0°C in an ice bath and trifluoroacetic anhydride (0.756 g, 0.5 mL, 3.6 mmol) was added. The reaction mixture turned to a white slurry in 1 minute but continued to stir in the ice bath for 30 minutes. The white slurry was then filtered, dried, and collected to afford acetylated dimethylaminopyridine (0.777 g, 98%) ^{1}H NMR (600 MHz; $CDCl_3$): δ 8.22 (d, 2H), 6.734 (d, 2H), 3.25 (s, 6H).

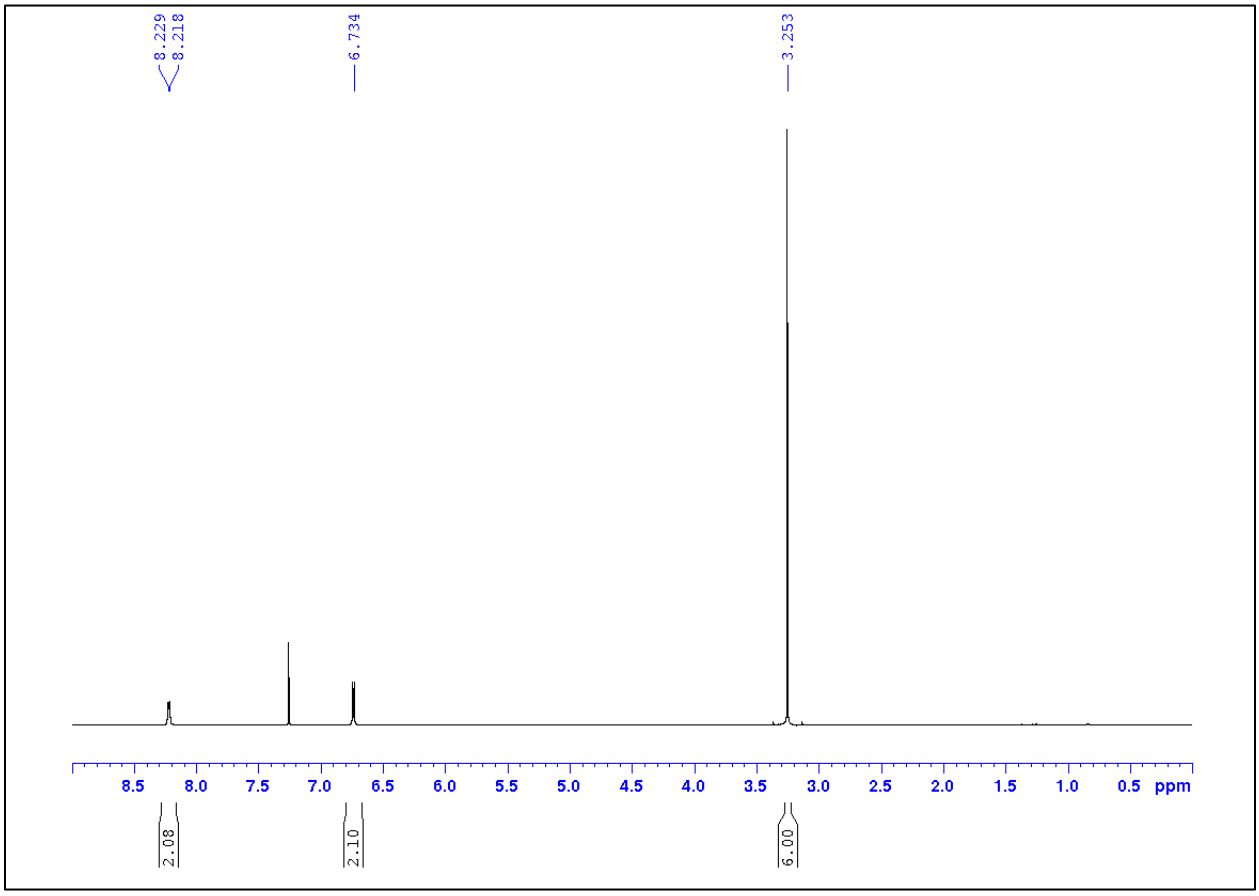

Figure 31: ^{1}H NMR spectrum of acetylated dimethylaminopyridine in $CDCl_3$.

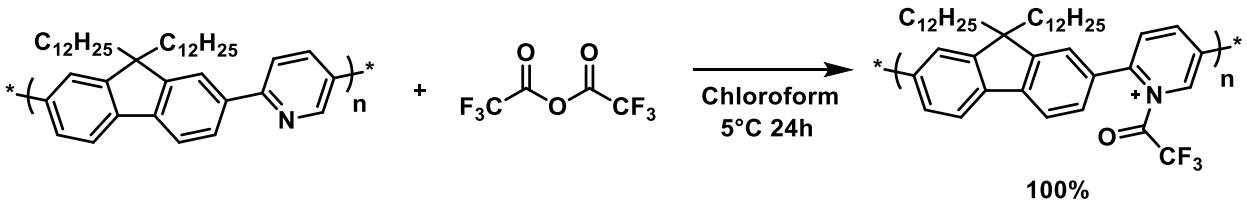

Scheme 26: Synthesis of Acetylated PF-Py (A-PF-Py).

Acetylated PF-Py (A-PF-Py)

A 20 mL vial equipped with a magnetic stir bar was charged with PF-Py (0.050 g, 84 µmol, Mn 13 kDa), and chloroform 1 mL. The reaction mixture was cooled to 0°C in an ice bath and trifluoroacetic anhydride (1.82 g, 1.17 mL, 8.6 mmol) was added. The reaction mixture turned dark red after a few minutes. The solution was left stirring in ice for 24 hours. The product was then dried under high vacuum for 24 hours to afford acetylated PF-Py (0.058 g, 100%). ^{1}H NMR (600 MHz; $CDCl_3$): δ 9.26-9.14 (1H, d), 8.66-7.69 (8H, m), 2.14 (4H, m), 1.22 (40H, m), 0.87 (6H, s).

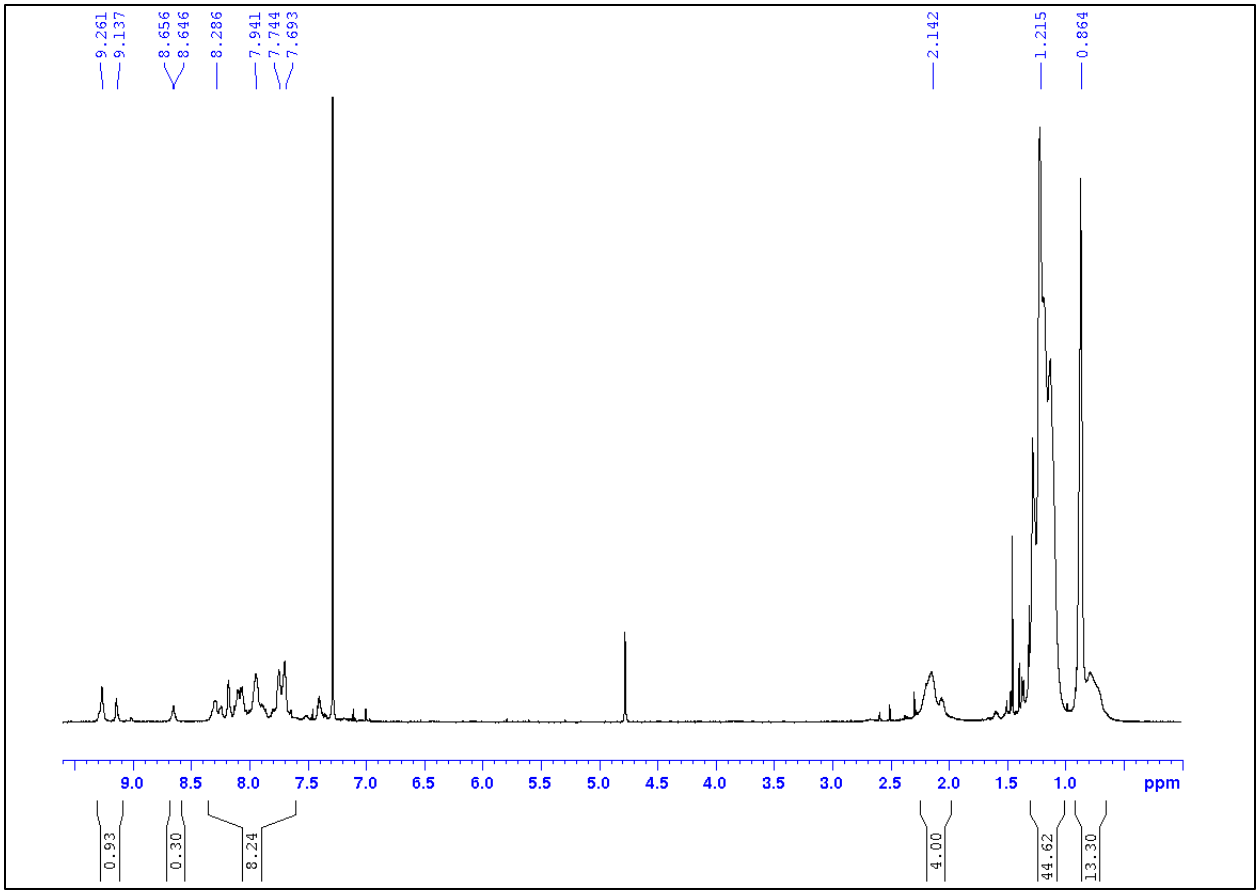

Figure 32: ^{1}H NMR spectrum of acetylated PF-Py $CDCl_3$ and D_2O.

3.5 Supporting Information

3.5.1 Atomic Force Microscopy (AFM)

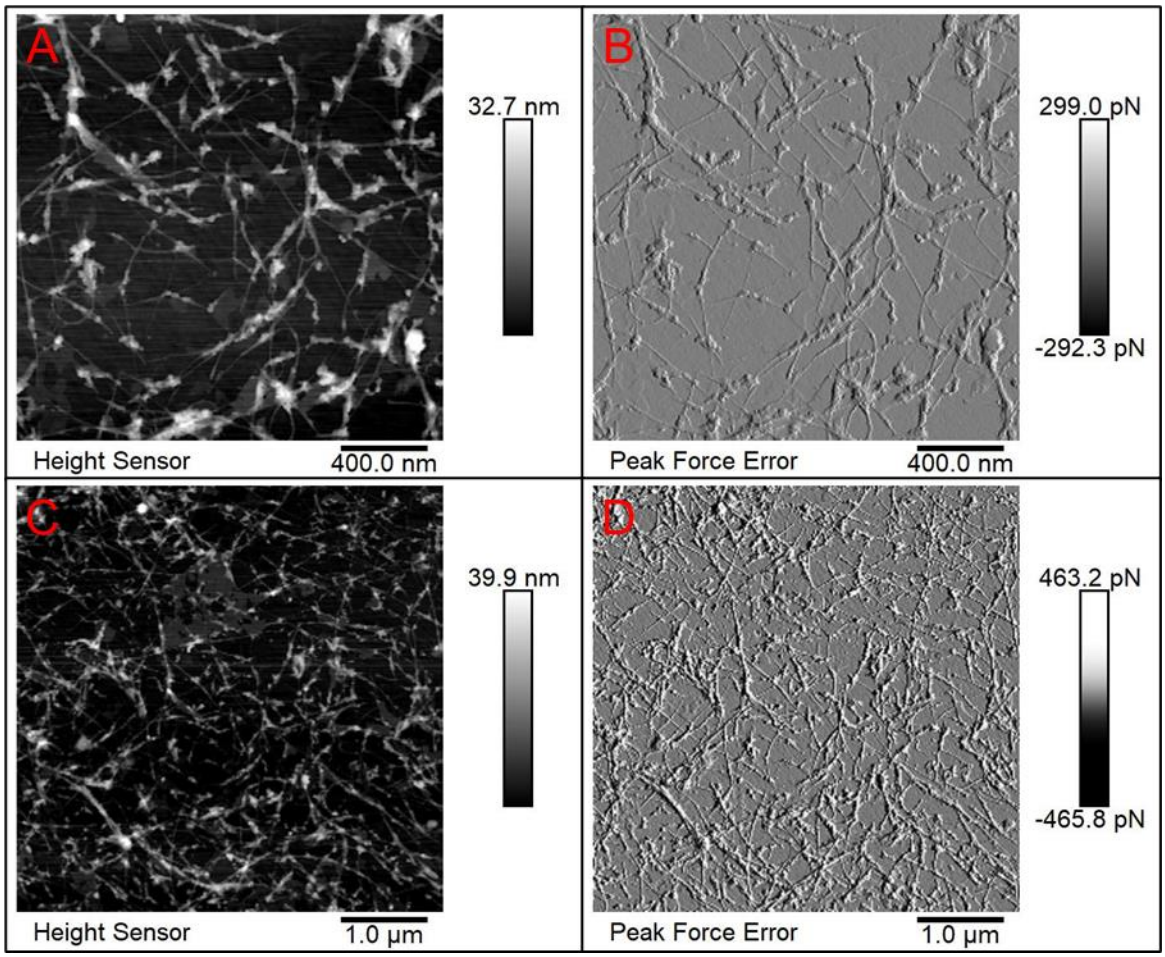

Figure 33: Atomic force microscopy (AFM) of 0.5:1 A-PF-Py dispersions showing polymer wrapped SWNTs. a) and b) 2 µm scale, c) and d) 5 µm scale.

3.5.2 Additional UV-vis-NIR Absorption Spectra

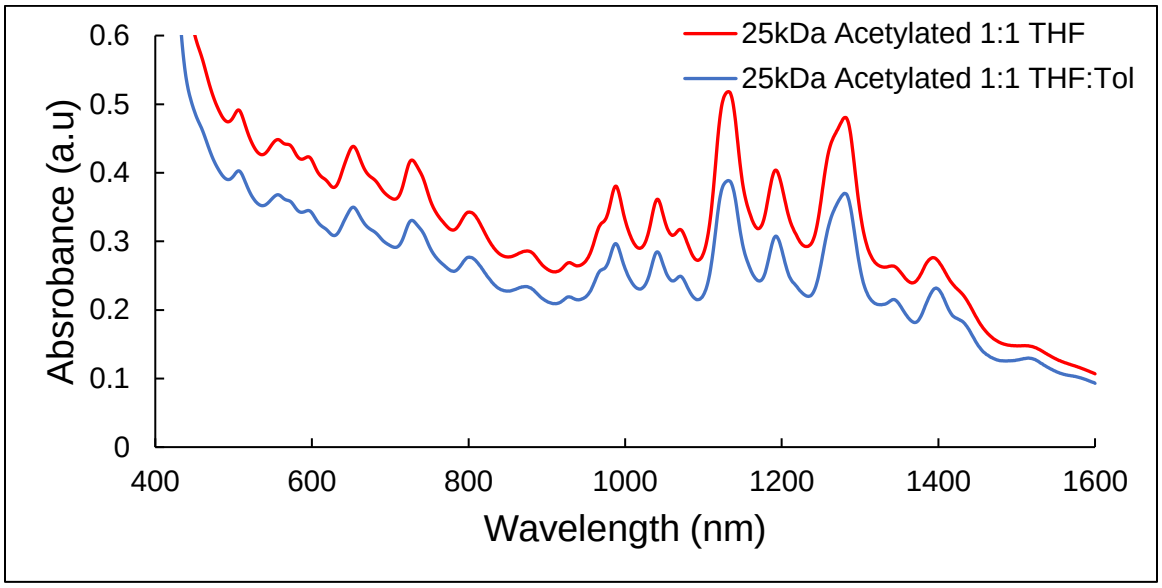

Figure 34: Unnormalized UV-vis-NIR absorption spectra for the A-PF-Py-SWNTs dispersant solvent study using HiPCO SWNTs. 25 kDa Acetylated 1:1 THF diluted 1:20. 25 kDa Acetylated 1:1 THF:Tol diluted 1:20.

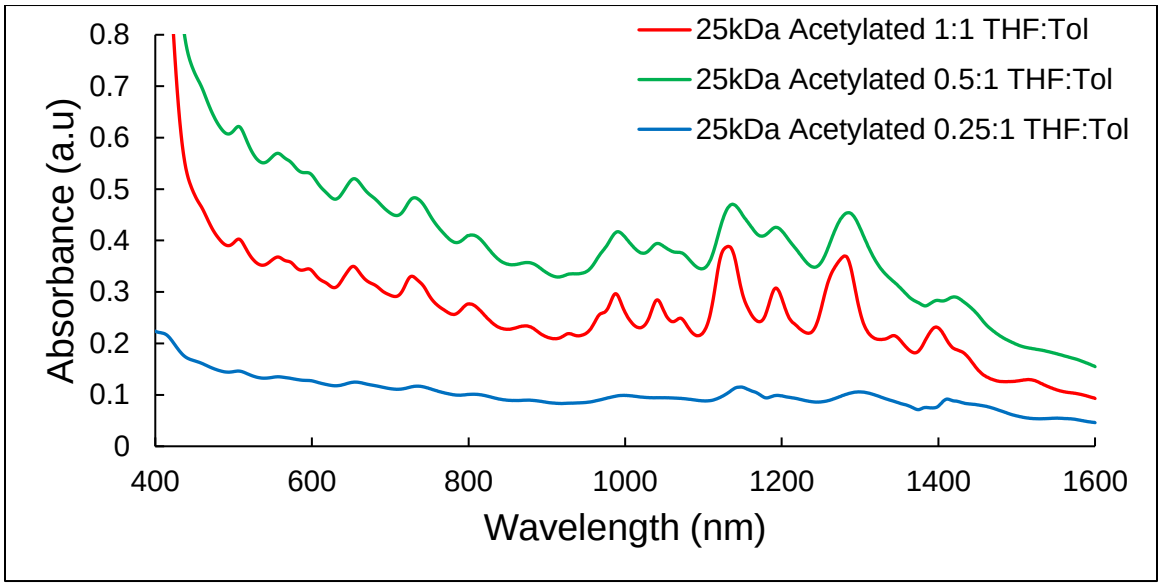

Figure 35: Unnormalized UV-vis-NIR absorption spectra for the A-PF-Py-SWNTs ratio study using HiPCO SWNTs. 25 kDa Acetylated 1:1 THF:Tol diluted 1:20. 25 kDa Acetylated 0.5:1 THF:Tol undilute. 25 kDa Acetylated 0.25:1 THF:Tol undilute.

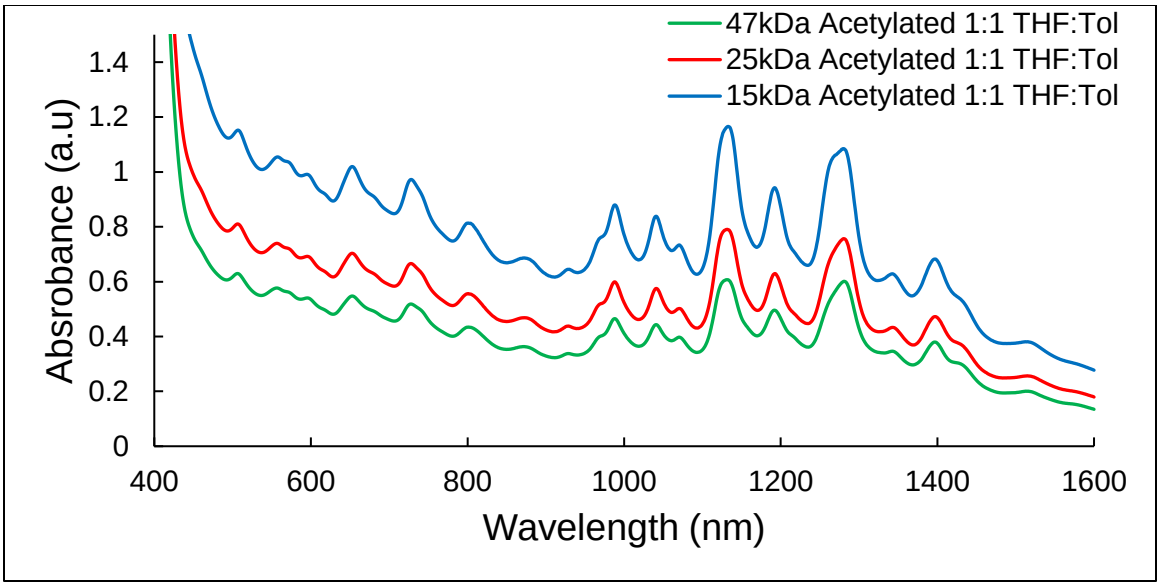

Figure 36: Unnormalized UV-vis-NIR absorption spectra for the A-PF-Py-SWNTs molecular weight study using HiPCO SWNTs. 47 kDa Acetylated 1:1 THF:Tol diluted 1:10. 25 kDa Acetylated 1:1 THF:Tol 1:10. 13 kDa Acetylated 0.25:1 THF:Tol 1:10.

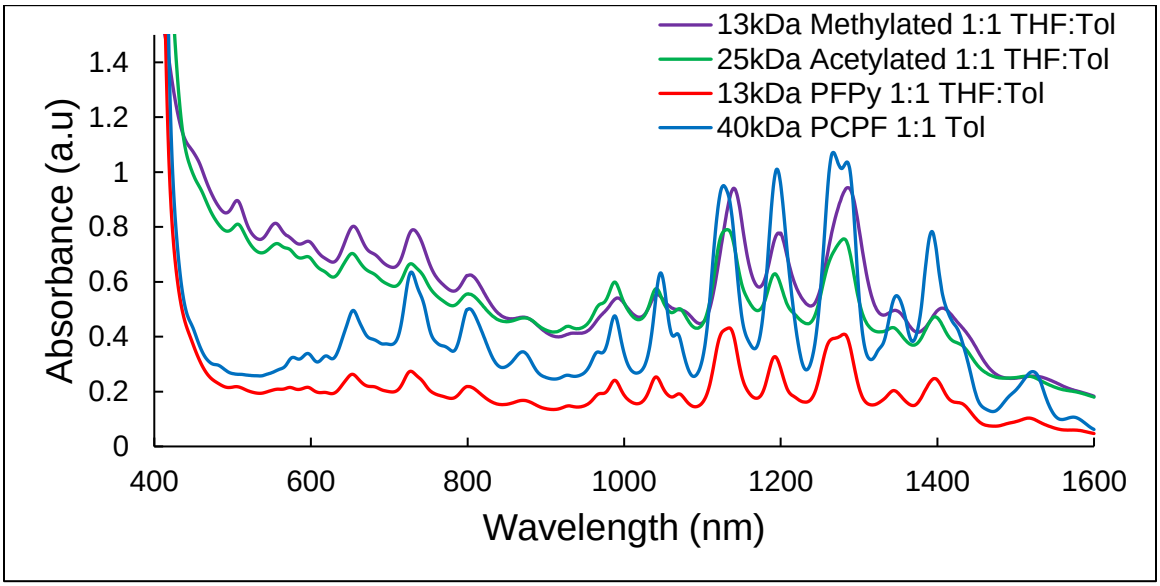

Figure 37: Unnormalized UV-vis-NIR absorption spectra for all polymer-SWNT study using HiPCO SWNTs. 13 kDa Methylated 1:1 THF:Tol Undilute. 25 kDa Acetylated 1:1 THF:Tol 1:10. 13 kDa PF-Py 1:1 THF:Tol 1:4 Dilution, 40 kDa PCPF 1:1 Tol Undilute.

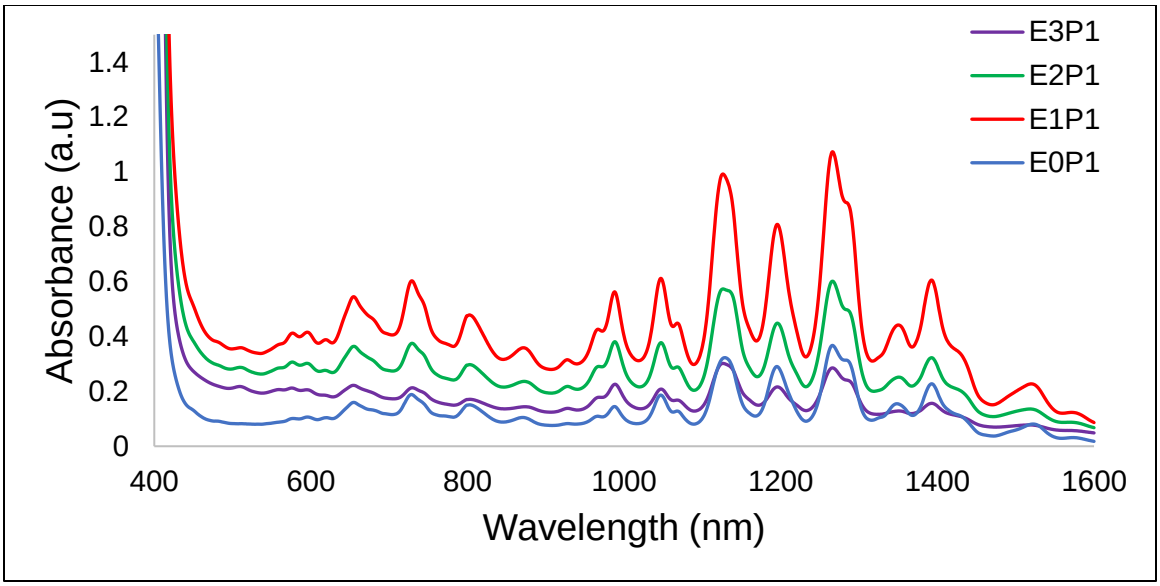

Figure 38: Unnormalized UV-vis-NIR absorption spectra for the P1-SWNTs molecular extraction study using HiPCO SWNTs. All 1:4 dilution in 1:1 Toluene.

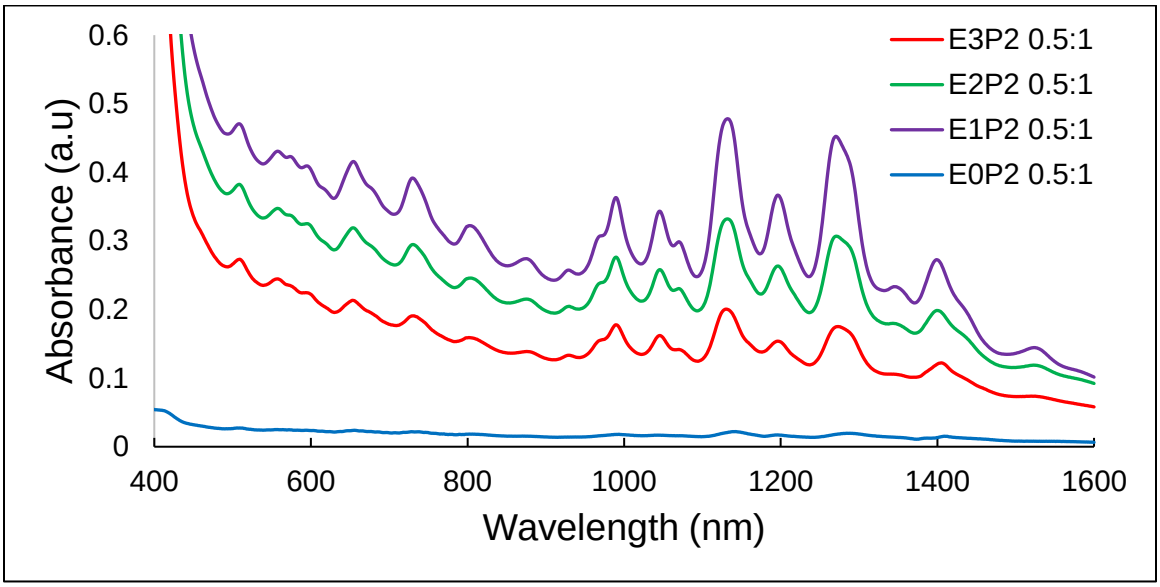

Figure 39: Unnormalized UV-vis-NIR absorption spectra for the 0.5:1, A-PF-Py-SWNTs molecular extraction study using HiPCO SWNTs. All 1:20 dilution in 1:1 THF:Toluene.

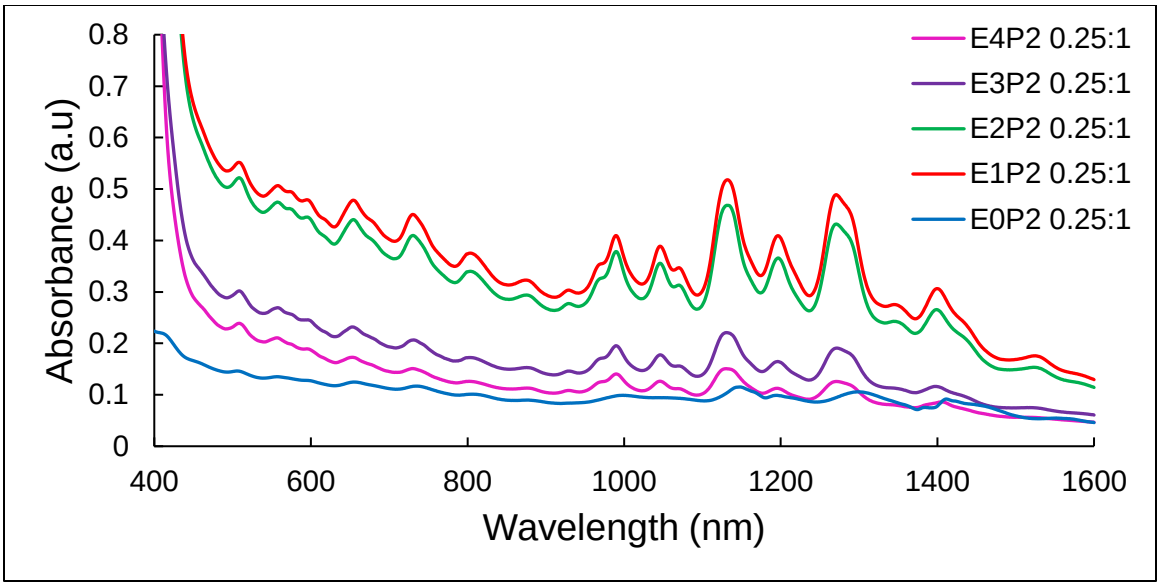

Figure 40: Unnormalized UV-vis-NIR absorption spectra for the 0.25:1, A-PF-Py-SWNTs molecular extraction study using HiPCO SWNTs. All 1:20 dilution in 1:1 THF:Toluene, except E0P2 which is undilute.

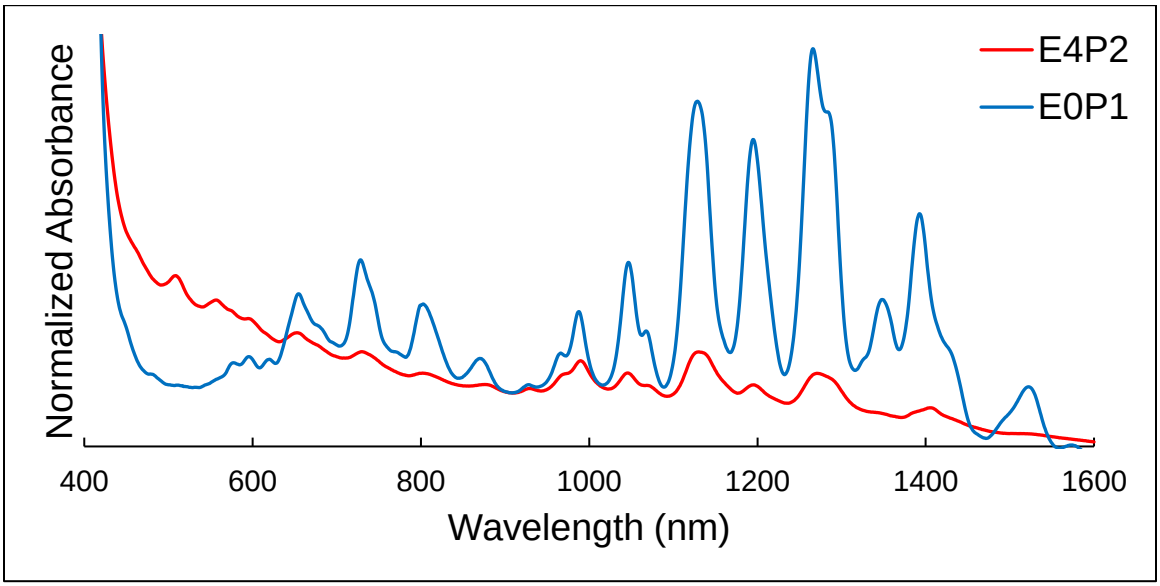

Figure 41: Normalized UV-vis-NIR absorption spectra for the E4P2 0.25:1 vs. E0P1 comparison using HiPCO SWNTs.

3.5.3 Photographs of Polymers and SWNT Dispersions

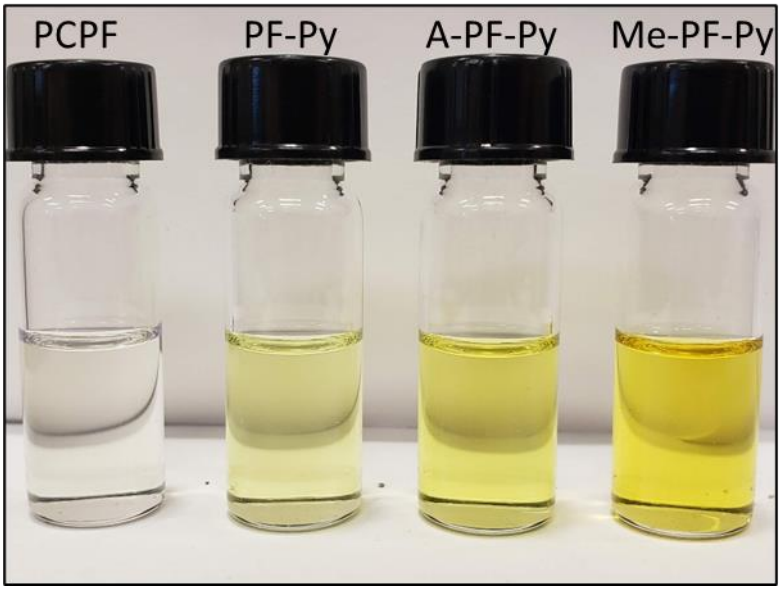

Figure 42: Photograph of polymers dissolved in 1:1 THF:Tol (left to right): PCPF, PF-Py, A-PF-Py, Me-PF-Py.

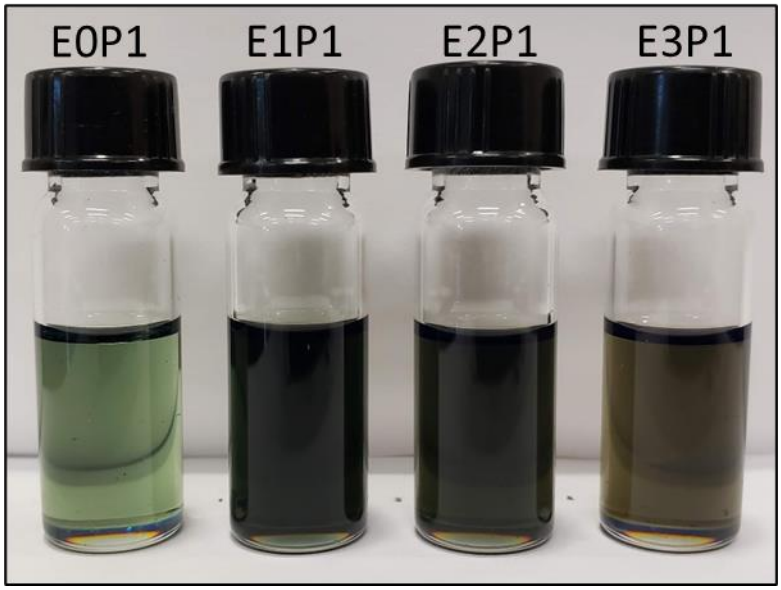

Figure 43: Photograph of PC-PF-SWNT dispersions produced using HiPCO SWNTs (left to right): E0P1, E1P1, E2P1, E3P1.

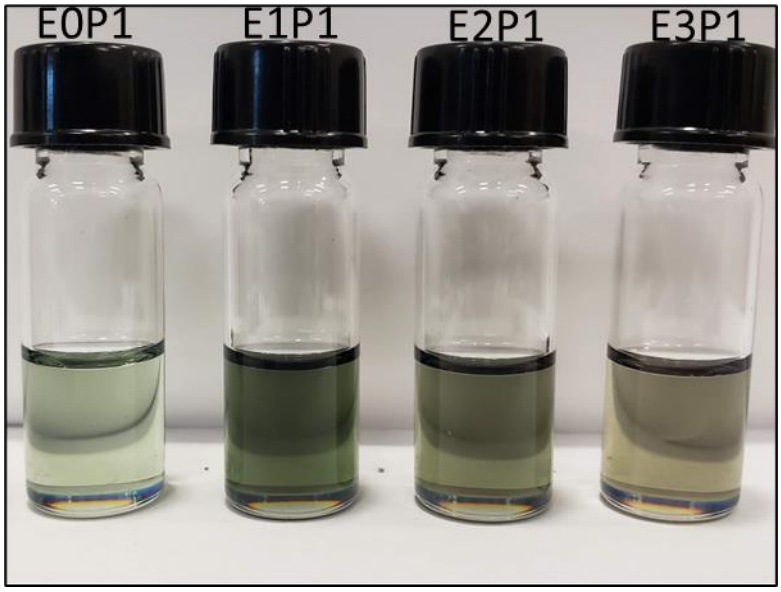

Figure 44: Photograph of PC-PF-SWNT dispersions, diluted 1:2, produced using HiPCO SWNTs (left to right): E0P1, E1P1, E2P1, E3P1.

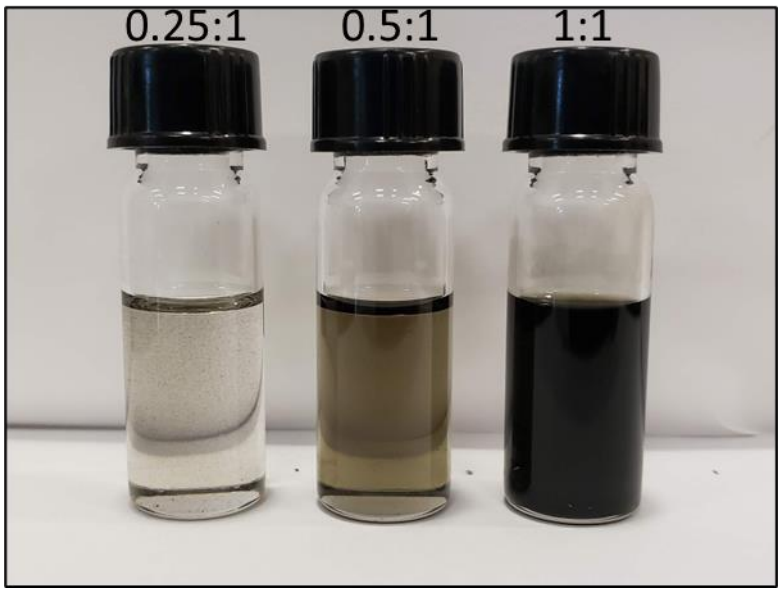

Figure 45: Photograph of A-PF-Py-SWNT dispersions produced using HiPCO SWNTs (left to right): 0.25:1, 0.5:1, 1:1.

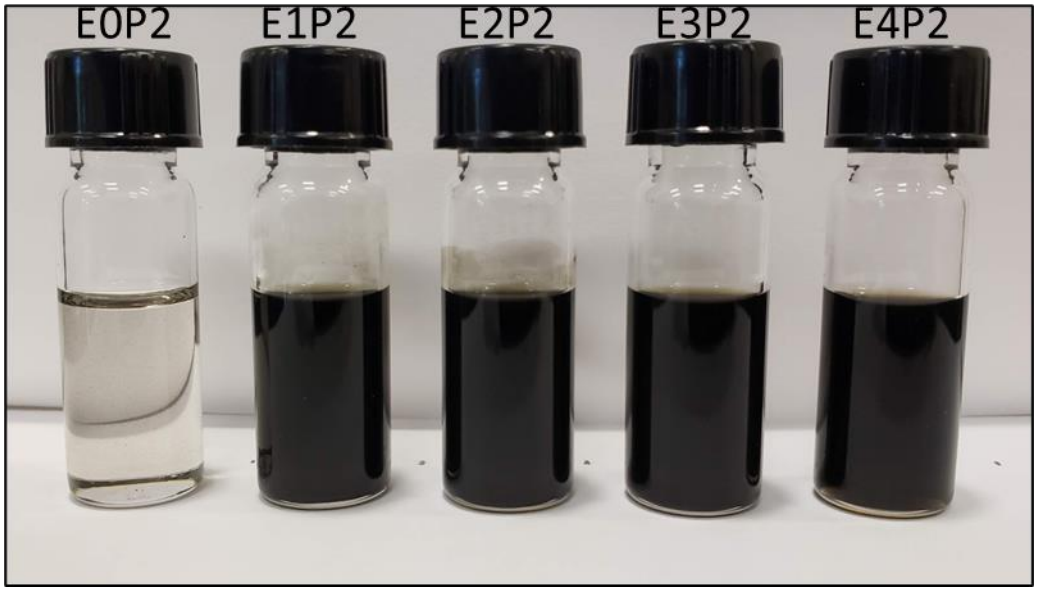

Figure 46: Photograph of 0.25:1, A-PF-Py-SWNT dispersions produced using HiPCO SWNTs (left to right): E0P2, E1P2, E2P2, E3P2, and E4P2.

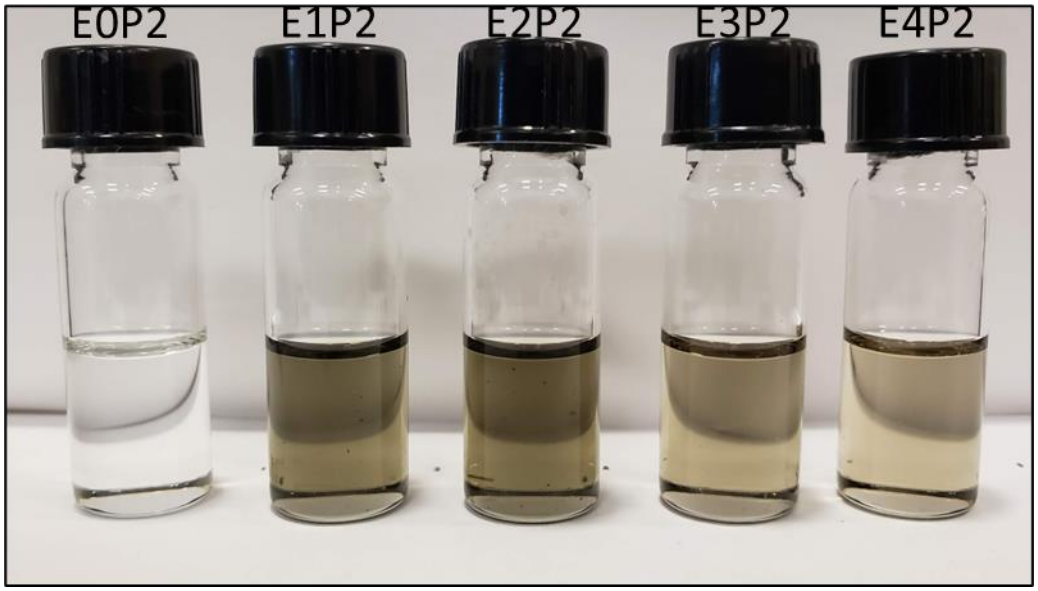

Figure 47: Photograph of 0.25:1, A-PF-Py-SWNT dispersions, dilute 1:20, produced using HiPCO SWNTs (left to right): E0P2, E1P2, E2P2, E3P2, and E4P2.

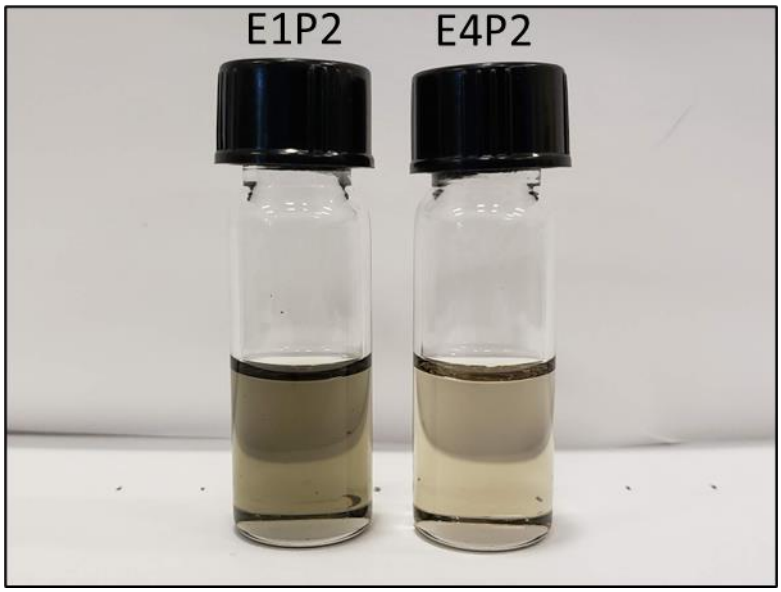

Figure 48: Photograph of 0.25:1, A-PF-Py-SWNT dispersions, dilute 1:20, produced using HiPCO SWNTs (left to right): E1P2, and E4P2.

3.5.4 Thermogravimetric Analysis (TGA) Data

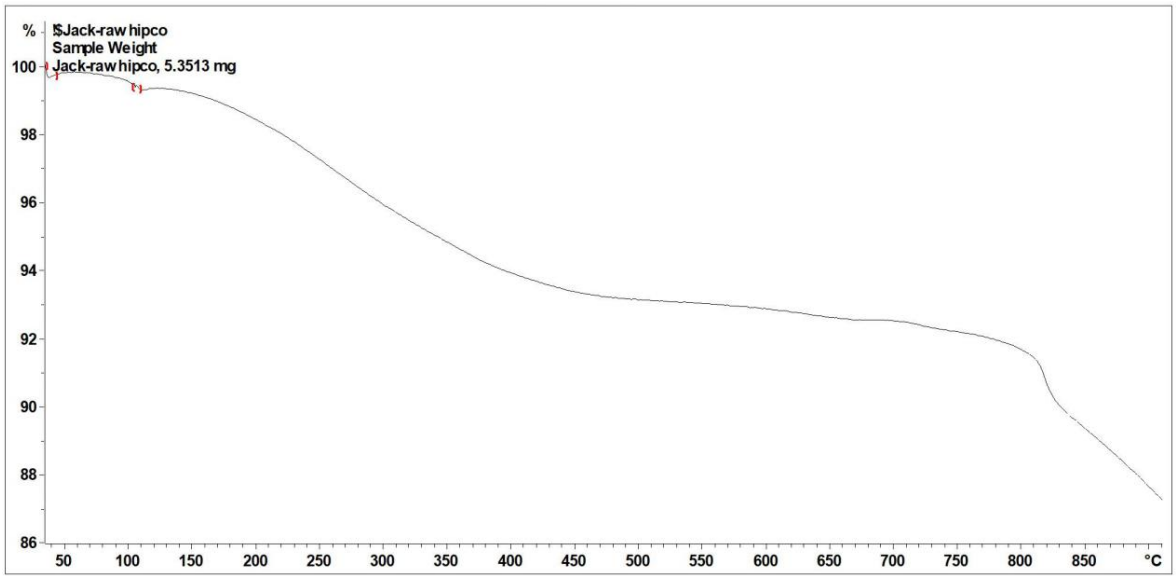

Figure 49: TGA of raw HiPCO SWNTs.

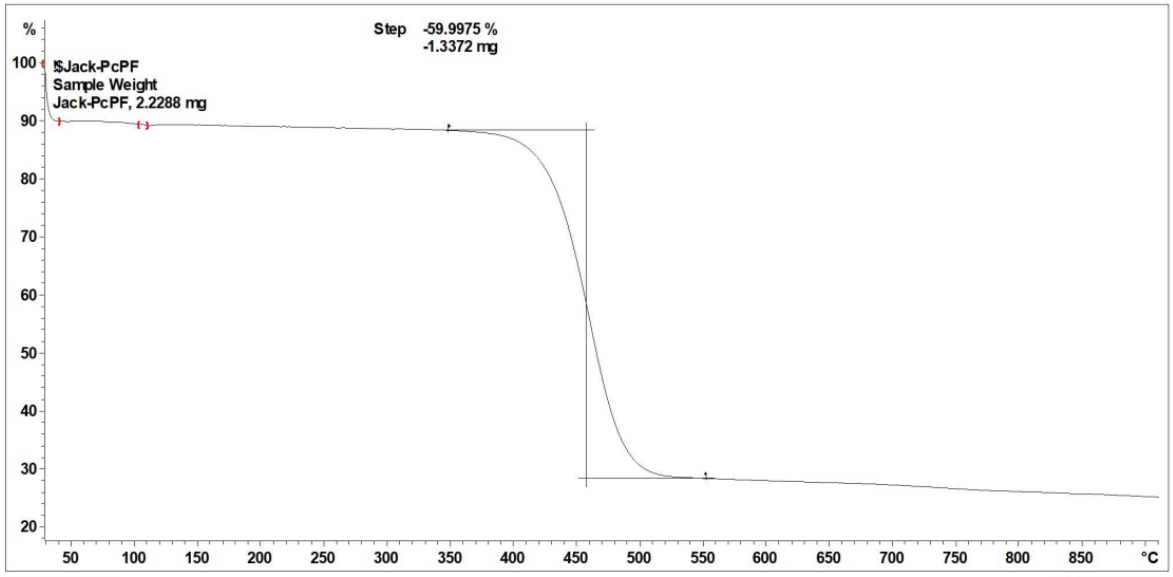

Figure 50: TGA of PC-PF.

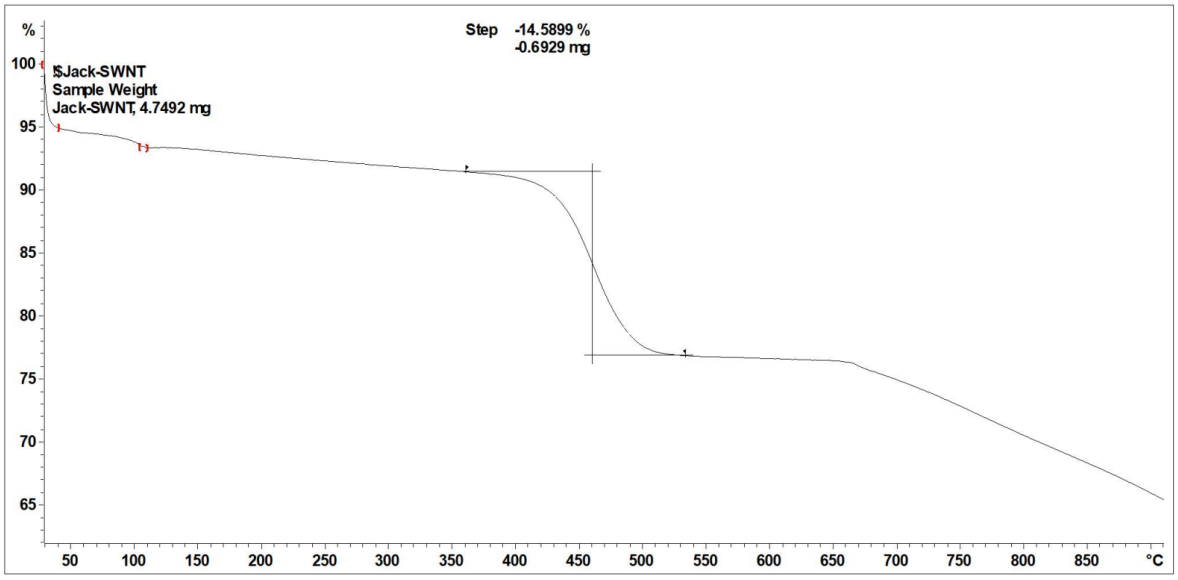

Figure 51: TGA of residue after dispersion with PCPF:HiPCO SWNTs and rinsed thoroughly with THF.

Chapter 4: Overall Conclusions and Future Work

4.1 General Conclusions

Despite CNTs being the subject of intensive research since their discovery, there remain challenges for incorporating them into materials to produce devices. The heterogenous nature of produced SWNT sample precludes immediate device incorporation without a purification method. To purify SWNTs, conjugated polymers have been an increasingly important dispersant option. Other techniques remain difficult and expensive making them not suitable for production on the industrial scale. Conjugated polymers can be synthesized on a large scale with high yields and have shown selectivity toward different SWNTs species based on diameter or electronic type. The most intriguing method for m-SWNT enrichment involves the use of a two-polymer system composed of an electron-rich PCPF and an electron-poor Me-PF-Py. By first selectively removing the sc-SWNT using the electron-rich polymer multiple times and then dispersing with an electron-poor polymer to disperse the m-SWNTs, ~70% m-SWNTs dispersions have been obtained. However, this system still had the potential to be further improved by modification of the architecture of the electron poor polymer through substitution of a more electron withdrawing functional group.

In Chapter 2, the addition of a dinitrobenzene group to PF-Py was investigated. This reaction was unsuccessful, despite modifying reaction conditions including, temperature, solvent, molecular weight, reaction concentration, and reaction time. In Chapter 3, we explored the possibility of the addition of a trifluoroacetyl group. The synthesis was successful and allowed for a straightforward functionalization of 100% of the pyridine groups, compared to only ~50% for the methylated polymer. We also investigate how the newly discovered acetylated PF-Py (A-PF-Py) disperses SWNTs and discovered that the A-PF-Py was more selective toward m-SWTNs than

the previously investigated Me-PF-Py. Finally, we incorporate the A-PF-Py into the two-polymer extraction system and produced concentrated m-SWNT enriched samples.

The most-significant contribution of this thesis comes from the synthesis of the A-PF-Py. We were able to functionalize the PF-Py with a more electron withdrawing functional group that showed superior selectivity toward m-SWNTs than the previously used Me-PF-Py. The ability to disperse m-SWNTs on a large scale using the conjugated polymer sorting, would allow for a decrease in cost and more widespread implementation of m-SWNTs into applications. This work offers a step forward and guides the future direction of m-SWNT enrichment using conjugated polymers.

4.2 Future Work

The characterization of the SWNTs dispersion requires further work to confirm the electronic purity. The main characterization tool used to monitor the amount of m- and sc-SWNTs in each dispersion was UV-vis-NIR spectroscopy, which although is a powerful characterization method, needs to be confirmed with other techniques. Specifically, Raman spectroscopy is an important characterization tool for SWNT dispersions. Unfortunately, access to the Raman instrument was unavailable prior to the completion of this thesis due to an upgrade of the instrument. Additionally, photoluminescence (PL) mapping would be a useful tool to further characterize the SWNT dispersions. PL mapping would allow for qualitative monitoring of both sc- and m-SWNT species depending on how intense the PL is for the sc-SWNT species. Atomic force microscopy (AFM) may also be a potential characterization method and can allow the detection of SWNT electronic species via the conductivity. The ability to precisely detect the species of each SWNT was not yet possible during the present studies. Similarly, conductivity testing requires further exploration. The conductivity of all dispersions should be measured in

triplicate. It is expected that the conductivity will increase as the quantity of m-SWNT increases. In summary, the characterization methods of Raman, PL, AFM, and four-point probe conductivity in addition to the UV-vis-NIR spectroscopy data in this thesis is necessary to fully characterize the presence of each SWNT electronic species.

The main benefit of conjugated polymer sorting is the scalability to an industrial scale. Dispersions investigated in this thesis were on a 10mL scale, which can purify a 5mg sample of SWNTs, already three orders of magnitude more sample than what other existing purification techniques, such as DGU, achieve. However, this scale is expected to be able to be increased further and experiments increasing the scale need to be performed with the A-PF-Py polymer to confirm enrichment is still possible at higher scales.

There also remains work to be done investigating plasma torch-SWNTs. The dispersion protocols have been optimized for HiPCO SWNTs and will need to be reoptimized for the plasma-torch dispersions.

The development of a removable polymer-SWNT process is also required, to fully benefit from the m-SWNT electronic properties. The conjugated polymer strongly adheres to the SWNT surface through non-covalent interactions which makes the removal of the polymer difficult. To address this issue, attempts have been made to anneal polymer-SWNT samples at high temperatures to remove the polymer side chains or to decompose the polymer backbone. This technique may be possible to be apply to the currently designed polymer-SWNT complexes.

Finally, this thesis established that acetylation is straightforward reaction that can be used post polymerization on the pyridine unit. Preparing a polymer containing a pyrazine monomer unit and adding two acetyl groups may be possible. This could increase the electron deficiency of the

polymer backbone and may enhance m-SWNT selectivity. Another interesting study would involve functionalization of the pyridine with difluoroacetyl or monofluoroacetyl moieties which would allow for direct comparison of more electron withdrawing substituents.

References

(1) Iijima, S. Growth of Carbon Nanotubes. *Mater. Sci. Eng. B* **1993**, *19* (1–2), 172–180. https://doi.org/10.1016/0921-5107(93)90184-O.

(2) Kiang, C. H.; Devries, M. S.; Gorman, G.; Savoy, R.; Bethune, D. S.; Klang, C. H.; De-Vries, M. S.; Vazquez, J.; Beyers, R. Cobalt-Catalysed Growth of Carbon Nanotubes with Single-Atomic-Layer Walls. *Nature* **1993**, *363* (6430), 605–607. https://doi.org/10.1038/363605a0.

(3) Terrones, M. Science and Technology of the Twenty-First Century: Synthesis, Properties, and Applications of Carbon Nanotubes. *Annu. Rev. Mater. Res.* **2003**, *33*, 419–501. https://doi.org/10.1146/annurev.matsci.33.012802.100255.

(4) Yu, M. F.; Files, B. S.; Arepalli, S.; Ruoff, R. S. Tensile Loading of Ropes of Single Wall Carbon Nanotubes and Their Mechanical Properties. *Phys. Rev. Lett.* **2000**, *84* (24), 5552–5555. https://doi.org/10.1103/PhysRevLett.84.5552.

(5) Avouris, Phaedon, Chen Zhihong, P. V. Carbon-Based Electronics. *Nat. Nanotechnoloy* **2007**, *2* (10), 605–615. https://doi.org/10.1038/nnano.2007.300.

(6) Avouris, P. Molecular Electronics with Carbon Nanotubes. *Acc. Chem. Res.* **2002**, *35* (12), 1026–1034. https://doi.org/10.1021/ar010152e.

(7) Han, Z.; Fina, A. Thermal Conductivity of Carbon Nanotubes and Their Polymer Nanocomposites: A Review. *Prog. Polym. Sci.* **2011**, *36* (7), 914–944. https://doi.org/10.1016/j.progpolymsci.2010.11.004.

(8) Collins, P. G.; Avouris, P. Nanotubes for Electronics. *Sci. Am.* **2000**, *283* (December), 62–

69. https://doi.org/10.1038/scientificamerican1200-62.

(9) Kataura, H.; Kumazawa, Y.; Maniwa, Y.; Umezu, I.; Suzuki, S.; Ohtsuka, Y.; Achiba, Y. Optical Properties of Single-Wall Carbon Nanotubes. *Synth. Met.* **1999**, *103* (1–3), 2555–2558. https://doi.org/10.1016/S0379-6779(98)00278-1.

(10) William James Bodnaryk. Purification of Semiconducting and Metallic Single-Walled Carbon Nanotubes Using Conjugated Polymers, 2020.

(11) Cruz-silva, E.; Cullen, D. A.; Gu, L.; Romo-herrera, J. M.; Muñoz-sandoval, E.; López-urías, F.; Sumpter, B. G.; Meunier, V.; Charlier, J.; Smith, Ḱ. D. J.; Terrones, H.; Terrones, M. Heterodoped Nanotubes: Theory, Synthesis, and Characterization of Phosphorus-Nitrogen Doped Multiwalled Carbon Nanotubes. *ACS Nano* **2008**, *2* (3), 441–448. https://doi.org/10.1021/nn700330w.

(12) Dürkop, T.; Getty, S. A.; Cobas, E.; Fuhrer, M. S. Extraordinary Mobility in Semiconducting Carbon Nanotubes. *Nano Lett.* **2004**, *4* (1), 35–39. https://doi.org/10.1021/nl034841q.

(13) Demirkol, D. O.; Timur, S. Chitosan Matrices Modified with Carbon Nanotubes for Use in Mediated Microbial Biosensing. *Microchim. Acta* **2011**, *173* (3–4), 537–542. https://doi.org/10.1007/s00604-011-0596-1.

(14) Cai, B.; Su, Y.; Tao, Z.; Hu, J.; Zou, C.; Yang, Z.; Zhang, Y. All-Carbon Photodetectors: Highly Sensitive Broadband Single-Walled Carbon Nanotube Photodetectors Enhanced by Separated Graphene Nanosheets (Advanced Optical Materials 23/2018). *Adv. Opt. Mater.* **2018**, *6* (23), 1870089. https://doi.org/10.1002/adom.201870089.

(15) Bindl, D. J.; Brewer, A. S.; Arnold, M. S. Semiconducting Carbon Nanotube/Fullerene Blended Heterojunctions for Photovoltaic near-Infrared Photon Harvesting. *Nano Res.* **2011**, *4* (11), 1174–1179. https://doi.org/10.1007/s12274-011-0167-0.

(16) Xiang, L.; Zhang, H.; Hu, Y.; Peng, L. M. Carbon Nanotube-Based Flexible Electronics. *J. Mater. Chem. C* **2018**, *6* (29), 7714–7727. https://doi.org/10.1039/c8tc02280a.

(17) Jung, D.; Lee, K. H.; Kim, D.; Burk, D.; Overzet, L. J.; Lee, G. S. Highly Conductive Flexible Multi-Walled Carbon Nanotube Sheet Films for Transparent Touch Screen. *Jpn. J. Appl. Phys.* **2013**, *52* (3). https://doi.org/10.7567/JJAP.52.03BC03.

(18) Wei, T.; Fan, Z.; Luo, G.; Wei, F. A New Structure for Multi-Walled Carbon Nanotubes Reinforced Alumina Nanocomposite with High Strength and Toughness. *Mater. Lett.* **2008**, *62* (4–5), 641–644. https://doi.org/10.1016/j.matlet.2007.06.025.

(19) Patel, D. K.; Kim, H.; Dutta, S. D.; Ganguly, K.; Lim, K. Carbon Nanotubes-Based Nanomaterials and Their Argicultral and Biotechnological Applications. *Materials* **2020**, *13* (1679), 1–28. https://doi.org/10.3390/ma13071679.

(20) Shah, K. A.; Tali, B. A. Synthesis of Carbon Nanotubes by Catalytic Chemical Vapour Deposition: A Review on Carbon Sources, Catalysts and Substrates. *Mater. Sci. Semicond. Process.* **2016**, *41*, 67–82. https://doi.org/10.1016/j.mssp.2015.08.013.

(21) Iijima, S. Helical Microtubules of Graphitic Carbon. *Nature* **1991**, *354*, 56–58. https://doi.org/10.1038/354056a0.

(22) Lchihashi, S. lljima 8c T.; Fundamental. Single-Shell Carbon Nanotubes of 1-Nm Diameter. *Nature* **1993**, *363* (3), 603–605. https://doi.org/10.1038/363603a0.

(23) Guo, T.; Nikolaev, P.; Thess, A.; Colbert, D. T.; Smalley, R. E. Catalytic Growth of Single-Walled Manotubes by Laser Vaporization. *Chem. Phys. Lett.* **1995**, *243* (1–2), 49–54. https://doi.org/10.1016/0009-2614(95)00825-O.

(24) Kong, J.; Cassell, A. M.; Dai, H. Chemical Vapor Deposition of Methane for Single-Walled Carbon Nanotubes. *Chem. Phys. Lett.* **1998**, *292* (4–6), 567–574. https://doi.org/10.1016/S0009-2614(98)00745-3.

(25) Kim, K. S.; Cota-sanchez, G.; Kingston, C. T.; Imris, M.; Simard, B.; Soucy, G. Large-Scale Production of Single-Walled Carbon Nanotubes by Induction Thermal Plasma. *J. Phys. D Appl. Phyics* **2007**, *40*, 2375–2387. https://doi.org/10.1088/0022-3727/40/8/S17.

(26) Nikolaev, P.; Bronikowski, M. J.; Bradley, R. K.; Rohmund, F.; Colbert, D. T.; Smith, K. A.; Smalley, R. E. Gas-Phase Catalytic Growth of Single-Walled Carbon Nanotubes from Carbon Monoxide. *Chem. Phys. Lett.* **1999**, *313* (1–2), 91–97. https://doi.org/10.1016/S0009-2614(99)01029-5.

(27) Zhang, J.; Gui, H.; Liu, B.; Liu, J.; Zhou, C. Comparative Study of Gel-Based Separated Arc- Discharge , HiPCO , and CoMoCAT Carbon Nanotubes for Macroelectronic Applications. *Nano Res.* **2013**, *6* (12), 906–920. https://doi.org/10.1007/s12274-013-0368-9.

(28) Rafique, M. M. A.; Iqbal, J. Production of Carbon Nanotubes by Different Routes-A Review. *J. Encapsulation Adsorpt. Sci.* **2011**, *01* (02), 29–34. https://doi.org/10.4236/jeas.2011.12004.

(29) Journet, C.; Maser, W. K.; Bernier, P.; Loiseau, A.; Lamy de la Chapelle, M.; Lefrant, S.; Deniard, P.; Lee, R.; Fischer, J. E. Large-Scale Production of Single-Walled Carbon

Nanotubes by the Electric-Arc Technique. *Nature* **1997**, *388* (6644), 756–758. https://doi.org/10.1038/41972.

(30) Ferreira, F.; Franceschi, W.; Menezes, B.; Biagioni, A.; Coutinho, A.; Cividanes, L. Chapter One - Synthesis, Characterization, and Applciations of Carbon Nanotubes. In *Carbon-Based Nanofillers and Their Rubber Nanocomposites*; 2019; pp 1–45. https://doi.org/10.1016/C2016-0-03648-3.

(31) Li, W. Z.; Xie, S. S.; Qian, L. X.; Chang, B. H.; Zou, B. S.; Zhou, W. Y.; Zhao, R. A.; Wang, G. Large-Scale Synthesis of Aligned Carbon Nanotubes. *Science* **1996**, *274* (5293), 1701–1703. https://doi.org/10.1126/science.274.5293.1701.

(32) Smiljanic, O.; Stansfield, B. L.; Dodelet, J. P.; Serventi, A.; Désilets, S. Gas-Phase Synthesis of SWNT by an Atmospheric Pressure Plasma Jet. *Chem. Phys. Lett.* **2002**, *356* (3–4), 189–193. https://doi.org/10.1016/S0009-2614(02)00132-X.

(33) Resasco, D. E.; Alvarez, W. E.; Pompeo, F.; Balzano, L.; Herrera, J. E.; Kitiyanan, B.; Borgna, A. A Scalable Process for Production of Single-Walled Carbon Nanotubes (SWNTs) by Catalytic Disproportionation of CO on a Solid Catalyst. *J. Nanoparticle Res.* **2002**, *4* (1–2), 131–136. https://doi.org/10.1023/A:1020174126542.

(34) Hamada, N.; Sawada, S. I.; Oshiyama, A. New One-Dimensional Conductors: Graphitic Microtubules. *Phys. Rev. Lett.* **1992**, *68* (10), 1579–1581. https://doi.org/10.1103/PhysRevLett.68.1579.

(35) Hu, J.; Odom, T. W.; Lieber, C. M. Chemistry and Physics in One Dimension: Synthesis and Properties of Nanowires and Nanotubes. *Acc. Chem. Res.* **1999**, *32* (5), 435–445. https://doi.org/10.1021/ar9700365.

(36) Nanot, S.; Hároz, E. H.; Kim, J. H.; Hauge, R. H.; Kono, J. Optoelectronic Properties of Single-Wall Carbon Nanotubes. *Adv. Mater.* **2012**, *24* (36), 4977–4994. https://doi.org/10.1002/adma.201201751.

(37) Kane, C. L.; Mele, E. J. Size, Shape, and Low Energy Electronic Structure of Carbon Nanotubes. *Phys. Rev. Lett.* **1997**, *78* (10), 1932–1935. https://doi.org/10.1103/PhysRevLett.78.1932.

(38) Ebbesen, T. W.; Lezec, H. J.; Hiura, H.; Bennett, J. W.; Ghaemi, H. F.; Thio, T. Electrical Conductivity of Individual Carbon Nanotubes. *Nature* **1996**, *382* (6586), 54–56. https://doi.org/10.1038/382054a0.

(39) Tasis, D.; Tagmatarchis, N.; Bianco, A.; Prato, M. Chemistry of Carbon Nanotubes. *Chem. Rev.* **2006**, *106* (3), 1105–1136. https://doi.org/10.1021/cr050569o.

(40) Hirsch, A.; Vostrowsky, O. Functionalization of Carbon Nanotubes. *Top. Curr. Chem.* **2005**, *245*, 193–237. https://doi.org/10.1007/b98169.

(41) Bahr, J. L.; Yang, J.; Kosynkin, D. V.; Bronikowski, M. J.; Smalley, R. E.; Tour, J. M. Functionalization of Carbon Nanotubes by Electrochemical Reduction of Aryl Diazonium Salts: A Bucky Paper Electrode. *J. Am. Chem. Soc.* **2001**, *123* (27), 6536–6542. https://doi.org/10.1021/ja010462s.

(42) Georgakilas, V.; Voulgaris, D.; Vázquez, E.; Prato, M.; Guldi, D. M.; Kukovecz, A.; Kuzmany, H. Purification of HiPCO Carbon Nanotubes via Organic Functionalization. *J. Am. Chem. Soc.* **2002**, *124* (48), 14318–14319. https://doi.org/10.1021/ja0260869.

(43) Liu, J.; Rinzler, A. G.; Dai, H.; Hafner, J. H.; Kelley Bradley, R.; Boul, P. J.; Lu, A.;

Iverson, T.; Shelimov, K.; Huffman, C. B.; Rodriguez-Macias, F.; Shon, Y. S.; Lee, T. R.; Colbert, D. T.; Smalley, R. E. Fullerene Pipes. *Science* **1998**, *280* (5367), 1253–1256. https://doi.org/10.1126/science.280.5367.1253.

(44) Wang, J.; Nguyen, T. D.; Cao, Q.; Wang, Y.; Tan, M. Y. C.; Chan-Park, M. B. Selective Surface Charge Sign Reversal on Metallic Carbon Nanotubes for Facile Ultrahigh Purity Nanotube Sorting. *ACS Nano* **2016**, *10* (3), 3222–3232. https://doi.org/10.1021/acsnano.5b05795.

(45) Campidelli, S.; Meneghetti, M.; Prato, M. Separation of Metallic and Semiconducting Single-Walled Carbon Nanotubes via Covalent Functionalization. *Small* **2007**, *3* (10), 1672–1676. https://doi.org/10.1002/smll.200700394.

(46) Hersam, M. C. Progress towards Monodisperse Single-Walled Carbon Nanotubes. *Nat. Nanotechnol.* **2008**, *3*, 387–394. https://doi.org/10.1038/nnano.2008.135.

(47) Hersam Mark, Arnold Micheal, Green Alexandar, Hulvat James, S. S. Sorting Carbon Nanotubes by Electronic Structure Using Denisty Differentiation. *Nat. Nanotechnoloy* **2006**, *1* (1), 60–65. https://doi.org/10.1038/nnano.2006.52.

(48) Ghosh, S.; Bachilo, S. M.; Weisman, R. B. Advanced Sorting of Single-Walled Carbon Nanotubes by Nonlinear Density-Gradient Ultracentrifugation. *Nat. Nanotechnol.* **2010**, *5* (6), 443–450. https://doi.org/10.1038/nnano.2010.68.

(49) Tanaka, T.; Jin, H.; Miyata, Y.; Kataura, H. High-Yield Separation of Metallic and Semiconducting Single-Wall Carbon Nanotubes by Agarose Gel Electrophoresis. *Appl. Phys. Express* **2008**, *1* (11), 1140011–1140013. https://doi.org/10.1143/APEX.1.114001.

(50) Tanaka, T.; Jin, H.; Miyata, Y.; Fujii, S.; Suga, H.; Naitoh, Y.; Minari, T.; Miyadera, T.; Tsukagoshi, K.; Kataura, H. Simple and Scalable Gel-Based Separation of Metallic and Semiconducting Carbon Nanotubes. *Nano Lett.* **2009**, *9* (4), 1497–1500. https://doi.org/10.1021/nl8034866.

(51) Arnold, M. S.; Stupp, S. I.; Hersam, M. C. Enrichment of Single-Walled Carbon Nanotubes by Diameter in Density Gradients. *Nano Lett.* **2005**, *5* (4), 713–718. https://doi.org/10.1021/nl050133o.

(52) Flavel, B. S.; Kappes, M. M.; Krupke, R.; Hennrich, F. Separation of Single-Walled Carbon Nanotubes by 1-Dodecanol-Mediated Size-Exclusion Chromatography. *ACS Nano* **2013**, *7* (4), 3557–3564. https://doi.org/10.1021/nn4004956.

(53) Tu, X.; Manohar, S.; Jagota, A.; Zheng, M. DNA Sequence Motifs for Structure-Specific Recognition and Separation of Carbon Nanotubes. *Nature* **2009**, *460* (7252), 250–253. https://doi.org/10.1038/nature08116.

(54) Zheng, M.; Jagota, A.; Semke, E. D.; Diner, B. A.; Mclean, R. S.; Lustig, S. R.; Richardson, R. E.; Tassi, N. G. DNA-Assisted Dispersion and Separation of Carbon Nanotubes. *Nat. Mater.* **2003**, *2* (May), 2–6. https://doi.org/10.1038/nmat877.

(55) Zheng, M.; Jagota, A.; Strano, M. S.; Santos, A. P.; Barone, P.; Chou, S. G.; Diner, B. A.; Dresselhaus, M. S.; Mclean, R. S.; Onoa, G. B.; Samsonidze, G. G.; Semke, E. D. Structure-Based Carbon Nanotube Sorting by Sequence-Dependent DNA Assembly. *Science* **2003**, *302*, 1545–1549. https://doi.org/10.1126/science.1091911.

(56) Vladimir, K. Post-Polymerization Click Functionalization of Conjugated Polymers, 2021.

(57) Chen, R. J.; Zhang, Y.; Wang, D.; Dai, H. Noncovalent Side-Wall Functionalization of Single-Walled Carbon Nanotubes. *J. Am. Chem. Soc.* **2001**, *123* (16), 3838–3839. https://doi.org/10.1021/ja010172b.

(58) Steuerman, D. W.; Star, A.; Narizzano, R.; Choi, H.; Ries, R. S.; Nicolini, C.; Stoddart, J. F.; Heath, J. R. Interactions between Conjugated Polymers and Single-Walled Carbon Nanotubes. *J. Phys. Chem. B* **2002**, *106* (12), 3124–3130. https://doi.org/10.1021/jp014326l.

(59) Samanta, S. K.; Fritsch, M.; Scherf, U.; Gomulya, W.; Bisri, S. Z.; Loi, M. A. Conjugated Polymer-Assisted Dispersion of Single-Wall Carbon Nanotubes: The Power of Polymer Wrapping. *Acc. Chem. Res.* **2014**, *47* (8), 2446–2456. https://doi.org/10.1021/ar500141j.

(60) Wang, H.; Bao, Z. Conjugated Polymer Sorting of Semiconducting Carbon Nanotubes and Their Electronic Applications. *Nano Today* **2015**, *10* (6), 737–758. https://doi.org/10.1016/j.nantod.2015.11.008.

(61) Lei, T.; Pochorovski, I.; Bao, Z. Separation of Semiconducting Carbon Nanotubes for Flexible and Stretchable Electronics Using Polymer Removable Method. *Acc. Chem. Res.* **2017**, *50* (4), 1096–1104. https://doi.org/10.1021/acs.accounts.7b00062.

(62) Adrian Nish, Jeong-Yuan Hwang, James Doig, R. N. Highly Selective Dispersion of Single-Walled Carbon Nanotubes Using Aromatic Polymers. *Nat. Nanotechnoloy* **2007**, *2* (10), 640–646. https://doi.org/10.1038/nnano.2007.290.

(63) Brady, G. J.; Joo, Y.; Wu, M. Y.; Shea, M. J.; Gopalan, P.; Arnold, M. S. Polyfluorene-Sorted, Carbon Nanotube Array Field-Effect Transistors with Increased Current Density and High on/off Ratio. *ACS Nano* **2014**, *8* (11), 11614–11621.

https://doi.org/10.1021/nn5048734.

(64) Toshimitsu, F.; Ozawa, H.; Nakashima, N. Hybrids of Copolymers of Fluorene and C60-Carrying-Carbazole with Semiconducting Single-Walled Carbon Nanotubes. *Chem. - A Eur. J.* **2015**, *21* (8), 3359–3366. https://doi.org/10.1002/chem.201405050.

(65) Pochorovski, I.; Wang, H.; Feldblyum, J. I.; Zhang, X.; Antaris, A. L.; Bao, Z. H-Bonded Supramolecular Polymer for the Selective Dispersion and Subsequent Release of Large-Diameter Semiconducting Single-Walled Carbon Nanotubes. *J. Am. Chem. Soc.* **2015**, *137* (13), 4328–4331. https://doi.org/10.1021/jacs.5b01704.

(66) Lei, T.; Chen, X.; Pitner, G.; Wong, H. S. P.; Bao, Z. Removable and Recyclable Conjugated Polymers for Highly Selective and High-Yield Dispersion and Release of Low-Cost Carbon Nanotubes. *J. Am. Chem. Soc.* **2016**, *138* (3), 802–805. https://doi.org/10.1021/jacs.5b12797.

(67) Barman, S. N.; Lemieux, M. C.; Baek, J.; Rivera, R.; Bao, Z. Effects of Dispersion Conditions of Single-Walled Carbon Nanotubes on the Electrical Characteristics of Thin Film Network Transistors. *ACS Appl. Mater. Interfaces* **2010**, *2* (9), 2672–2678. https://doi.org/10.1021/am1005223.

(68) Lee, H. W.; Yoon, Y.; Park, S.; Oh, J. H.; Hong, S.; Liyanage, L. S.; Wang, H.; Morishita, S.; Patil, N.; Park, Y. J.; Park, J. J.; Spakowitz, A.; Galli, G.; Gygi, F.; Wong, P. H. S.; Tok, J. B. H.; Kim, J. M.; Bao, Z. Selective Dispersion of High Purity Semiconducting Single-Walled Carbon Nanotubes with Regioregular Poly(3-Alkylthiophene)S. *Nat. Commun.* **2011**, *2* (541), 1–8. https://doi.org/10.1038/ncomms1545.

(69) Gomulya, W.; Rios, J. M. S.; Derenskyi, V.; Bisri, S. Z.; Jung, S.; Fritsch, M.; Allard, S.;

Scherf, U.; Dos Santos, M. C.; Loi, M. A. Effect of Temperature on the Selection of Semiconducting Single Walled Carbon Nanotubes Using Poly(3-Dodecylthiophene-2,5-Diyl). *Carbon* **2015**, *84*, 66–73. https://doi.org/10.1016/j.carbon.2014.11.037.

(70) Rice, N. A.; Subrahmanyam, A. V.; Laengert, S. E.; Adronov, A. The Effect of Molecular Weight on the Separation of Semiconducting Single-Walled Carbon Nanotubes Using Poly(2,7-Carbazole)S. *J. Polym. Sci. Part A Polym. Chem.* **2015**, *53* (21), 2510–2516. https://doi.org/10.1002/pola.27715.

(71) Ding, J.; Li, Z.; Lefebvre, J.; Cheng, F.; Dubey, G.; Zou, S.; Finnie, P.; Hrdina, A.; Scoles, L.; Lopinski, G. P.; Kingston, C. T.; Simard, B.; Malenfant, P. R. L. Enrichment of Large-Diameter Semiconducting SWCNTs by Polyfluorene Extraction for High Network Density Thin Film Transistors. *Nanoscale* **2014**, *6* (4), 2328–2339. https://doi.org/10.1039/c3nr05511f.

(72) Wang, H.; Hsieh, B.; Jiménez-Osés, G.; Liu, P.; Tassone, C. J.; Diao, Y.; Lei, T.; Houk, K. N.; Bao, Z. Solvent Effects on Polymer Sorting of Carbon Nanotubes with Applications in Printed Electronics. *Small* **2015**, *11* (1), 126–133. https://doi.org/10.1002/smll.201401890.

(73) Jakubka, F.; Schießl, S. P.; Martin, S.; Englert, J. M.; Hauke, F.; Hirsch, A.; Zaumseil, J. Effect of Polymer Molecular Weight and Solution Parameters on Selective Dispersion of Single-Walled Carbon Nanotubes. *ACS Macro Lett.* **2012**, *1* (7), 815–819. https://doi.org/10.1021/mz300147g.

(74) Qian, L.; Xu, W.; Fan, X.; Wang, C.; Zhang, J.; Zhao, J.; Cui, Z. Electrical and Photoresponse Properties of Printed Thin-Film Transistors Based on Poly(9,9-

Dioctylfluorene-Co -Bithiophene) Sorted Large-Diameter Semiconducting Carbon Nanotubes. *J. Phys. Chem. C* **2013**, *117* (35), 18243–18250. https://doi.org/10.1021/jp4055022.

(75) Fong, D.; Adronov, A. Recent Developments in the Selective Dispersion of Single-Walled Carbon Nanotubes Using Conjugated Polymers. *Chem. Sci.* **2017**, *8* (11), 7292–7305. https://doi.org/10.1039/c7sc02942j.

(76) Lemasson, F. A.; Strunk, T.; Gerstel, P.; Hennrich, F.; Lebedkin, S.; Barner-kowollik, C.; Wenzel, W.; Kappes, M. M.; Mayor, M. Selective Dispersion of Single-Walled Carbon Nanotubes. *J. Am. Chem. Soc.* **2011**, *133*, 652–655. https://doi.org/10.1021/ja105722u.

(77) Rice, N. A.; Adronov, A. Supramolecular Interactions of High Molecular Weight Poly(2,7-Carbazole)s with Single-Walled Carbon Nanotubes. *Macromolecules* **2013**, *46* (10), 3850–3860. https://doi.org/10.1021/ma400081d.

(78) Rice, N. A.; Adronov, A. Selective Interactions of a High-Molecular-Weight Polycarbazole with Different Commercial Nanotube Samples. *J. Polym. Sci. Part A Polym. Chem.* **2014**, *52* (19), 2738–2747. https://doi.org/10.1002/pola.27292.

(79) Kim, K. K.; Yoon, S. M.; Choi, J. Y.; Lee, J.; Kim, B. K.; Kim, J. M.; Lee, J. H.; Paik, U.; Park, M. H.; Yang, C. W.; An, K. H.; Chung, Y.; Lee, Y. H. Design of Dispersants for the Dispersion of Carbon Nanotubes in an Organic Solvent. *Adv. Funct. Mater.* **2007**, *17* (11), 1775–1783. https://doi.org/10.1002/adfm.200600915.

(80) Star, A.; Stoddart, J. F.; Steuerman, D.; Diehl, M.; Boukai, A.; Wong, E. W.; Yang, X.; Chung, S.; Choi, H.; Heath, J. R. Preparation and Properties of Polymer-Wrapped Single-Walled Carbon Nanotubes. *Angew. Chemie* **2001**, *113* (9), 1771–1775.

https://doi.org/10.1002/1521-3773.

(81) Cheng, F.; Adronov, A. Noncovalent Functionalization and Solubilization of Carbon Nanotubes by Using a Conjugated Zn-Porphyrin Polymer. *Chem. - A Eur. J.* **2006**, *12* (19), 5053–5059. https://doi.org/10.1002/chem.200600302.

(82) Sprafke, J. K.; Stranks, S. D.; Warner, J. H.; Nicholas, R. J.; Anderson, H. L. Noncovalent Binding of Carbon Nanotubes by Porphyrin Oligomers. *Angew. Chemie - Int. Ed.* **2011**, *50* (10), 2313–2316. https://doi.org/10.1002/anie.201007295.

(83) Yoon, S. M.; Sung, J. K.; Shin, H. J.; Benayad, A.; Seong, J. C.; Ki, K. K.; Soo, M. K.; Yong, J. P.; Kim, G.; Choi, J. Y.; Young, H. L. Selective Oxidation on Metallic Carbon Nanotubes by Halogen Oxoanions. *J. Am. Chem. Soc.* **2008**, *130* (8), 2610–2616. https://doi.org/10.1021/ja077449d.

(84) Hamon, M. A.; Stensaas, K. L.; Sugar, M. A.; Tumminello, K. C.; Allred, A. K. Reacting Soluble Single-Walled Carbon Nanotubes with Singlet Oxygen. *Chem. Phys. Lett.* **2007**, *447* (1–3), 1–4. https://doi.org/10.1016/j.cplett.2007.08.079.

(85) Varghese, N.; Ghosh, A.; Voggu, R.; Ghosh, S.; Rao, C. N. R. Selectivity in the Interaction of Electron Donor and Acceptor Molecules with Graphene and Single-Walled Carbon Nanotubes. *J. Phys. Chem. C* **2009**, *113* (39), 16855–16859. https://doi.org/10.1021/jp9075355.

(86) Rice, N. A.; Subrahmanyam, A. V.; Coleman, B. R.; Adronov, A. Effect of Induction on the Dispersion of Semiconducting and Metallic Single-Walled Carbon Nanotubes Using Conjugated Polymers. *Macromolecules* **2015**, *48* (15), 5155–5161. https://doi.org/10.1021/acs.macromol.5b00631.

(87) Fong, D.; Bodnaryk, W. J.; Rice, N. A.; Saem, S.; Moran-Mirabal, J. M.; Adronov, A. Influence of Polymer Electronics on Selective Dispersion of Single-Walled Carbon Nanotubes. *Chem. - A Eur. J.* **2016**, *22* (41), 14560–14566. https://doi.org/10.1002/chem.201602722.

(88) Bodnaryk, W. J.; Fong, D.; Adronov, A. Enrichment of Metallic Carbon Nanotubes Using a Two-Polymer Extraction Method. *ACS Omega* **2018**, *3* (11), 16238–16245. https://doi.org/10.1021/acsomega.8b02735.

(89) Weisman, R. B.; Bachilo, S. M.; Tsyboulski, D. Fluorescence Spectroscopy of Single-Walled Carbon Nanotubes in Aqueous Suspension. *Appl. Phys. A Mater. Sci. Process.* **2004**, *78* (8), 1111–1116. https://doi.org/10.1007/s00339-003-2461-5.

(90) O'Connell, M. J.; Bachilo, S. M.; Huffman, C. B.; Moore, V. C.; Strano, M. S.; Haroz, E. H.; Rialon, K. L.; Boul, P. J.; Noon, W. H.; Kittrell, C.; Ma, J.; Hauge, R. H.; Weisman, R. B.; Smalley, R. E. Band Gap Fluorescence from Individual Single-Walled Carbon Nanotubes. *Science* **2002**, *297* (5581), 593–597. https://doi.org/10.1126/science.1072631.

(91) Bachilo, S. M.; Strano, M. S.; Kittrell, C.; Hauge, R. H.; Smalley, R. E.; Weisman, R. B. Structure-Assigned Optical Spectra of Single-Walled Carbon Nanotubes. *Science* **2002**, *298* (5602), 2361–2366. https://doi.org/10.1126/science.1078727.

(92) Naumov, A. V.; Ghosh, S.; Tsyboulski, D. A.; Bachilo, S. M.; Weisman, R. B. Analyzing Absorption Backgrounds in Single-Walled Carbon Nanotube Spectra. *ACS Nano* **2011**, *5* (3), 1639–1648. https://doi.org/10.1021/nn1035922.

(93) Weisman, R. B.; Bachilo, S. M. Dependence of Optical Transition Energies on Structure for Single-Walled Carbon Nanotubes in Aqueous Suspension: An Empirical Kataura Plot.

Nano Lett. **2003**, *3* (9), 1235–1238. https://doi.org/10.1021/nl034428i.

(94) Mehlenbacher, R. D.; Wu, M. Y.; Grechko, M.; Laaser, J. E.; Arnold, M. S.; Zanni, M. T. Photoexcitation Dynamics of Coupled Semiconducting Carbon Nanotube Thin Films. *Nano Lett.* **2013**, *13* (4), 1495–1501. https://doi.org/10.1021/nl304591w.

(95) tephanie Reich, C. T. R. Raman Spectroscopy of Graphite. *Philos. Trans. R. Soc.* **2004**, *362* (1824), 2271–2288. https://doi.org/10.1098/rsta.2004.1454.

(96) Jorio, A.; Pimenta, M. A.; Souza Filho, A. G.; Saito, R.; Dresselhaus, G.; Dresselhaus, M. S. Characterizing Carbon Nanotube Samples with Resonance Raman Scattering. *New J. Phys.* **2003**, *5* (139). https://doi.org/10.1088/1367-2630/5/1/139.

(97) Lefrant, S.; Baibarac, M.; Baltog, I. Raman and FTIR Spectroscopy as Valuable Tools for the Characterization of Polymer and Carbon Nanotube Based Composites. *J. Mater. Chem.* **2009**, *19* (32), 5690–5704. https://doi.org/10.1039/b821136a.

(98) Dresselhaus, M. S.; Dresselhaus, G.; Saito, R.; Jorio, A. Raman Spectroscopy of Carbon Nanotubes. *Phys. Rep.* **2005**, *409* (2), 47–99. https://doi.org/10.1016/j.physrep.2004.10.006.

(99) Strano, M. S.; Doorn, S. K.; Haroz, E. H.; Kittrell, C.; Hauge, R. H.; Smalley, R. E. Assignment of (n, m) Raman and Optical Features of Metallic Single-Walled Carbon Nanotubes. *Nano Lett.* **2003**, *3* (8), 1091–1096. https://doi.org/10.1021/nl034196n.

(100) Doorn, S. K.; Heller, D. A.; Barone, P. W.; Usrey, M. L.; Strano, M. S. Resonant Raman Excitation Profiles of Individually Dispersed Single Walled Carbon Nanotubes in Solution. *Appl. Phys. A Mater. Sci. Process.* **2004**, *78* (8), 1147–1155.

https://doi.org/10.1007/s00339-003-2466-0.

(101) Strano, M. S.; Dyke, C.; Usrey, M.; Barone, P.; Mathew, A.; Shan, H.; Kittrell, C.; Hauge, R.; James, T.; Smalley, R. Electronic Structure Control of Single-Walled Carbon Nanotube Functionalization. *Science* **2003**, *301* (5639), 1519–1521. https://doi.org/10.1126/science.1087691.

(102) Pimenta, M.; Marucci, A.; Empedocles, S.; Bawendi, M.; Hanlon, E.; Rao, A.; Eklund, P.; Smalley, R.; Dresselhaus, G.; Dresselhaus, M. Raman Modes of Metallic Carbon Nanotubes. *Phys. Rev. B - Condens. Matter Mater. Phys.* **1998**, *58* (24), R16016–R16019. https://doi.org/10.1103/PhysRevB.58.R16016.

(103) Zincke Th, Heuser G, M. W. I. Ueber Dinitrophenylpyridiniumchlorid Und Dessen Umwandlungsproducte. *European J. Org. Chem.* **1904**, *333* (2), 296–345. https://doi.org/10.1002/jlac.19043330212.

(104) Kunugi, S.; Okubo, T.; Ise, N. A Study on the Mechanism of the Reaction of N-(2,4-Dinitrophenyl)-3carbamoylpyridinium Chloride with Amines and Amino Acids with Reference to Effect of Polyelectrolyte Addition. *J. Am. Chem. Soc.* **1976**, *98* (8), 2282–2287. https://doi.org/10.1021/ja00424a047.

(105) Elliot, N.; Caple, G. Formation of Phenylpyridinium Chloride from 5-Anilino-N-Phenyl-2,4-Pentadienylideniminium Chloride. Kinetics in Basic Media. *Am. Chem. Soc.* **1970**, *661* (8), 5641–5645. https://doi.org/10.1021/ja00722a016.

(106) Eda, M.; Kurth, M. J.; Nantz, M. H. The Solid-Phase Zincke Reaction: Preparation of ω-Hydroxy Pyridinium Salts in the Search for CFTR Activation. *J. Org. Chem.* **2000**, *65* (17), 5131–5135. https://doi.org/10.1021/jo0001636.

(107) Yves Genisson, CHristian Marazano, Maryam Mehmandoust, Dino Ginecco, B. C. Das. Zincke's Reaction with Chiral Primary Amines: A Practical Entry to Pyridinium Salts of Interest in Asymmetric Synthesis. *Synlett* **1992**, *1992* (5), 431–434. https://doi.org/10.1055/s-1992-21371.

(108) Barbier, D.; Marazano, C.; Das, B. C.; Potier, P. New Chiral Isoquinolinium Salt Derivatives from Chiral Primary Amines via Zincke Reaction. *J. Org. Chem.* **1996**, *61* (26), 9596–9598. https://doi.org/10.1021/jo961539b.

(109) Genisson, Y.; Marazano, C.; Das, B. A Stereocontrolled Alkylation of Chiral Pyridinium Salts with Grignard Reagents: Synthesis of (+)-Normetazocine and (+)-Nordextrorphan. *J. Org. Chem.* **1993**, *58* (8), 2052–2057. https://doi.org/10.1021/jo00060a019.

(110) Carpino, L. A. Convenient Prepartion of (9-Fluorenyl)Methanol and Its 2,7-Dihalo Derivatives. *Am. Chem. Soc.* **1980**, *45* (21), 4250–4252. https://doi.org/10.1021/jo01309a045.

(111) Gomulya, W.; Costanzo, G. D.; De Carvalho, E. J. F.; Bisri, S. Z.; Derenskyi, V.; Fritsch, M.; Fröhlich, N.; Allard, S.; Gordiichuk, P.; Herrmann, A.; Marrink, S. J.; Dos Santos, M. C.; Scherf, U.; Loi, M. A. Semiconducting Single-Walled Carbon Nanotubes on Demand by Polymer Wrapping. *Adv. Mater.* **2013**, *25* (21), 2948–2956. https://doi.org/10.1002/adma.201300267.